EINDHOVEN UNIVERSITY OF TECHNOLOGY

Eindhoven University of Technology

MASTER

Beam quality determination methods for focused ion beams

Penterman, K.E.M.

Award date:
2019

Link to publication

Disclaimer
This document contains a student thesis (bachelor's or master's), as authored by a student at Eindhoven University of Technology. Student theses are made available in the TU/e repository upon obtaining the required degree. The grade received is not published on the document as presented in the repository. The required complexity or quality of research of student theses may vary by program, and the required minimum study period may vary in duration.

General rights
Copyright and moral rights for the publications made accessible in the public portal are retained by the authors and/or other copyright owners and it is a condition of accessing publications that users recognise and abide by the legal requirements associated with these rights.

• Users may download and print one copy of any publication from the public portal for the purpose of private study or research.
• You may not further distribute the material or use it for any profit-making activity or commercial gain

Eindhoven University of Technology
Department of Applied Physics
Coherence and Quantum Technology (CQT)

Beam Quality Determination Methods for Focused Ion Beams

Master's Thesis

K.E.M. Penterman

CQT – 2019 - 18

Supervisors:
dr. ir. E.J.D. Vredenbregt
dr. ir. S.H.W. Wouters
dr. ir. G. ten Haaf

Abstract

In this thesis methods of determining the beam quality of a focused ion beam (FIB) are researched. FIBs are important instruments in the field of nanomachining, particularly because of their ability to directly modify structures at the nanometer length scale. As the semiconductor industry has need of smaller features, more precise FIBs are also needed. For this reason, two methods to determine FIB beam quality are evaluated in this thesis. The chosen methods focus on three of the most important properties of the FIB: resolution, spot size and beam brightness.
The first evaluated method is a method for determining resolution, proposed by Orloff et al [1]. It determines the contrast response to spatial frequencies of FIB created images, by investigating the contrasts between sharp edges at different distances from one another. To do so an image of a sample with many such sharp edges, in this case broken graphite, is made using the imaging capabilities of the FIB and subsequently analysed to find the contrasts between the different edges.
The use of this method results in a decent estimate of the resolution, but only as a range in which it can be found, such as 2-7 nm or 4-10 nm, found at image magnifications of $M = 120000$ and $M = 65000$ respectively. This method becomes less accurate at lower magnifications, as can be seen by the resolution range of 15-35 nm found at $M = 25000$.
It is a slow method, however, since the positions of the edges have to be determined manually to gain an accurate result. The possibility of determining edge positions automatically is researched, but no practicable method is found within the scope of this thesis, though the use of specific software that focuses on finding shapes (the lines of the edges) instead of local maxima is proposed.
The second evaluated method is a method for using knife edge measurements to determine both the spot size and the reduced brightness of the beam. A knife edge measurement works by scanning the beam over a single sharp edge and determining the size of the beam from the resulting so-called rise distance. For the purposes of determining the spot size and reduced brightness, the explored method used a number of knife edge measurements at different positions along the beam axis at and surrounding the focal point of the beam.
The use of this method results in rough estimates for the spot size and beam brightness. The greatest problem is caused by the use of an insufficiently sharp knife edge, which results in finding erroneous spot sizes. The experimental values are always within an order of magnitude from the expected result, however, and greater effort in using a sufficiently sharp knife edge as well as other improvements, may result in a more accurate determination of these values.
The trends of the spot size and reduced brightness' dependency on other beam parameters can be inferred from the results quite well, however, and are also useful towards determining beam quality. This Knife Edge method can thus best be used to gain understanding of the important trends in the ion beam properties, like the spot size versus current curve, instead of as a method to accurately determine spot size and brightness. It has the benefit that it can determine these trends without the beam current density being known and that this method can be performed almost fully automatically.
The main limit to using both of these methods on FIBs of higher quality and thus better resolution, smaller spot size and higher beam brightness is expected to be the sharpness of the edges, since when the beam size decreases, the edges need to be proportionally sharper as well, as not to interfere with the accuracy of the results.

Contents

1 **Introduction** ... 6
1.1 **Context of this thesis** ... 6
1.1.1 *The Focused Ion Beam* ... 6
1.1.2 *Demand for more precise FIBs* ... 7
1.2 **Beam quality** ... 8
1.3 **Current state of the field** ... 9
1.3.1 *Resolution measurement* ... 9
1.3.2 *Spot Size measurements* ... 10
1.3.3 *Current density profile measurements* ... 10
1.4 **Focus of this thesis** ... 10
1.5 **Contents** ... 11
2 **FIB Setup** ... 12
2.1 **Introduction** ... 12
2.2 **The LMIS FIB** ... 12
2.2.1 *The FIB setup* ... 12
2.2.2 *Imaging with the FIB* ... 15
2.2.3 *Specifications* ... 16
3 **Resolution Measurement** ... 18
3.1 **Introduction** ... 18
3.2 **Underlying Principles** ... 18
3.2.1 *The Rayleigh definition of resolution* ... 18
3.2.2 *Expected beam parameters* ... 19
3.3 **Implementation** ... 22
3.3.1 *Implementation of the Technique* ... 22
3.3.2 *Manual Determination of Edges* ... 23
3.3.3 *Automatic Determination of Edges* ... 24
3.3.4 *Expected experimental difficulties* ... 26
3.4 **Results** ... 27
3.4.1 *Manual Determination of the Edges* ... 27
3.4.2 *Automatic Determination of the Edges* ... 30
3.4.3 *Difficulties of this method* ... 34
3.5 **Conclusion** ... 35
4 **The Knife Edge Method** ... 38
4.1 **Introduction** ... 38

4.2 Underlying Principles ... 38
4.2.1 Brightness ... 38
4.2.2 Expected beam parameters ... 40
4.3 Implementation ... 42
4.3.1 The model ... 42
4.3.2 Experimental Implementation ... 46
4.3.3 Expected Experimental Difficulties ... 51
4.4 Results ... 56
4.4.1 Experimental measurements ... 56
4.4.2 Difficulties of the Knife Edge Method ... 62
4.5 Conclusion ... 63
5 Conclusion and discussion ... 64
5.1 Conclusions ... 64
5.1.1 The resolution measurement ... 64
5.1.2 The knife-edge measurement ... 65
5.2 Discussion ... 66
5.3 Recommendations for future research ... 67
Bibliography ... 70
Appendix: Code ... 72
A.1 Matlab codes for the experiments in Chapter 3 ... 72
A.1.1 Code for manual edge determination ... 72
A.1.2 Code for automatic edge determination ... 74
A.1.3 Code for adding artificial noise ... 78
A.2 Matlab code for the experiment in Chapter 4 ... 79
A.3 FIB instruction code used for Chapter 4 ... 85

1 Introduction

1.1 Context of this thesis

1.1.1 The Focused Ion Beam

In the last few decades the Focused Ion Beam (FIB) (see Figure 1.1.2) has become an important part of the semiconductor industry. Its ability to image and modify structures at the nanometer length scale makes it a valuable tool [2]. FIBs can be used for microscopy and to create or modify nanostructures by removing material through sputtering or by adding material through beam-activated chemistry with a precursor gas [3] (see Figure 1.1.1). More specifically they are often used for maskless depositioning or milling, error-correction or analysis of a sample [4,5].

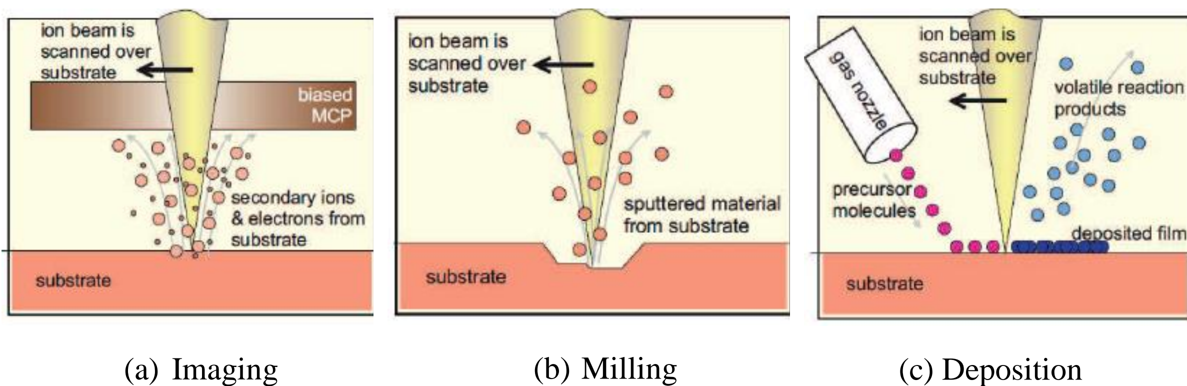

(a) Imaging (b) Milling (c) Deposition

Figure 1.1.1: Capabilities of a FIB. Imaging (a) in which secondary electrons are detected while the beam is scanned over the substrate. Milling (b) in which the momentum of the ions is used to sputter material away. And deposition (c) in which material is added through beam activated chemistry with a precursor gas. This image is taken from [6].

Compared to electron microscopy, ion microscopy with a FIB has the advantages of higher surface sensitivity and distinct contrast mechanisms [3]. FIBS also enable spatially resolved elemental analysis using secondary ion mass spectrometry (SIMS) [5]. Use of a FIB instead of an electron microscope is not without drawbacks, however, since the imaging resolution is often severely limited by sputtering damage [7] (also see Section 4.3.3). The greater ion mass does make FIBs useful for lithography, though, since scattering effects are usually less important in determining feature size and limiting pitch than for electron beam techniques [8].

Figure 1.1.2: Picture of a Ga LMIS FIB. This particular FIB is the FEI FIB 200TEM used in the experiments detailed in Chapters 3 and 4 and is further described in Chapter 2.

1.1.2 Demand for more precise FIBs

Over the past decades the semiconductor industry has been striving for smaller and smaller features on integrated circuits. In that time the semiconductor industry has managed to match Moore's law [9], stating that the number of transistors in a dense integrated circuit will double every two years. This goal asks for smaller and smaller components that can be placed ever more closely together. This has currently led to features as small as 10 nm, as Samsung reports about their newest phones [10,11].

The performance of FIBs is determined primarily by a system's ion source [12]. In current state of the art FIBs, namely the Liquid Metal Ion Source (LMIS), there are relatively few ionic species that can be focused to the nanometer scale and even then this typically requires beam energies of 10 keV or more, because of the inherent energy spread of the ion beam [3]. New sources that achieve better results are already in development [12]. One of these is the ABLIS project [2,5,6,13]. Compared to the LMIS, this new source should have at least a smaller longitudinal energy spread, higher brightness (in the order of 10^7 A/m^2 sr V) and be able to produce currents up to at least 0.6 nA [13]. Another is the LoTIS source, presented by Steele et al [14]. For comparison with the Ga LMIS, which is currently the most used type of LMIS [13], see Table 1.1.1. An explanation of these measures for beam quality (including the brightness) is given in Section 1.2.

When working on smaller scales, the evaluation methods also need to become more precise and finding fitting analysis methods becomes more challenging. Older techniques such as edge resolution analysis or ion beam spot burns provide only a limited understanding of the ion beam probe current distribution [15]. To understand which of the currently available analysis methods can still be used on the new FIBs that are being created today, it is important to know the limitations of these techniques and to fully understand how these techniques can best be implemented.

Table 1.1.1: The measured spot size and reduced brightness of the old Ga LMIS compared to new atomic sources as proposed by Steele et al. (the LoTIS) and Ten Haaf et al. (the ABLIS). The spot size and reduced brightness are important measures of beam quality, as is further explained in Section 1.2. While the ABLIS project does not yet have measurements of the final ionic beam, they have measured the quality of the atomic beam their source creates pre-ionization and extrapolated their results from there.

	Ga LMIS	**LoTIS [14]**	**ABLIS [13]**
Spot Size (nm)	5 - 10	(2.1 ± 0.2)	3.2 (preliminary)
Reduced Brightness ($Am^{-2}Sr^{-1}eV^{-1}$)	10^6	$(2.4 \pm 0.1) \cdot 10^7$	10^7 (preliminary)

1.2 Beam quality

Beam quality is determined by how well an ion beam can be used to achieve a certain goal. For imaging, the resolution of the beam should be high (see Section 3.2.1 for more information about resolution). For milling, depositioning and other nanomachining applications, the spot size of the beam (the beam size at its focal point) should be small, since that makes higher accuracy possible [16]. Since the imaging resolution of a FIB can be difficult to determine, the spot size has actually become a common measure of FIB beam quality [17]. The spot size is highly dependent on another important beam property, however: the beam current. One of the most important properties of a FIB is thus the spot size versus current curve (see Section 4.2.2 for more information about the spot size versus current curve). This is largely determined by the beam's transverse reduced brightness and the longitudinal energy spread of the source [2]. Thus, high reduced brightness and low energy spread are also generally accepted measures for beam quality [12] (see Section 4.2.1 for more information about beam brightness).

This leaves out the exact current density distribution of the beam. Spot size is often defined as the diameter of the beam containing at least 50% (or another percentage) of the current [17], yet this part of the beam does not determine its entire effect. Particularly at low currents the shape of the beam in a FIB can best be described by a narrow Gaussian function in the central parts and the so-called beam "tails", consisting of a second broader overlapping Gaussian and exponential functions in the edges [18]. At higher currents, the exponential functions at the edges widen faster than the central Gaussian. Thus, the higher the current, the larger these so-called beam "tails" are. [19]. These edges are normally of an intensity a few orders lower than the central part of the beam and can thus be ignored for many applications in less sensitive materials (see Figure 1.2.1). Since progress has been made in reducing the spot size of focused ion beams, however, evidence shows larger tails in the current density distribution [8], causing a large effect on nanomachining precision. Thus, a current density distribution with small tails is preferable and knowing the exact current density distribution of a beam can be very useful towards determining its possible precision and thus the beam's quality [4,15].

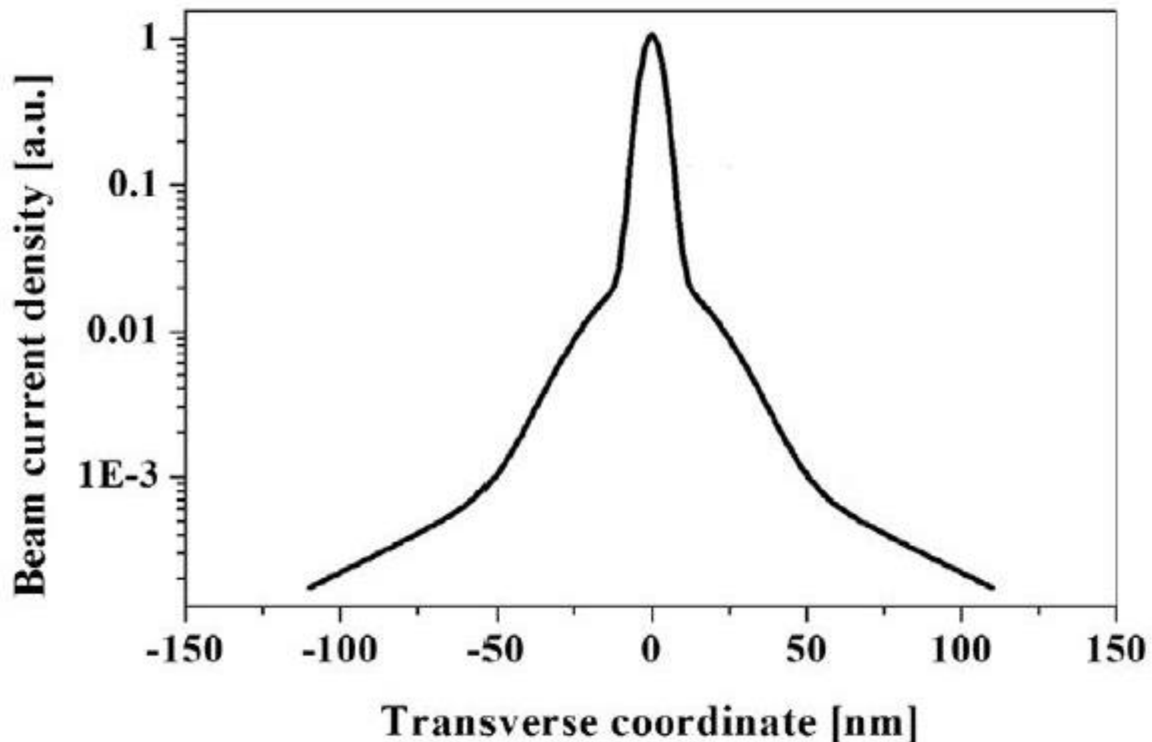

Figure 1.2.1: An example beam profile of a focused ion beam, showing a narrow central Gaussian and the beam "tails", consisting of a broader overlapping Gaussian and exponential functions at the edges. The narrow central Gaussian is basically governed by the virtual beam size. The broader overlapping Gaussian is attributed to chromatic aberrations in the lens system and the exponential edge functions are governed by ion collisions with residual gas molecules in the FIB column. This image is adapted from [18].

1.3 Current state of the field

Given the importance of knowing the precision and quality of a FIB, there are already many analysis methods in existence that are used to determine its properties. As an overview of the existing methods some of these are detailed here.

1.3.1 Resolution measurement

There is some difficulty in measuring the imaging resolution of a FIB [17]. It is possible to calculate it from the source current density distribution, but this does not give an accurate representation of the actual resolution, because interaction between the beam and the sample is not taken into account [20]. Because of this it has become common to define FIB performance in terms of the focused beam size [17].

One method to directly determine the resolution of a FIB has been proposed by Orloff et al [1], however. This method works by analysing a picture created with the FIB of a sample containing several sharp edges. The picture is created by scanning the ion beam over the sample and measuring the emitted secondary electrons. After this the contrasts between edges in the picture are determined. It is a slow method, since the positions of the edges in the picture have to be determined by hand, but should result in a relatively accurate measurement of the resolution of a FIB that does take sample interaction into account. More about this method can be found in Chapter 3.

1.3.2 Spot Size measurements

The most common method for measuring the spot size of a FIB is the Knife Edge Measurement [17]. Some variations of this have been proposed [21,22], but all of them follow the same principle. The method works by scanning the beam across a sample consisting of a single sharp edge. Since the beam has a finite size, during part of the scan the beam will only be partially on the sample. From this scan the size of the beam can then be determined. While this method is not known to be very accurate, resulting in the need for many measurements to account for statistical variations, it is quick and easy to implement [17]. More about this method can be found in Chapter 4.

Another common method is used not to determine the exact size of the beam itself, but its effect on a sample, by using the beam to burn away part of the sample material (like a spot or a line) and measuring the effect [19,23]. The beam size thus found is usually called the apparent beam size. While these measurements do give information about the FIB, the results are of course highly dependent on the substrate material.

1.3.3 Current density profile measurements

To accurately measure the current density profile of a FIB by measuring the effect of the beam on a substrate material (for example by sputtering or milling) is difficult, since the effect of a FIB on a sample material is subject to a variety of effects, including statistical effects in the sputtering, amorphization of the sample and implantation of the beam ions. The methods mentioned before in Section 1.3.2, while using the entire beam, are therefore better used to only determine spot size, since trying to determine the exact current density profile of the entire beam in such a way is highly inaccurate.

Most usable methods to measure the current density profile thus use a way to take the effect of the beam on a substrate into account. They either model the damage done by each beam particle [15,24] or use repeated measurements on the same substrate material with different intensities to experimentally determine the effect of the beam [4].

These methods do make it possible to determine the current density profile of a FIB, though they require use of a TEM (Transmission Electron Microscope) or in the case of Lugstein et al. [4] AFM (atomic force microscopy) for accurate further substrate analysis.

1.4 Focus of this thesis

The focus of this thesis is on two measurement methods: the before described resolution measurement (see Section 1.3.1) and Knife Edge measurement (see Section 1.3.2). These methods were chosen, because they can be used to give clear indications of the properties of a FIB (namely resolution, spot size and brightness) and should be relatively easy to implement. In this thesis these methods will be tested and evaluated, to find their limitations. The goal is to eventually determine whether they can be used to measure the beam quality of future FIBs with higher reduced brightness and smaller spot size than the Ga LMIS, like the ABLIS (see Section 1.1.2) and other FIBs like it. To this end, the practicability of possibly automating these methods will also be researched.

1.5 Contents

The Introduction (Chapter 1) of this thesis gives a general overview of the need for accurate measurement methods to determine the quality of a Focused Ion Beam, how FIB quality can be quantified and what sort of methods are currently extant. It also explains the focus of this thesis. The rest of the thesis starts with the experimental setup used for both of the experiments in Chapters 3 and 4, giving an overview of the used FIB (Chapter 2). Chapter 3 focuses on a resolution measurement method for a FIB and contains the underlying principles used in this method, its experimental implementation, the results of testing the method and the resulting conclusion. Chapter 4 focuses on the knife edge measurement method and contains that method's underlying principles, its experimental implementation and a way of modelling the results, as well as the results of testing the method experimentally compared to the results of the modelling and the conclusions about the knife edge measurement.

Finally, Chapter 5 shows the conclusion of the thesis, focusing on the practicability of the researched methods and the possibility of using them in future analysis of the quality of more accurate FIBs.

2 FIB Setup

2.1 Introduction

To test the methods in this thesis a gallium liquid metal ion source (LMIS) FIB was used, particularly a FEI FIB 200TEM (see Figure 1.1.2 in Chapter 1). The gallium liquid metal ion source (LMIS) is the most commonly used source in FIB instruments. Unlike its counterpart, the gas field ionization source (GFIS), the LMIS has a higher sputter yield, which makes it more useful for milling, and causes less subsurface damage, since the used ions have a smaller penetration depth. This makes the LMIS more suited for nanomachining [2,5]. Since higher quality sources will particularly be needed for nanomachining purposes in the future (see Section 1.1.2), it seemed most useful to test the methods discussed in this paper on an LMIS FIB. Also, the particular FIB used for these measurements (see Section 2.2.3) is the same LMIS FIB on the ion beam column of which the new source created by the ABLIS project [2,5,6,13] will be mounted.
In this chapter the experimental setup of the used LMIS FIB will be detailed.

2.2 The LMIS FIB

2.2.1 The FIB setup

The FIB used in the setup consists of a liquid metal ion source followed by a series of extractors and lenses that extract a particle stream and focus it onto a sample stage (see Figure 2.2.2). The liquid metal ion source itself is made out of a tungsten wire etched into a blunt tip (see Figure 2.2.1).

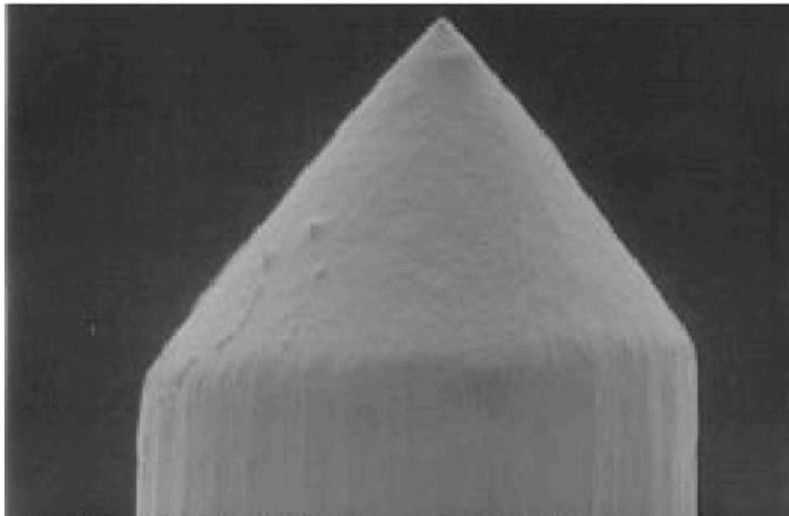

Figure 2.2.1: The tip of a properly heated LMIS source during operation.

Liquid gallium is supplied to the tip and is formed into a cone by the electric field from the extractor. This is called the Taylor cone and has a spherical tip far smaller than the tip etched into the tungsten wire [25]. Positive Ga ions are emitted from the tip of the cone by field evaporation. The distance between the extractor and the tip is set so that stable emission occurs at a voltage difference of 12 kV. To prevent the extractor from extracting too much current and keep the emission current between 2.2 and 2.4 μA, the suppressor uses an electrical field of opposing polarity, which is varied between -2 kV and +2 kV.
After this, the ion beam is directed down the column by the field of the first lens (hereafter called the condenser lens), which has a tension that can be set from 0 to -40 kV with respect to ground. The distance between the tip and the condenser lens is in the order of centimeters. The

initial focusing of the beam by the condenser lens largely determines the eventual spot size of the beam.
Several apertures are in place in this part of the column to mechanically control beam size and shape. The first is the Beam Acceptance Aperture (BAA) near the extractor cap. After passing through the condenser lens the beam is accelerated down the column through the second of these mechanically controllable apertures: the Automatic Variable Aperture (AVA), located on the AVA strip.
Having passed the condenser lens and the apertures, the beam then passes through a set of blanking plates that can be used to divert the beam away from the sample by using a negatively charged plate for when the FIB is in operation, but scanning is not desired. Diverting the beam away when not scanning protects the sample from unnecessary damage by the beam. Before final focusing the beam also passes through the deflection octupole, which can be used to shift the beam across the sample, to enable scanning.
The second lens assembly (hereafter called the objective lens) finally focuses the beam onto the sample stage, to which a sample can be mounted. The objective lens can be set to a tension from 0 to 30 kV with respect to ground and is set roughly thirty centimeters apart from the condenser lens. The distance between the stage and the objective lens is in the order of centimeters.
The sample stage can move the sample around independently of the rest of the FIB setup. It can tilt the entire sample holder around the x axis, which also tilts the y axis and z axis accordingly, it can rotate the sample along the z axis (which, at zero tilt, lies along the ion beam axis) and move the sample in the three axial directions (see Figure 2.2.3). The stage can be moved manually or through software commands.
During operation the beam current can be measured directly within the setup. When the blanking plates are used, they divert the beam into a Faraday cup, which measures the total beam current. While scanning is in progress, End Point Detection (EDP) measures the absorbed current at the specimen stage. This makes it possible to monitor current changes while scanning. To enable EDP and to prevent charge build-up in the sample, the sample needs to be conductive (or treated to be so) and electrically grounded to the sample holder.

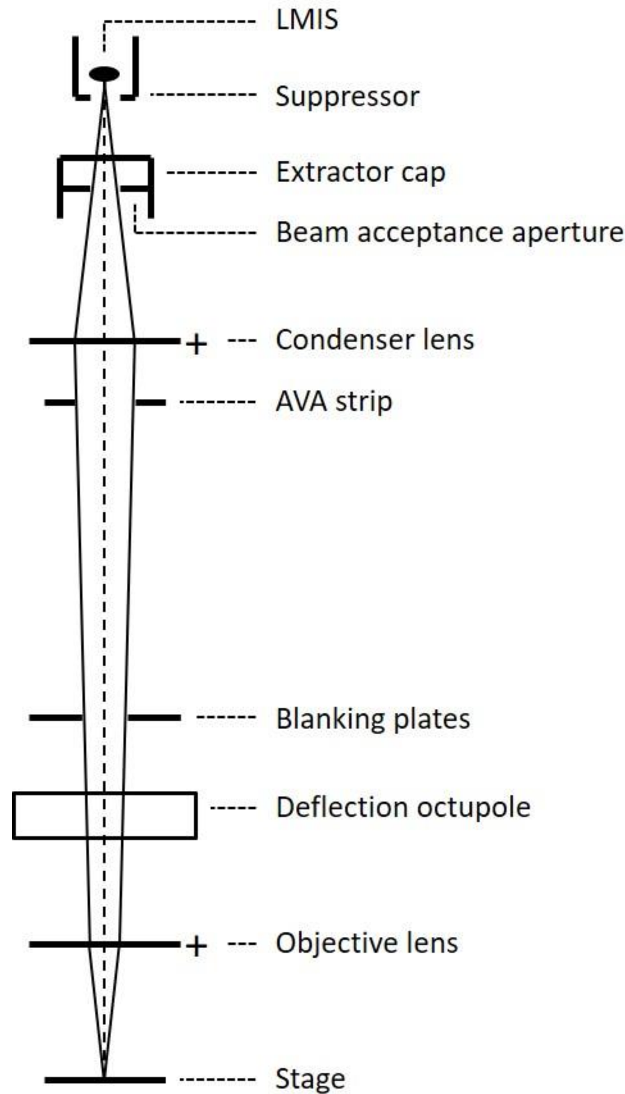

Figure 2.2.2: Functional schematic of the ion beam column of the used FIB. A gallium reservoir supplies liquid gallium to the tip portion of the LMIS. There a Taylor cone is formed from the liquid gallium by application of the electric field from the extractor. The process of field evaporation then produces ion emission. The extractor cap ensures stable emission with a positive field, while the suppressor supplies a field of opposing polarity to retard the flow of ions and obtain an emission current of 2.2 to 2.4 µA. The ion beam formed by the flow of positive gallium ions is further directed down the column by the fields of the condenser lens assembly, of which the voltage can be set from 0 to -40 kV with respect to ground. The condenser lens also provides initial focusing and largely determines the eventual spot size. The two mechanical apertures it passes through, the beam acceptance aperture (BAA) and the automatic variable aperture (AVA), are used to mechanically control the size and shape of the beam. The beam blanking plates can be used to divert the beam away from the sample when scanning is not desired. After the initial focusing of the beam by the condenser lens assembly it passes through the deflection octupole, which provides the scanning, shift and tilt function of the beam via a deflection amplifier. Finally, the beam is focused onto the stage by the objective lens assembly of which the voltage can be set from 0 to 30 kV with respect to ground. The stage can hold and move a sample for the beam to affect. Distances in the FIB range from a couple of centimeters between the source and the condenser lens as well as between the objective lens and the stage to about thirty centimeters between the two lenses.

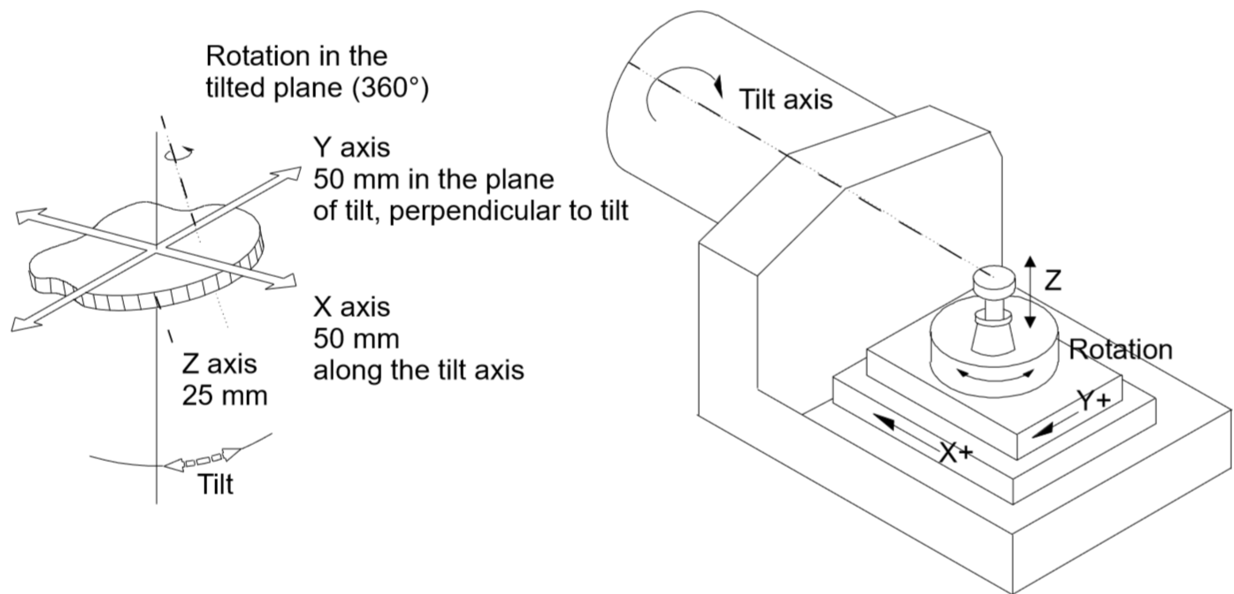

Figure 2.2.3: Figure detailing possible sample motion within the FIB. Tilting the sample along the tilt axis changes the direction of the y axis and z axis as shown. The direction of the x axis does not change, since it lies along the tilt axis. The z axis lies along the ion beam axis at zero tilt. The sample can rotate 360° around the z axis and can move 50 mm along the x axis, 50 mm along the y axis and 25 mm along the z axis.

2.2.2 Imaging with the FIB

While scanning a sample with the FIB, secondary electrons are emitted from the sample, due to collisions of the incident ions with the sample. By detecting these secondary electrons as the ion beam scans over the sample a secondary electron intensity image can be formed (see Figure 2.2.4). The beam is scanned across the sample surface in a regular pattern, called a raster. The raster consists of a series of lines in the horizontal axis (the x axis) shifted slightly across the surface from one another across the vertical axis (the y axis). The raster consists of typically one million locations (also called pixels) the beam visits during the scan.

The detector that detects the secondary electrons is a continuous dynode electron multiplier detector. It offers an off-axis view of the sample (see Figure 2.2.4) that is helpful in determining topographical information that may not be seen from a top-down view.

Thus, these secondary electron images show a clear surface morphology of the sample. They are limited by two factors, however. Firstly, when making a secondary electron scan, the amount of electrons gained is dependent on the intensity of the beam. Since the ion beam also causes sputtering and thus deterioration of the sample, this means there is a trade-off between information gained, in the form of secondary electrons, and sample deterioration [1]. Secondly, the secondary electron yield dependent on the incident ions can be inconstant across the surface of the sample, due to statistical properties, which will lead to additional noise in the image [17].

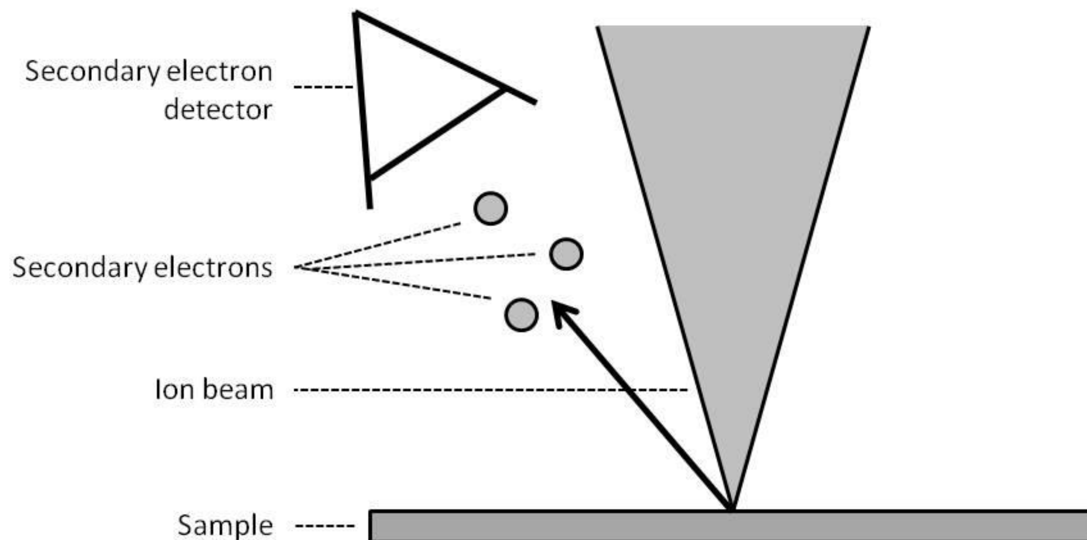

Figure 2.2.4: When the ion beam scans over a sample, the incident ions cause electrons to be emitted from the sample. These so-called secondary electrons are detected by a secondary electron detector and can be used to form a secondary electron image of the sample.

The used FIB contains software that can be used to automatically instruct the FIB to move the sample stage (and thus the sample) and/or make secondary electron images and save them, thus making it possible to automatically let the FIB generate images of a sample at different positions.
While operating the FIB, aside from setting the voltage of the lenses and the beam current, it is also possible to directly set the magnification which is used to capture images. The magnification of an image is the part of the sample viewed or scanned. At higher magnification a smaller part of the image will be scanned in more detail. Since the exact magnifications of the FIB corresponding to its settings can be calibrated with a standard sample, it is possible to directly set the wanted magnification for capturing an image.

2.2.3 Specifications

The used LMIS is a FEI FIB 200TEM (see Figure 1.1.2 in Chapter 1). It should have a resolution $D \leq 7$ nm at a beam current of 1 pA, at least while the magnification $M > 30$k. FIBs of this type generally also have a Reduced Brightness B_R of about 10^6 Am^{-2}sr^{-1}eV^{-1} and can produce a beam of 1 pA with a 5-10 nm spot size [2,5,12,25].
The beam potential of the FIB equals 30.0 kV and the beam energy equals 30.0 keV.

3 Resolution Measurement

3.1 Introduction

The first method explored to determine performance of a FIB is focussed on measuring its resolution. This particular resolution measurement should be a relatively quick and easy way to determine the resolution of a FIB. It is performed by making a secondary electron picture of a sample with many sharp edges and analysing the contrast between those edges. It is also, according to Orloff et al [1], supposed to be quite accurate, unlike the Knife Edge Method explored in the next chapter. Thus, it seemed like a good way to both determine the resolution of the ion beam and get an estimate for beam size. Particularly if the calculations needed to determine the resolution from a secondary electron picture could be automated.
In this chapter this method is described and tested, starting with the underlying principles and the explanation of the exact implementation of this method and ending with the results the method produces in terms of resolution and a reflection on its accuracy and usability.

3.2 Underlying Principles

3.2.1 The Rayleigh definition of resolution

Resolution can be defined as the ability to spatially distinguish two objects. The Rayleigh-criterion [1,20] uses this definition, specifying that there must be a discernible difference between the intensity at which the objects show up in the image and the intensity at which the space between them is shown (see Figure 3.2.1). This difference is defined in the contrast. Two objects are named spatially distinguishable when the contrast between them is high enough.
The contrast C in any part of an image is given by

$$C = \frac{I_{max} - I_{min}}{I_{max} + I_{min}}, \quad (3.2.1)$$

in which I_{max} is the maximum intensity in that part of the image and I_{min} the minimum intensity in that same region.
Thus, an image with several distinguishable features can be used to determine the change in contrast for features at different distances from each other. The resolution is then the distance between features corresponding to a chosen minimum contrast at which features are considered to just be spatially distinguishable.
According to the Rayleigh definition two point sources are defined as being just distinguishable, when the maximum of the intensity distribution of one point source coincides with the first minimum of the distribution of the second. This can particularly be applied to electron beam instruments. In a diffraction-limited electron beam system, the image of a point source will have an intensity distribution described by an Airy-function [20]. Overlapping two Airy-functions as in the Rayleigh definition, such that the maximum of the first falls on the first minimum of the second, results in Figure 3.2.1. The contrast between the peaks of the functions is then close to 10% of the maximum contrast of the image C_{max}. Note that, unlike in the example of the two Airy-functions, in actual images the intensity is usually never zero even in the darkest parts of the image, meaning that, since I_{min} is not equal to 0, C_{max} will not be equal to 1 (see Equation 3.2.1).

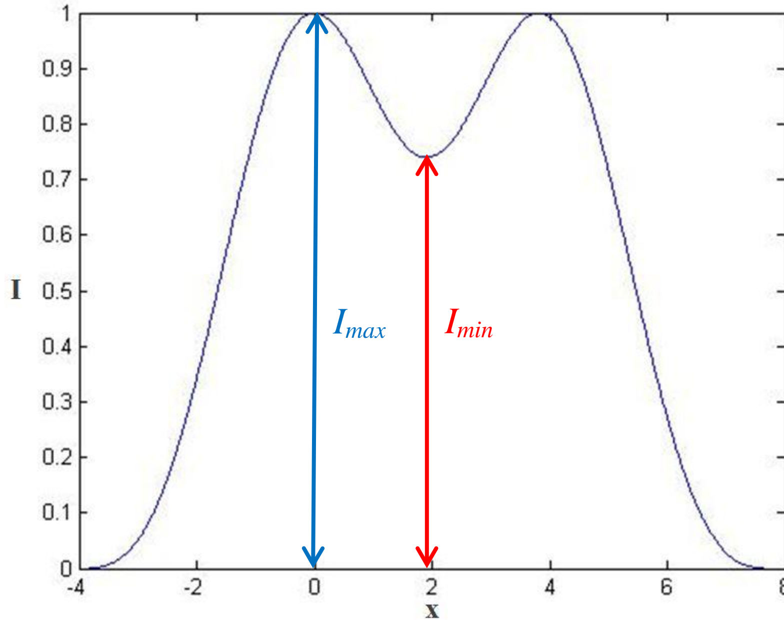

Figure 3.2.1: Illustration of the Rayleigh-criterion. The Graph shows the sum of two overlapping Airy-functions, placed so that the maximum of each function coincides with the first minimum of the other. These Airy-functions represent the intensity distributions of two point sources. The Rayleigh-criterion uses the difference between the minimum intensity between these features, I_{min}, and the maximum intensity at these features, I_{max}, as the minimal contrast at which two features are still considered spatially distinguishable (see Equation 3.2.1).

The image of an ion beam does not automatically result in an Airy-function, however. With an ion beam, where the wavelength of the ions in the system is effectively zero, and when aberrations are negligible, the source current density distribution J_s can be used as the analogue of the diffraction pattern that is described by an Airy-function in electron beam systems. The approximately Gaussian shape of the source current density distribution in ion beams (see Section 1.2) makes it not feasible to simply look for the distance at which the first minimum overlaps with the maximum. Instead, Orloff et al. [1] uses the contrast level of 10% corresponding to the Rayleigh-criterion applied on electron beam systems as the limit for the resolution.

This means that the resolution D corresponds to the distance between two features in the image at which the contrast between those features drops to 10% of the maximum contrast in the image $d_{10\%}$:

$$D = d_{10\%} \,. \qquad (3.2.2)$$

This reworked definition makes it possible to use the Rayleigh-criterion for other optical systems.

3.2.2 Expected beam parameters

To determine the usability of this method for determining the resolution, its results have to be compared to the expected beam parameters. The FIB on which these measurements are performed should have a resolution $D \leq 7$ nm at a current of 1 pA, at least while the magnification $M > 30$k (see Section 2.2.3). At a higher current the resolution should worsen (and may thus be > 7 nm) and at higher magnifications the resolution should get better (and may thus be even lower than expected). While either the current or the magnification changes no more than an order of magnitude, however, the resolution can also be expected to remain within one order of magnitude of the aforementioned 7 nm.

To determine the expected shape of the contrast C as a function of the spatial distances d in the image the Optical Transfer Function (OTF) can be used. The OTF is the contrast C as a function of the spatial frequencies f in the image. It shows how well an optical system can resolve details at each frequency. The ability of an optical ion beam system to resolve details at different distances depends on its current density distribution, since the image of a point source will be equal to the current density distribution of the beam at the sample. The image of all the points in a sample is thus a super addition of the current density distribution images of each point, from which the contrasts in the image can be determined (see Figure 3.2.1). This means that, to find the contrast dependency on the spatial frequencies, the Fourier transform of the current density distribution can be used. In fact, the OTF of an optical ion system equals the Fourier transform of its current density distribution [20]. This means the OTF can be calculated, if the current density distribution is known.
To determine the expected shape of the contrast C as a function of the spatial distance between features, the contrast response to differing spatial distances in the images is needed however, instead of the contrast response to different spatial frequencies. For this the OTF needs to be transformed to be dependent on the spatial distances d instead of the spatial frequencies f. This can be done using Equation 3.2.3:

$$f = \frac{1}{d}. \tag{3.2.3}$$

This transformation results in the transformed optical transfer function or OTF_d. The OTF_d is the contrast response to differing spatial distances in the image instead of spatial frequency.
The shape of the current density distribution itself is expected to be a narrow Gaussian distribution in the central parts with so-called beam “tails”, consisting of a second broader overlapping Gaussian and exponential functions at the edge of the beam (see Chapter 1.2). The lower the current, the smaller the addition of the exponential functions to the beam shape becomes and thus the closer the beam shape resembles the central Gaussian functions. Furthermore, the shape of the central-most Gaussian is most important for determining resolution [18].
Thus, for resolution purposes, the current density distribution can be approximated by using only the central Gaussian. The expected shape of the OTF of an optical beam system with a Gaussian current density distribution is equal to the Fourier transform of the Gaussian current density distribution:

$$C = e^{-\frac{1}{2}(\sigma f)^2}, \tag{3.2.4}$$

in which σ is the standard deviation of the Gaussian (see Figure 3.2.2).
Thus, assuming the current density distribution is (roughly) Gaussian in shape, the OTF (see Equation 3.2.4) can be transformed using Equation 3.2.3 into the OTF_d (see Figure 3.2.3):

$$C = e^{-\frac{1}{2}(\frac{\sigma}{d})^2}. \tag{3.2.5}$$

This would be the expected shape of the contrast as a function of the spatial distances in the image.
Since the OTF_d is the expected contrast as a function of the spatial distances in the image, the resolution of the image can be found at the spatial distance where the contrast is equal to 10% of its maximum: $OTF_{d,10\%}$ (see Section 3.2.1).

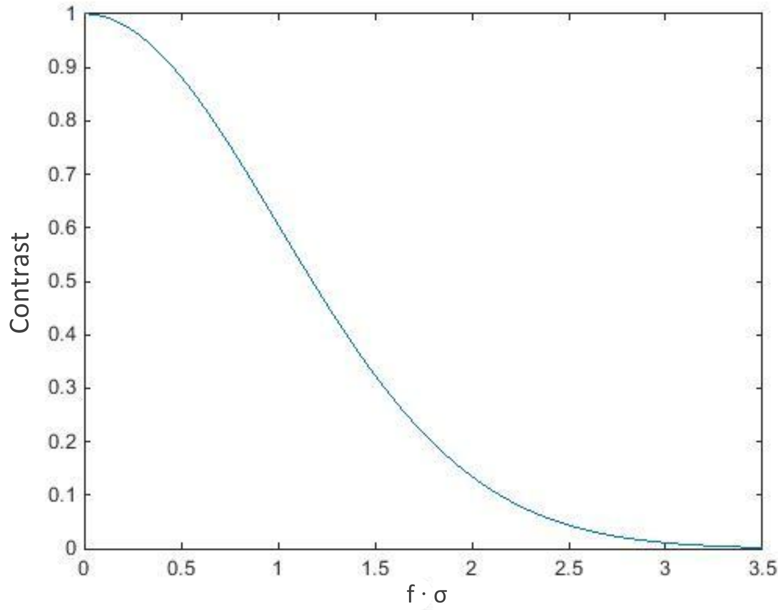

Figure 3.2.2: An illustration of the OTF of a system in which the current density distribution is a Gaussian (see Equation 3.2.4). The OTF equals the current density distribution's Fourier transform.

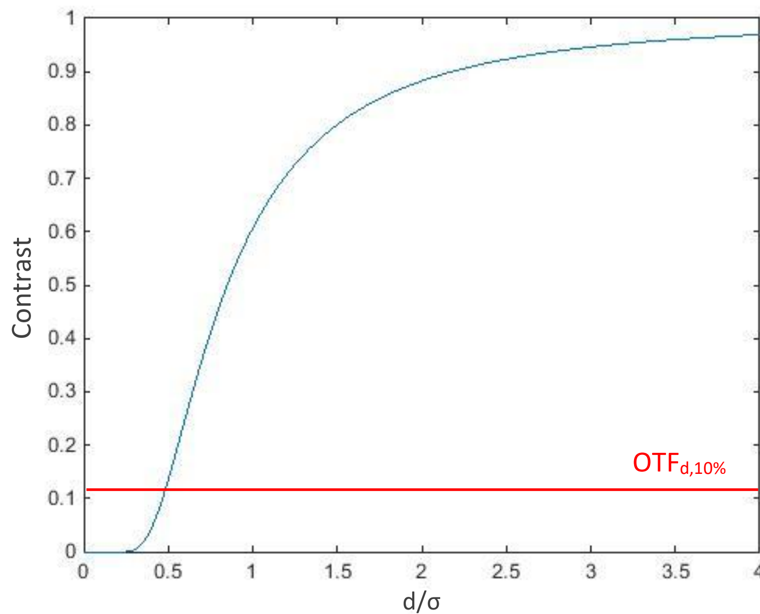

Figure 3.2.3: An illustration of the transformed optical transfer function OTF_d of a system in which the current density distribution is a Gaussian (see Equation 3.2.5). The red line marked $OTF_{d,10\%}$ marks where the contrast is at 10% of its maximum. Where the blue line of the OTF_d intersects the red line, $d = d_{10\%}$ and thus equals the resolution D (see Equation 3.2.2).

3.3 Implementation

In this section the implementation of the method to measure resolution that is tested in this chapter is described. The goal is not to determine the imaging resolution of the FIB, but to investigate the applicability and limits of this method. To that purpose the method described in this section will be tested and its results will be compared to expectations (see Section 3.4).

3.3.1 Implementation of the Technique

The method used in this chapter closely follows the method proposed by Orloff et al [1]. In this experiment secondary electron pictures are made of a broken graphite sample. When graphite breaks it leaves many sharp edges and these sharp edges can be used to determine the imaging resolution of the FIB.

The secondary electron pictures are made using the FIB setup described in Chapter 2. Once the scan is made, the locations of the edges in the image are determined either manually or automatically. After this, the distance d and the minimum intensity I_{min} between each pair of edges and the maximum intensity I_{max} at those two edges are determined. Pairs of edges are always next to each other (with no edges in between). Edge pairs are also only picked along horizontal lines of the scan (see Figure 3.3.1 & 3.3.2). This makes comparison with the automatically determined edges easier and makes it possible to easily calculate the distance and minimum and maximum intensity between the edges. From the measured intensities the contrast C for each pair of edges is determined using Equation 3.2.1, resulting in the contrast as a function of several distances: the OTF_d.

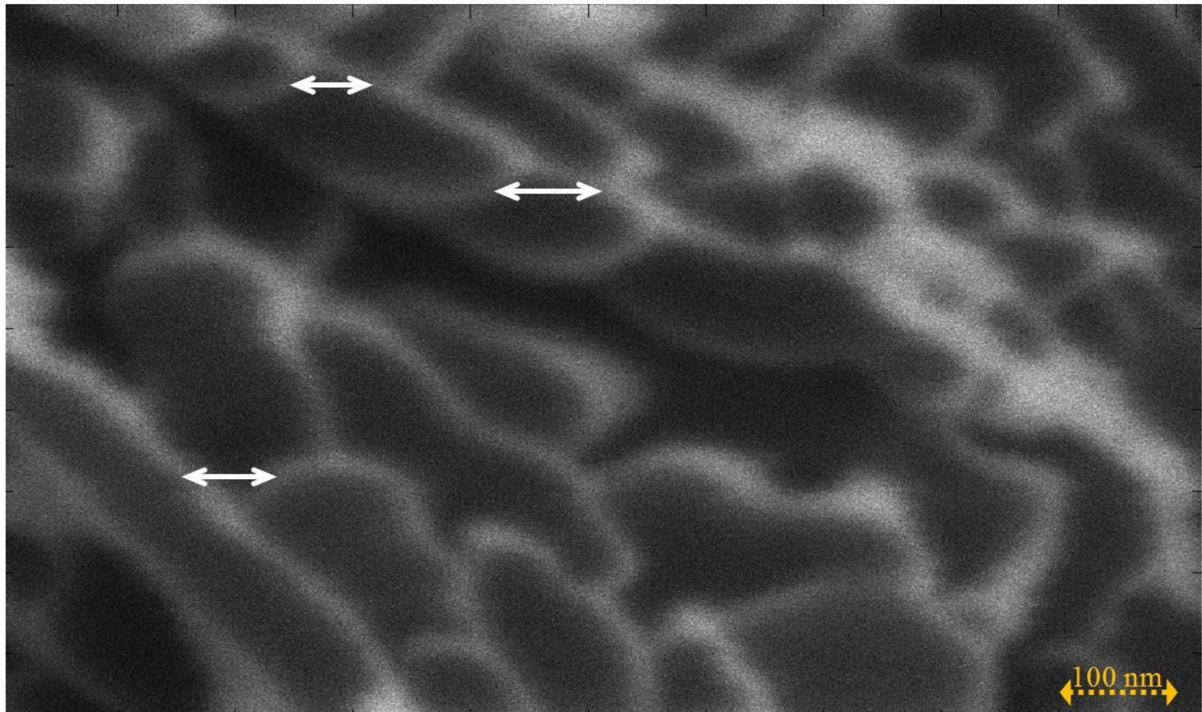

Figure 3.3.1: A secondary electron scan of graphite, showing the edges of the material. The white arrows indicate some examples of the horizontal distance between two edges. The maximum intensity at such edges and the minimum intensity between them is used to find the contrast between the edges and the resolution of the picture. The scan was made with the FIB at a magnification of 120000 with an ion current of 40 pA and a beam voltage of 30.0 kV.

To find the resolution, the OTF_d is first normalized by dividing it by a factor C_{max}, which should equal the maximum contrast that can be achieved by increasing the distance between two edges.

C_{max} may be determined by calculating the contrast of the picture as a whole, which is the highest possible contrast to be found in the picture. This is how it was done for the measurements from the manually determined edges. C_{max} is technically the highest possible contrast between two edges and not the highest contrast in the entire picture, however. The amount of data gleaned from the measurements with automatic edge determination, made it possible to define C_{max} that way for those measurements, and in those measurements C_{max} was thus determined by averaging the 100 highest measured contrasts. The averaging was done to account for error and noise.
The difference between this second determination of C_{max}, as the average of the 100 highest contrasts found, and the former determination, as the highest contrast in the image, was found to be less than 10%, which means both methods could be used.
The normalized contrast C_{norm} is then defined as:

$$\boldsymbol{C_{norm}} = \frac{\boldsymbol{C}}{\boldsymbol{C_{max}}}. \tag{3.3.1}$$

The division by C_{max} means the normalized contrast C_{norm} should approach a maximum of 1. This makes it easy to find the edge separation distance d at which the contrast dips to 10% of its maximum (at $C_{norm} = 0.1$), which corresponds to the Rayleigh definition of resolution (see Equation 3.2.2).

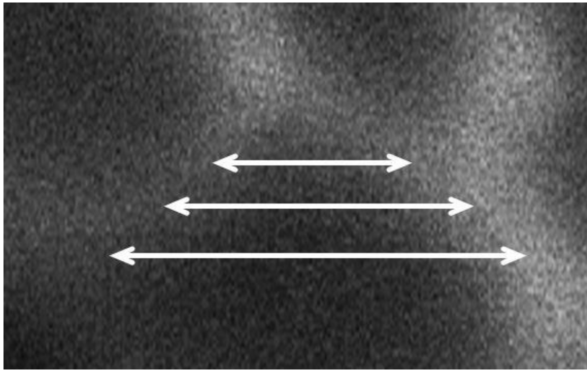

Figure 3.3.2: Part of the scan of Figure 3.3.1, showing where two edges come together, making it possible to determine how the contrast changes at different distances between the features. The arrows show possible lines along which the contrast can be measured, corresponding to lessening distances between the features.

3.3.2 Manual Determination of Edges

Much like in Figures 3.3.1 and 3.3.2, manual determination of the edges is done by picking some of the clearly perceivable edges in the picture. Preference is given to spots where two edges get together (as can be seen in Figure 3.3.2), since there it is possible to do several measurements, showing how the contrast changes as the features get closer together.
The code used to calculate the contrast from two manually picked edges can be found in Appendix A.1.1.

3.3.3 Automatic Determination of Edges

The automatic determination of the edges is done with Matlab. This script looks at the image intensity for each horizontal line of the secondary electron scan. The positions of the edges on each line are then determined, by finding local maxima in the intensity. To filter out maxima caused by noise, these maxima are compared to the intensity of the area around them as can be seen in Figure 3.3.3. Only maxima that denote a broader peak in the intensity spectrum are accepted as edges. Once the maxima are found, the contrast between a pair of maxima can easily be determined (see Figures 3.2.1 and 3.3.4).

The code used to automatically find the edges and determine the contrasts between them can be found in Appendix A.1.2.

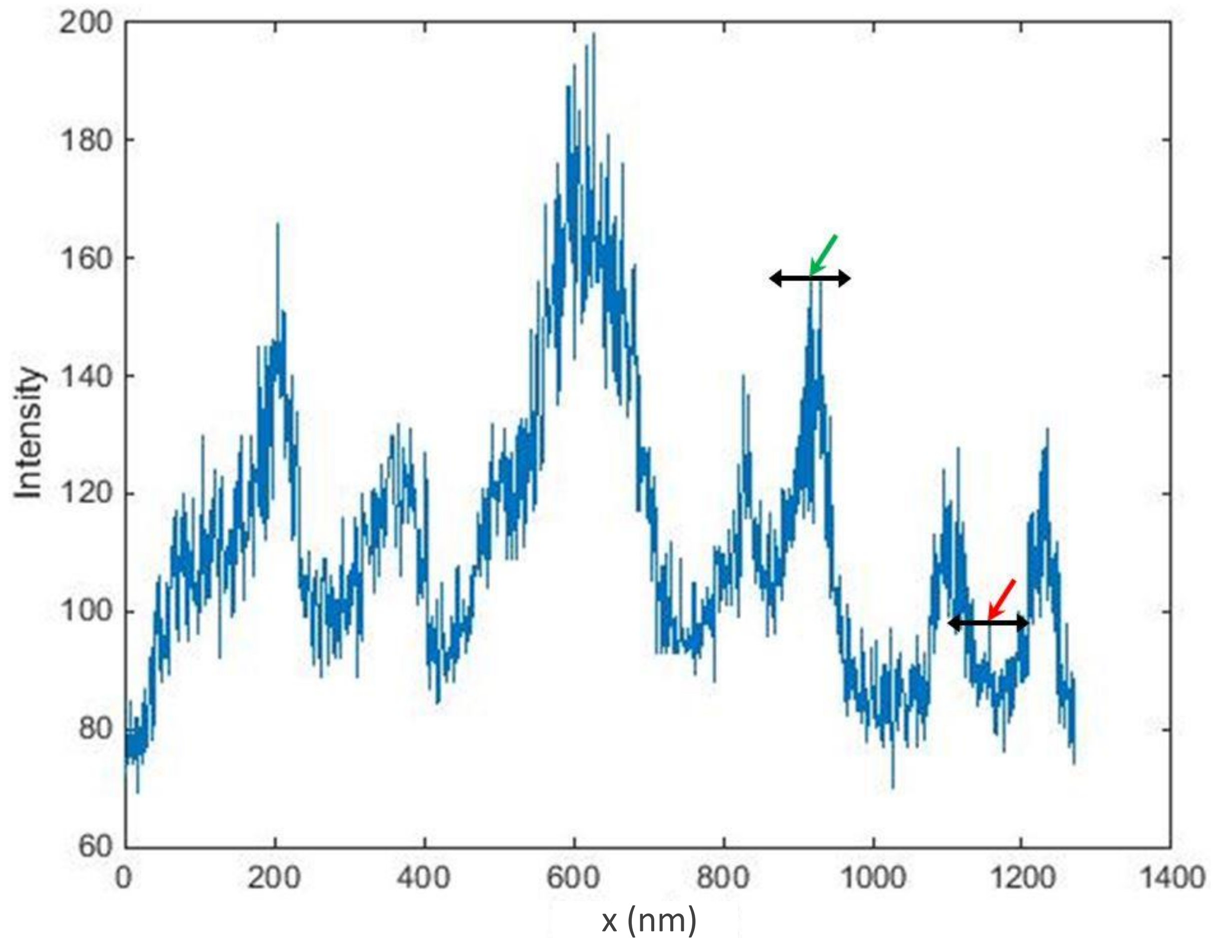

Figure 3.3.3: A horizontal line from the secondary electron scan of graphite of Figure 3.3.1, showing the intensity as a function of position x. While the noise causes thin local maxima to appear, the broader peaks in the intensity line correspond to the edges of the graphite. The green and red arrow point to two maxima. The horizontal ranges show the area used to determine whether these are local maxima that indicate edges or simply the effect of noise. As can be seen the green (left) arrow is an actual local maximum indicating an edge and the red (right) arrow is a peak caused by noise.

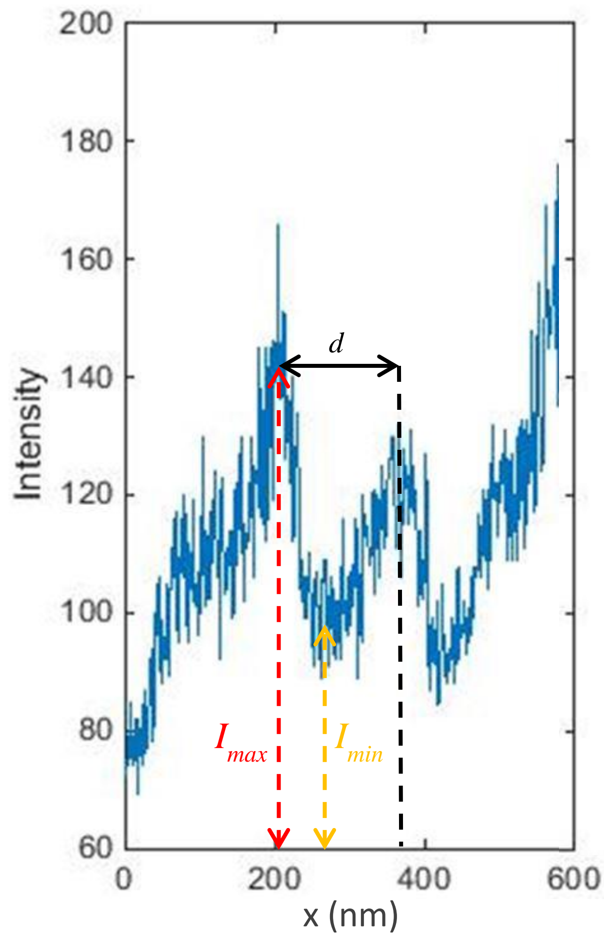

Figure 3.3.4: Part of a horizontal line from the secondary electron scan of graphite of Figure 3.3.1, showing the intensity as a function of position x. The intensity along the complete line is shown in Figure 3.3.3. The peaks correspond to edges of the graphite. The red and orange ranges show the maximum intensity I_{max} and minimum intensity I_{min} between two of these edges respectively. The horizontal range shows the distance d between these edges. From this information the contrast C between those edges, which thus corresponds to that value of d, can be determined using Equation 3.2.1.

3.3.4 Expected experimental difficulties

This method of measuring resolution is supposed to be straight forward, so long as the signal-to-noise ratio of the system is good enough to detect a given level of contrast [1]. Reducing noise can be difficult, however. When the sample is exposed to the beam, it is subjected to sputtering, implantation and other damages by the ions. While a larger exposure time reduces noise, it will also increase damage to the sample, deteriorating the image in turn.

This is mainly a problem for determining the locations of the edges automatically, since the noise interferes with accurate detection. Noise may cause maxima to appear where there are no edges. On the other hand, many methods of countering this may in turn cause real edges to be overlooked. For instance, with the method described in Section 3.3.3, which is also shown in Figure 3.3.3, the range chosen to determine whether a maximum is an edge or the effect of noise makes a large difference. When choosing a too small range noise peaks are detected as edges. Yet when choosing a too large range existing edges are overlooked. When, at that point, the contrast between two apparently neighbouring edges is determined, and there is an overlooked edge between them, I_{min} in this contrast determination will be higher, than if there had been no edge in the middle. This will result in a lower contrast C being found at this distance of edge separation d than there should be (see Equation 3.2.1).

These difficulties should not occur when manually determining the edges, however, since this will only be done with images in which the difference between edges and noise can clearly be seen, as in Figure 3.3.1.

3.4 Results

To evaluate the usability of this method, the experimental results gained by using this method will first be explained and compared to expectations. Both the results of determining the edges manually (see Section 3.3.2) and the effects of using the described method to automatically determine the edges (see Section 3.3.3) are shown. On the basis of this the effectiveness and possibilities of this method will be described.

3.4.1 Manual Determination of the Edges

These are the results of the resolution measurements that were gained by manually determining the positions of the edges in a scan of a broken graphite sample (see Figures 3.4.1, 3.4.2 and 3.4.3). The scans were made at three different magnifications M to get an indication of the difference in resolution between those. The goal of these measurements was, firstly, to get comfortable with the techniques involved and find out its limits and practicality and, secondly, to compare these results later to the same technique used with automatic edge determination. The secondary electron scans from which these results were obtained were all made using the FIB setup described in Chapter 2, with an ion current of 40 pA and a beam voltage of 30.0 kV. The highest magnification at which the resolution was determined was 120000. At higher magnifications the noise became too great to easily process the images, therefore no results from higher magnifications are shown.

Figure 3.4.1 shows the normalized OTF_d at a magnification of 120000. The figure shows that the spread of the contrast increases at higher distances. In this case it does not make it impossible to determine the resolution, since the accuracy at 10% is high.

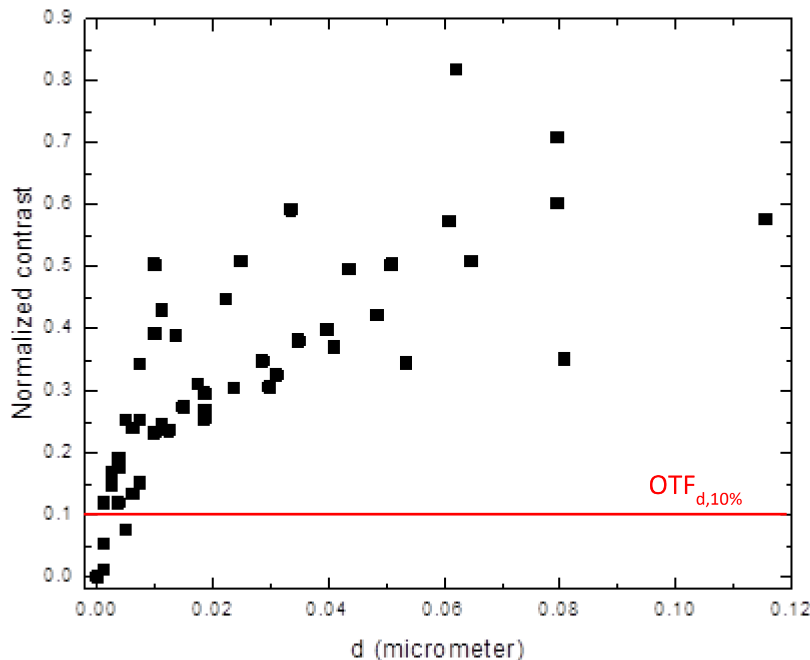

Figure 3.4.1: The normalized contrast between two sharp edges, as a function of the distance between those edges, at M = 120000. The edges have been picked manually. The electron scan from which these results were determined can be seen in Figure 3.3.1. It was taken at a beam current of 40 pA and a beam voltage of 30.0 kV. The red line marked $OTF_{d,10\%}$ shows where the contrast is at 10% of its maximum.

The shape of the normalized OTF_d in Figure 3.4.1 can be compared to the expected OTF_d for a Gaussian beam current density distribution as seen in Figure 3.2.3. Firstly, the contrast increases with distance, as expected. Secondly, the shape matching the Gaussian current density

distribution can clearly be detected in the low distance region, but then flattens out. This is probably caused by the current density distribution not being perfectly Gaussian in shape. The exact shape of the current density distribution in a LMIS FIB has been observed to closely approximate a narrow Gaussian in the centre of the distribution, but added with an overlapping broader Gaussian and tails on the side (see Section 1.2). This second broader Gaussian may account for the perceived flattening of the current density distribution, since this is the effect caused by the addition of a second flatter, broader OTF_d (see Figure 3.2.3 for the shape of the OTF_d). This is as such not an unexpected result.
The resolution found at 10% of the maximum contrast (where the normalized contrast equals 0.1) lies between 2-7 nm. When comparing this to Figure 3.3.3, which shows the image intensity along a horizontal line from the picture from which these results were calculated, this seems rather small. In retrospect, contrast between two edges was calculated by determining I_{max} and I_{min} between those points without properly taking noise into account, which means that the maximum intensity found would be skewed upward and minimum intensity found would be skewed downward by noise, making the contrast between most edges appear greater than it should be. This may in turn have made the resolution appear smaller.
On the other hand, the resolution of this particular FIB should be below 7 nm at a current of 1 pA and a magnification above 30000. While a higher current (40 pA instead of 1 pA) should result in a lower resolution, the higher magnification (120000 instead of 30000) would in turn result in increased resolution. Overall the expectation of the resolution in this measurement being below 7 nm cannot be made, but it shows at least that a resolution in the order of 2-7 nm is not unexpected and that, even with the noise, it seems to be in the same order of magnitude as what would be expected.
The resolution was also determined with this method at a magnification of 65000 and a magnification of 25000. Figure 3.4.2 shows the normalized OTF_d at a magnification of 65000. Here, unlike the measurement at a M = 120000 (see Figure 3.4.1) the spread is not greatest at the highest distances, but at the 20 to 40 nm range. This does not yet cause a problem at the 10% cut off, since the shape of the OTF_d is still visible and the accuracy at the cut off is still high enough.

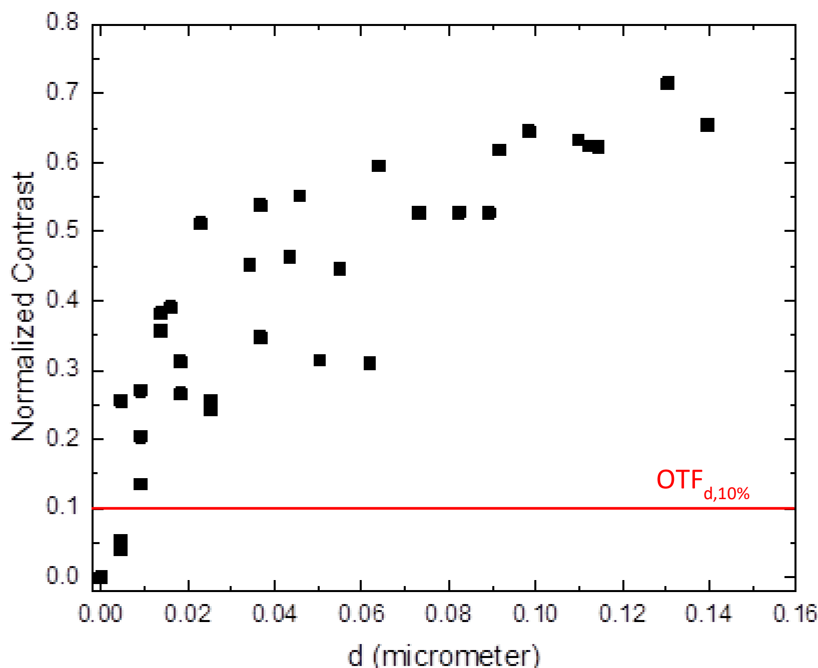

Figure 3.4.2: The normalized contrast between two sharp edges, as a function of the distance between those edges, at M = 65000. The edges have been picked manually. The electron scan from which these results were determined was taken at a beam current of 40 pA and a beam voltage of 30.0 kV. The red line marked $OTF_{d,10\%}$ *shows where the contrast is at 10% of its maximum.*

When the shape of the normalized OTF_d in Figure 3.4.2 is compared to the expected OTF_d for a Gaussian beam current density distribution (see Figure 3.2.3), once again the similarities can be seen. The contrast rises with distance between edges and in the lower ranges the shape matching the Gaussian current density can clearly be seen, though at higher distances, like in Figure 3.4.1, it flattens out. This emphasizes the probable difference between the actual beam current density distribution at the focal point and a Gaussian current density distribution once more as well as the fact that the second broader Gaussian contributing to the current density distribution should be taken into account.
The resolution here at 10% of the maximum contrast lies between 4-10 nm. This is once again in the order of the resolution being below 7 nm, if the higher current (40 pA instead of 1 pA) is somewhat offset by the higher magnification (65000 instead of 30000). Also, the resolution seems to worsen at lower magnification, as is expected.
Lastly, the resolution was determined at M = 25000. Figure 3.4.3 shows the normalized OTF_d at this magnification.

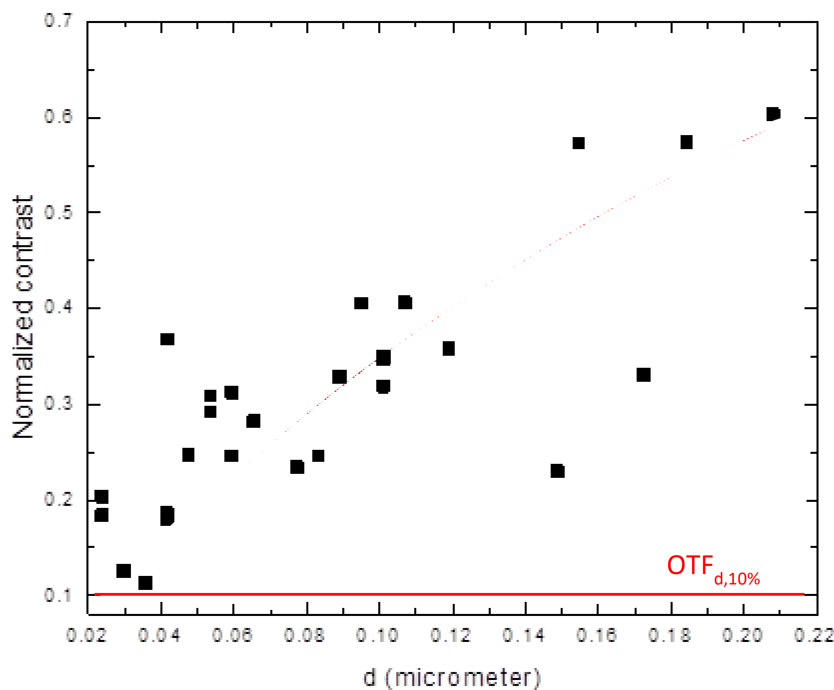

Figure 3.4.3: The normalized contrast between two sharp edges, as a function of the distance between those edges, at M = 25000. The edges have been picked manually. The electron scan from which these results were determined was taken at a beam current of 40 pA and a beam voltage of 30.0 kV. The red line marked $OTF_{d,10\%}$ *shows where the contrast is at 10% of its maximum.*

In Figure 3.4.3 it can be seen that the expected shape of the OTF_d is not necessarily visible in the results. While the contrast still rises with increasing distance between the edges, the characteristic shape of the OTF_d of a Gaussian current density distribution in the lower distance regions is no longer visible. It is possible that this is caused by the lower magnification, which makes it harder to determine the exact resolution, since the edges are less easy to spot (see Figure 3.4.4).

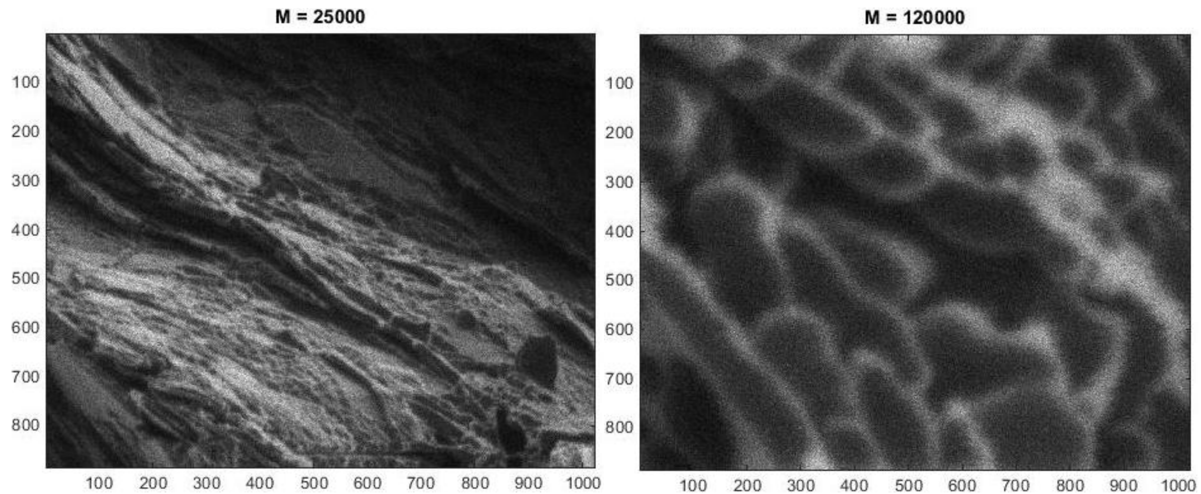

Figure 3.4.4: Secondary electron scans of graphite made with the FIB at two different magnifications. At M = 120000 the image shows clear edges which can be easily spotted. At M = 25000 the individual edges are harder to see. This might cause the lower accuracy of the OTF_d calculated from these results (see Figure 3.4.3).

At this magnification it was difficult to find any edges close enough to each other to match 10% of the maximum contrast. Extrapolating from the graph, the contrast appears to lie between 15-35 nm. The resolution was expected to be higher here, than in the measurements at *M* = 120000 and *M* = 65000, since the magnification is lower here than the *M* = 30000 from the expectations and the current is still 40 pA instead of 1 pA.

Overall, it can be seen that the resolution rises with lower magnifications, as is expected and the lowest measured resolutions (at magnifications greater than 30000) match the expectation of being below 7 nm. The shape of the OTF_d matched that of a Gaussian current density distribution in the lower contrast ranges, at least while the magnification is high enough, and the difference in the higher contrast ranges is not unexpected and can be explained. This seems to indicate that the contrast profile found with this method is a decent reflection of reality and can thus be used to determine resolution.

3.4.2 Automatic Determination of the Edges

<u>Limitations</u>

The biggest problem in the automatic determination of the edges in a scan is caused by the noise. Noise makes it very difficult to accurately determine the minima and maxima in a scan, as illustrated in Figure 3.4.5.

As stated (see Section 3.3.3), noise is currently accounted for by comparing a local maximum to the intensities around it (see Figure 3.3.3). Thus, an easy solution to this problem might seem to be to compare a local maximum to a larger range of neighbours. Alternatively, it may be possible to smooth the picture, using a noise filter of some sort. The option to compare to more neighbours has been tried, but it proved difficult to find a standard comparison distance that filtered out most of the noise without missing out on many edges in the image. Smoothing the picture likewise deteriorated the information in a scan by smoothing away many of the edges, when trying to remove enough of the noise.

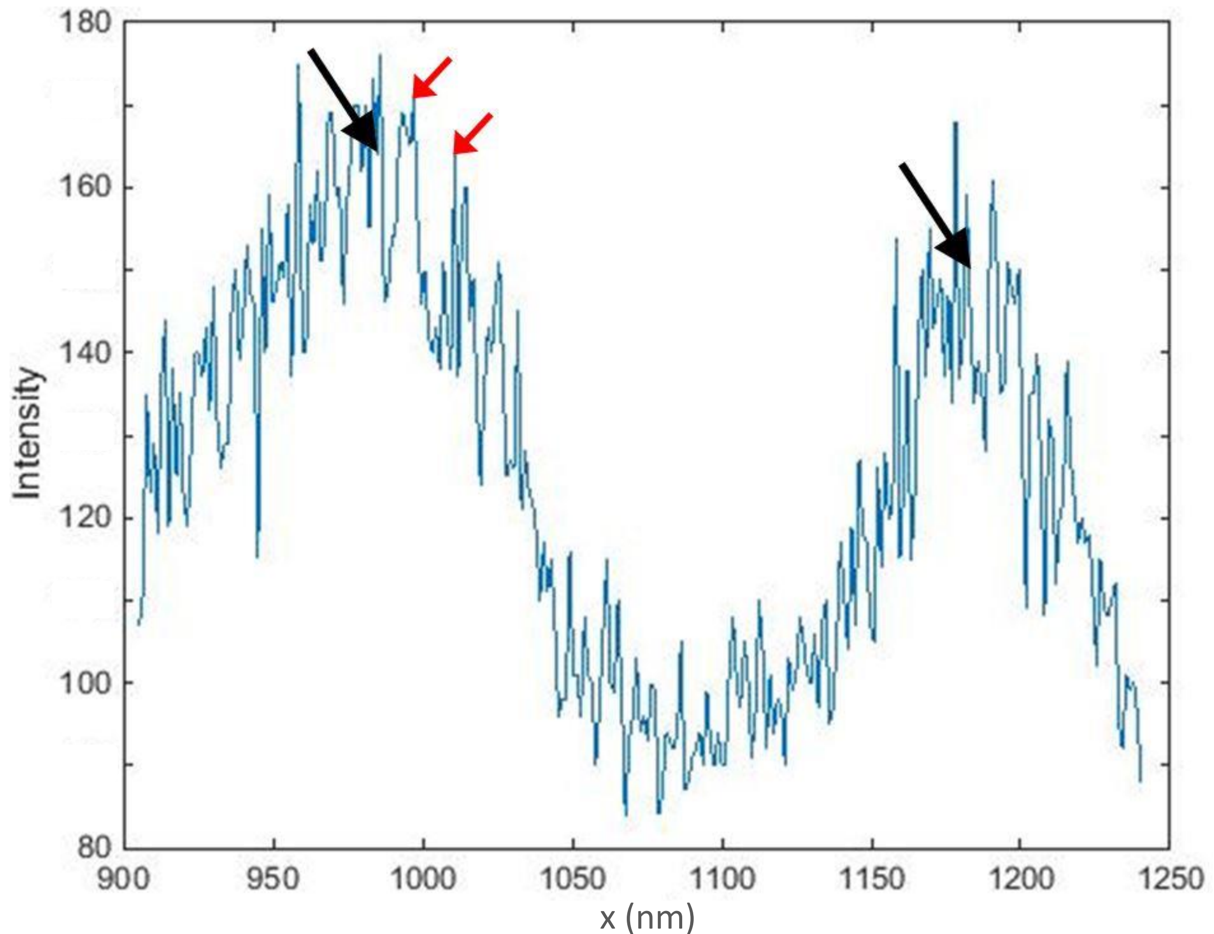

Figure 3.4.5: The intensity of a part of one line from the scans of broken graphite. The large peaks show two edges, marked by the large black arrows, which can be used to determine the contrast. The small red arrows show two of the maxima that are caused by noise, that may easily be falsely identified as edges. The line comes from the scan shown in Figure 3.3.1.

The effect of noise

To gain more insight into the effect of the noise on this method, it has been modelled by adding artificial amounts of noise to an image sample before again determining the contrast as a function of the distance between pairs of edges. The noise was simulated by adding a random positive or negative amount of noise to the intensity at each point. The maximum noise thus added was set equal to a chosen percentage of the maximum of the image and care was taken that the new intensity values were never below zero or above the maximum image intensity.
The code used to add artificial noise to the images can be found in Appendix A.1.3. The effect of this on the apparent OTF_d, when using automatically picked edges, is illustrated in Figures 3.4.6 and 3.4.7.

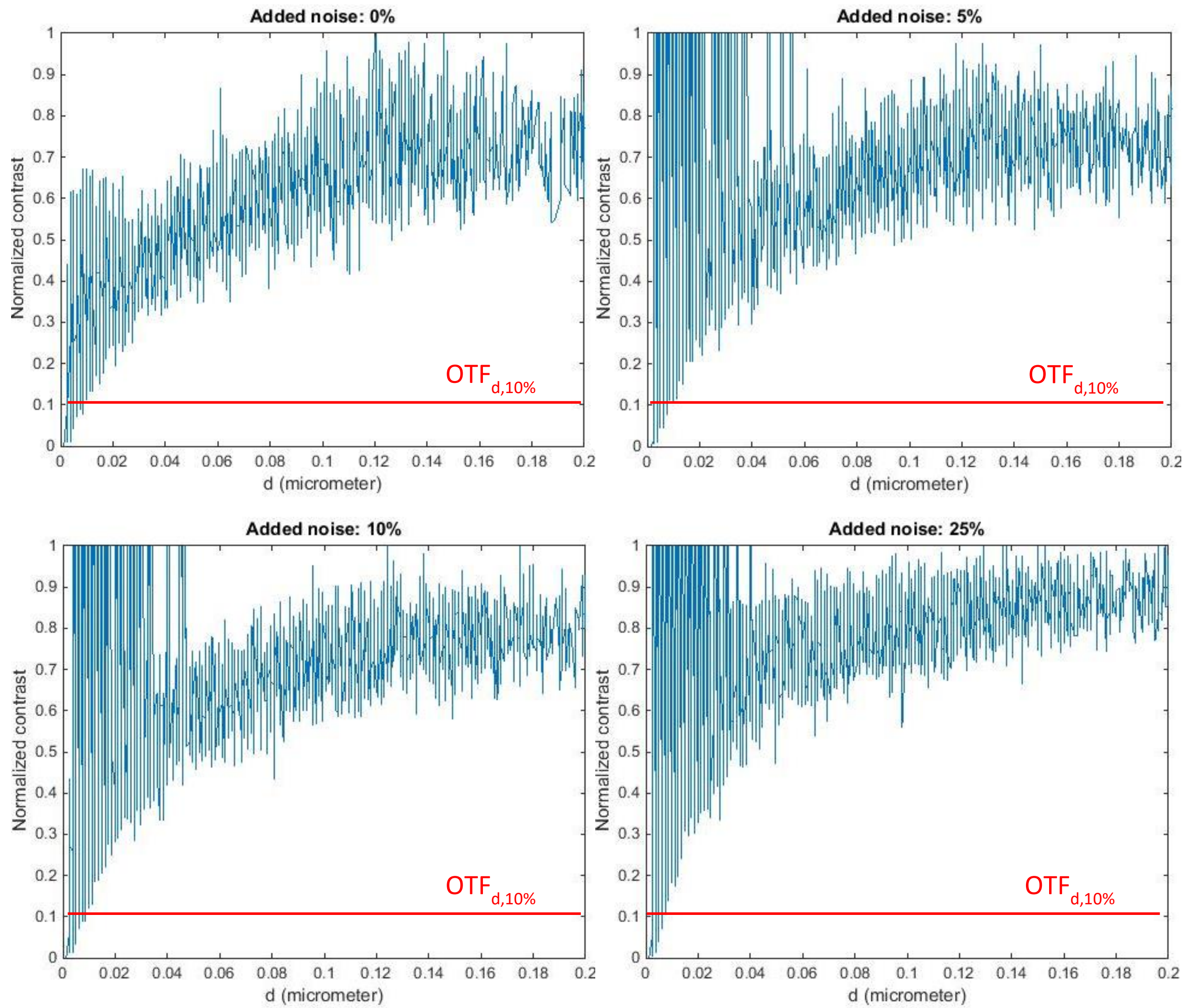

Figure 3.4.6: The effect of added noise on the calculated normalized contrast as a function of the distance between pairs of edges. The places of the edges were determined automatically. The added noise is random and the maximum added noise is given as a percentage of the maximum line intensity. The data points at maximum contrast at the lower distances that can be seen in all but the top left image are caused by the function that adds noise and can thus be ignored, in favour of the general trend of the normalized contrast. The result without added noise comes from the scan shown in Figure 3.3.1. The red lines marked $OTF_{d,10\%}$ *show where the contrast is at 10% of its maximum.*

Figure 3.4.6 shows the effect of errors induced by noise on the normalized contrasts found, showing that at low distances (where the 10% cut off to determine the resolution can be found) the OTF_d will appear steeper. What cannot be seen in Figure 3.4.6 is that the maximum contrast C_{max} also changes, since the contrast is divided by C_{max} to normalize the OTF_d. Figure 3.4.7 shows the effect on the contrast before normalization. Here it can be seen that not only does the noise cause the OTF_d to seem steeper, it also enlarges the perceived maximum contrast, from 0.38 to 0.5 in Figure 3.4.7 respectively.
The spread in contrasts found itself does not appear to change much from one image to another, however. The data points at the top that can be seen at lower *d* in all images where noise was added (all but the top left image in Figure 3.4.6 and the left image in Figure 3.4.7) are artefacts of the function that adds noise and can be ignored.

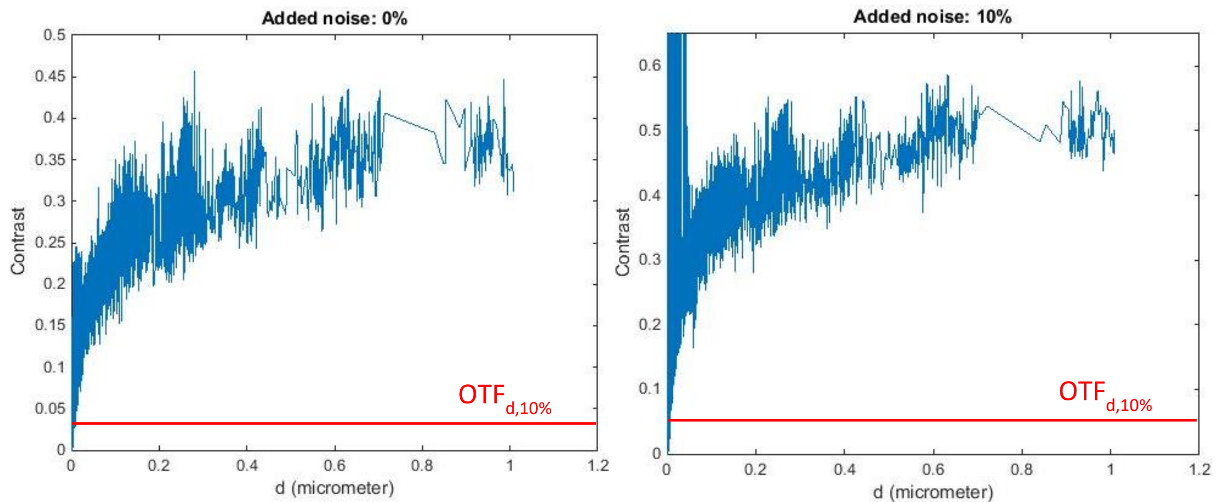

Figure 3.4.7: The effect of added noise on the calculated contrast (before normalization) as a function of the distance between pairs of edges. The places of the edges were determined automatically. The added noise is random and the maximum added noise is given as a percentage of the maximum line intensity. The data points at maximum contrast around 0 distance that can be seen in the right image are caused by the function that adds noise and can thus be ignored, in favour of the general trend of the normalized contrast. The result without added noise comes from the scan shown in Figure 3.3.1. Since in these graphs the contrast was not normalized, the red line marked $OTF_{d,10\%}$ *showing 10% of the maximum contrast will not be found at 0.1.*

Noise is thus a significant problem for automatically determining the edges, as can also be seen in the comparison with the results gained by manually picking the edges (see Figure 3.4.8). This was expected, since noise may cause invalid edges to be found, as explained in Section 3.3.4. The shift in contrasts found is probably caused by noise peaks being seen as edges, which can lead to larger found intensity differences and thus larger found contrasts (see Equation 3.2.1). This effect can especially be seen at smaller d, where the contrast between real edges is small.

Comparison

The validity of the results when the edges are determined automatically, can easily be seen in Figure 3.4.8. It shows that when using the automatic edge finding method, the proper edges will be found, but due to the noise many extra data points are found as well, that result in a large spread of the data. The effect of the noise (shown in Figure 3.4.6) can also be seen here, causing the overall trend of the normalized contrast to shift slightly upward. Altogether these effects make it impossible to find the proper 10% resolution from these results.

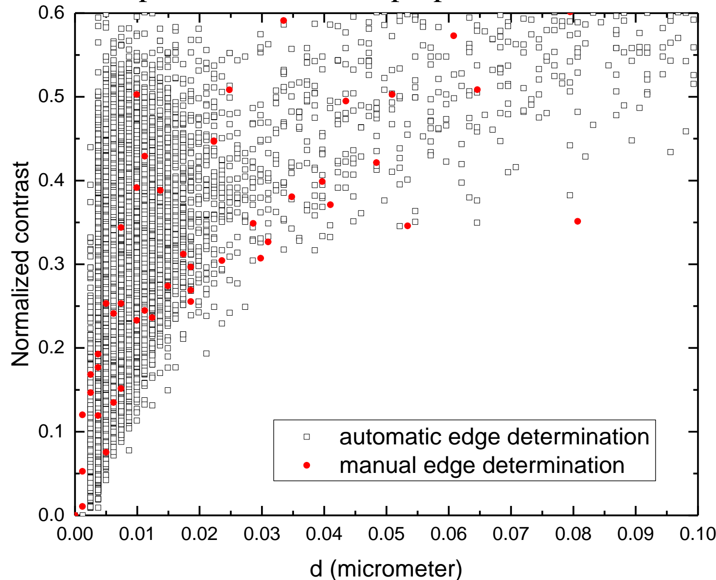

Figure 3.4.8: The normalized contrast between two sharp edges, as a function of the distance between those edges, at M = 120000 with an ion current of 40 pA and a beam voltage of 30.0 kV. Both the results in which the edges were determined manually and the results from automatic edge determination are shown. Both results come from the same electron scan, shown in Figure 3.3.1. The values from the manual edge determination in this graph can also be found in Figure 3.4.1.

To properly determine the edges automatically a better edge finding method or a proper way to filter the noise is therefore necessary.

3.4.3 Difficulties of this method

The manual determination of edges was easy, yet somewhat time intensive to perform. The resolution could be determined from these results, though not very precisely. While at the higher magnifications ($M = 120000$ and $M = 65000$) a reasonable estimate of resolution could be made, the spread in data points found by the method at lower magnification ($M = 25000$) rose greatly. The automatic determination of edges was highly noise sensitive and lead to a high spread in the data points, which makes it impossible to determine the resolution from these measurements. A better automatic edge detection method would be necessary.

Contrast determination itself once pairs of edges were found showed little difficulty, though it may be better to also take noise into account when determining the maximum and minimum intensities needed. Once the positions of these maxima and minima are known this should not be difficult, however, and can simply be done by averaging the intensities over a very small surrounding area.

3.5 Conclusion

First of all, the method described in this chapter makes it possible to determine an optical transfer function for a FIB, using nothing but a secondary electron image made with that FIB. Particularly the shapes of the OTF_d generated by the measurements at M = 120000 and M = 65000 closely resembled the expected shape of an OTF_d. Being able to determine the optical transfer function without needing to know the current density distribution is useful, since, as the several resulting OTF_d show (by comparing Figures 3.4.1, 3.4.2 and 3.4.3 to Figure 3.2.3), the shape of the current density distribution does not exactly correspond to a simple Gaussian and can in fact not easily be determined (see Section 1.3.3).

The actual results for the resolution at these magnitudes, between 2-7 nm at M = 120000 and 4-10 nm at M = 65000, are in the same order of magnitude as the expected resolution. They do in fact coincide with the indication of resolution that it should be below 7 nm (see Section 2.2.3). This indication was given at 1 pA (instead of the here used 40 pA), however, which means the resolution should not be as high in these measurements, since resolution worsens with increasing current. On the other hand the used magnifications were higher than M = 30000, which was the magnification for which the resolution should be below 7 nm, which should lead to a better resolution, since, as long as the noise does not overpower the signal, the resolution gets better at higher magnifications. All in all, while these results may be skewed by noise so that the resolutions lie slightly lower, and the expectation of the resolution being below 7 nm corresponds to a lower current (1 pA instead of 40 pA) and a lower magnification (30000 instead of 65000 or 1200000), the resolution was still expected to be about the same order of magnitude as 7 nm, since the higher current (which decreases resolution) and the higher magnification (which increases resolution) should somewhat compensate for one another. Since the found resolutions at these magnifications are indeed within the same order of magnitude, this indicates that, at the very least, this method can thus be used to gain a decent estimate of resolution.

A method for accurate automatic determination of the edges has not yet been shown. In fact, the noise makes it very difficult to do so easily. While by eye the edges are visible, noise creates many extra maxima in the picture that can easily be falsely recognized as an edge. Using simple methods to filter out the noise tends to smooth away several of the edges, also leading to a false result. While many 'false' edges are found, the proper ones are found as well, however (see Figure 3.4.8), which might mean that with more sophisticated software it is possible to do automatic edge determination in future.

It might be easier to do this with software that does not find line maxima, but rather recognizes shapes and draws lines in the two-dimensional picture corresponding to the higher intensity spots. This sort of software is already available and thus it should be possible to create a reliable method for accurate automatic edge determination. Creating software that can determine the OTF_d directly from a picture taken inside the FIB would be very useful to the focused ion beam field, since it allows for easy direct determination of the resolution of the FIB at several magnifications, even if the current density distribution is not exactly known. This makes it very worthwhile to try and create a method for determining the edges automatically.

While this may be possible, however, and may in fact have been done by others by now, this report does not go so far as to find or create the needed software, since it requires a software heavy focus that has so far not been a part of this work. The manual method of edge determination is useable enough to determine resolution and, for the purposes of future research, the kind of software needed for automatic edge determination has become clear. Furthermore, beam quality is indicated by more than just resolution (see Section 1.2), thus the

rest of this report focuses on a different measurement method which is used to determine spot size and brightness and is expected to have high applicability in the field.

4 The Knife Edge Method

4.1 Introduction

The other method explored to determine performance of a FIB is focussed on measuring the beam quality, in terms of its spot size, emittance and brightness. It is called the Knife Edge method and it makes use of the knife edge measurement, a technique regularly used in the field. The knife edge measurement is a quick and relatively easy method to determine the spot size of an ion beam. While, as discussed (see Section 1.3.2), it does have its problems, it is a direct method without a convoluted secondary analysis process. It is also the most commonly used method to determine beam performance. As such it is expected to prove valuable, if not to determine exact numbers, then at least to make an accurate estimate of the beam quality.

In this chapter the Knife Edge method will be described and tested. It starts with the underlying principles and the explanation of the exact implementation of this method. After this the results the method produces in terms of spot size, emittance and brightness dependent on several varying settings of the FIB will be determined, so that the results can be compared to the expected trends and a reflection can be made on the accuracy and usability of this method. The chapter concludes with this reflection.

4.2 Underlying Principles

4.2.1 Brightness

When analysing beam quality, the brightness of the beam is one of its most important properties. High brightness is the result of several other optimized beam properties, such as high energy, high current and low energy spread [6] (see Equation 4.2.1 [20]):

$$B = \frac{\partial^2 I}{\partial \Omega \partial A}. \tag{4.2.1}$$

The brightness can also be expressed as a function of the emittance (see Equation 4.2.2) [26]:

$$B = \frac{I}{\pi^2 \varepsilon_x \varepsilon_y}, \tag{4.2.2}$$

in which B is the beam brightness I is the beam current and ε_x and ε_y are the beam emittances in the two directions perpendicular to the beam axis.

The emittance ε of the beam is here defined as the area in phase-space the particles of the beam take up, divided by π [27]. Assuming that the motion of the particles between cardinal directions is only weakly coupled and that the momentum of the particles in the direction of beam propagation (hereafter called the z-direction) is far greater than in the other cardinal directions (the x- and y-directions respectively), phase-space can directly be defined as the position of a particle (x or y for its position on the x or y axis respectively) and its angle with respect to the z axis (x' or y' respectively) at a certain position z along the beam propagation in the FIB.

Weakly coupled motion of the particles between directions, also means that their movement can be described by the Twiss parameters. The optical parameter $\beta(z)$ is the Twiss parameter that describes how the beam optics influence the particles of the beam at each position along the beam axis. The other two Twiss parameters, $\alpha(z)$ and $\gamma(z)$ are defined as functions of β:

$$\alpha(z) \equiv -\frac{1}{2}\frac{d\beta(z)}{dz}, \tag{4.2.3}$$

$$\gamma(z) \equiv \frac{1 + \alpha(z)^2}{\beta(z)}. \tag{4.2.4}$$

Assuming that no heating in the beam takes place, emittance is a conserved quantity [13]. In that case it is possible to describe the emittance of the beam by using the Twiss parameters,

instead of just the movement of a single particle. This is done by setting the possible distance of the described particle to the beam axis at each point (its amplitude of movement as defined by $\beta(z)$) equal to the radius of particle positions in the entire beam (defined either as the standard deviation or some other radius that denotes the size of the main part of the beam), thus using $\beta(z)$ to describe the movement of the entire beam. The area in phase space taken up by the beam at a certain point in the FIB is then described by the Twiss parameters as in Figure 4.2.1 and the emittance of the beam at that point can be defined as the area in phase space shown [27].

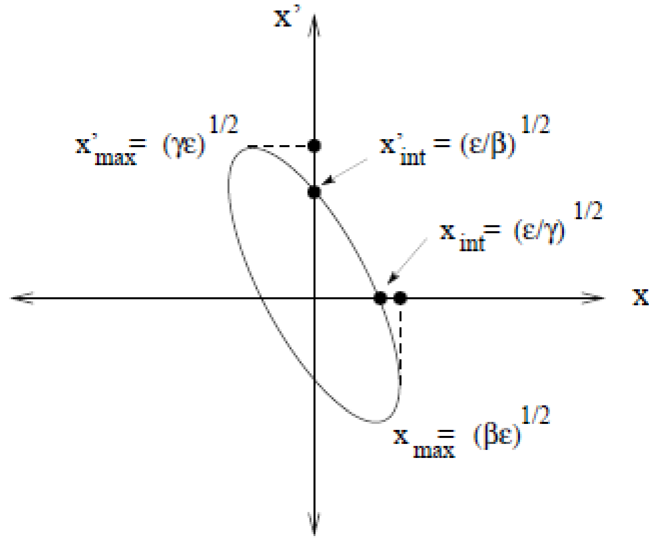

Figure 4.2.1: A representation of the area in phase space a particle in a particle beam can take up at a specific position along the FIB column. α, β and γ are the Twiss parameters, here shown in relation to the maximum distance x_{max}, maximum divergence x'_{max} and the intersection of the phase space area edge with the zero divergence axis x_{int} and with the zero distance axis x'_{int}. If the radius of this area of possible position of this particle is taken equal to the size of the beam (defined as either the standard deviation or some other radius that denotes the size of the main part of the beam), this area in phase space can be taken as the equivalent of the emittance of the beam. This then means that x_{max} is equal to the beam radius and x'_{max} is equal to the beam half divergence.

Emittance is then equal to:

$$\varepsilon = \frac{x_{max}^2}{\beta}, \tag{4.2.5}$$

in which x_{max} is now the radius of the beam or beam half size at that point in the FIB column (see Figure 4.2.1). Thus, when beam size and β are known at a certain point, the emittance there (and thus the emittance in the entire beam, since the emittance is conserved) can be determined. And it is possible to determine x_{max} and β at the focal point of the beam, as $x_{max,0}$ and β_0 respectively.

While the beam half size $x_{max,0}$ can directly be measured in the focal point of the beam, β_0 can be found from α_0 and γ_0 (see Equation 4.2.4). As can be seen in Figure 4.2.1, the focal point (also called the waist of the beam) occurs when x_{max} is of minimal size and thus equal to x_{int} which means that:

$$x_{max,0} = x_{int,0} \rightarrow \sqrt{\beta_0 \varepsilon_0} = \sqrt{\frac{\varepsilon_0}{\gamma_0}} \rightarrow \gamma_0 = \frac{1}{\beta_0}. \tag{4.2.6}$$

Together with Equation 4.2.4 this results in:

$$\alpha_0 = 0\,. \tag{4.2.7}$$

In these equations $x_{max,0}$ and $x_{int,0}$ are x_{max} and x_{int} at the waist respectively and β_0, α_0 and γ_0 are the Twiss parameters at the waist. A beam particle drifting over a distance L to or from the waist of the beam is thus affected as:

$$\begin{pmatrix}\beta_L\\\alpha_L\\\gamma_L\end{pmatrix}=\begin{pmatrix}1 & -2L & L^2\\0 & 1 & -L\\0 & 0 & 1\end{pmatrix}\begin{pmatrix}\beta_0\\0\\\gamma_0\end{pmatrix}=\begin{pmatrix}\beta_0+L^2\gamma_0\\-L\gamma_0\\\gamma_0\end{pmatrix}, \tag{4.2.8}$$

where β_L, α_L and γ_L are the Twiss parameters at a distance L from the waist.

From Equations 4.2.5, 4.2.6 and 4.2.8 the emittance can then be determined as a function of beam half width at the waist and beam half width at a distance L from the waist:

$$\varepsilon=\frac{x_{max,0}}{L}\sqrt{x_{max,L}^2-x_{max,0}^2}, \tag{4.2.9}$$

in which $x_{max,0}$ is the beam half width at the waist and $x_{max,L}$ is the beam half width at a distance L from the waist.

This means that by measuring the beam width at both the waist and another position close to the waist the emittance can be calculated. This makes it possible, when the beam current is known, to calculate the Brightness (see Equation 4.2.2). The beam current is determined within the setup as explained in Section 2.2.1.

To allow for easy comparison between beams of different energy the beam energy U is divided out, leaving the reduced brightness B_r:

$$B_r=\frac{B}{U}=\frac{I}{\pi^2 U\varepsilon_x\varepsilon_y}. \tag{4.2.10}$$

4.2.2 *Expected beam parameters*

To determine the usability of the Knife Edge method, its results have to be compared to the expected beam parameters. As seen in Section 2.2.3, the expected spot size lies between 5-10 nm and the reduced brightness is expected to be about 10^6 $Am^{-2}sr^{-1}eV^{-1}$. The beam voltage of 30.0 kV corresponds to a beam energy U of 30.0 keV.

The shape of the current density distribution is expected to be a narrow Gaussian distribution in the central parts with so-called beam tails, which consist of a second broader overlapping Gaussian and exponential functions at the edge of the beam (see Chapter 1.2). These edges are normally of an intensity a few orders lower than the central part of the beam and can thus be ignored for many applications in less sensitive materials. For most measurements the current density distribution can thus be assumed to be a Gaussian. Yet, the higher the current, the larger the addition of these tails to the beam shape becomes, which may cause problems for measurements in the higher current ranges.

The spot size versus current curve will also be measured. Depending on whether the beam quality is mostly limited by spherical aberrations, chromatic aberrations or the brightness, this curve should follow one of the following equations [13]:

$$d_{50,S}\propto I^{\frac{3}{8}}, \tag{4.2.11}$$

$$d_{50,C}\propto I^{\frac{1}{4}}, \tag{4.2.12}$$

$$d_{50,B}\propto\left(\frac{I}{B_{r,25}}\right)^{\frac{1}{2}}, \tag{4.2.13}$$

in which $d_{50,S}$, $d_{50,C}$ and $d_{50,B}$ are the spherical aberration limited, chromatic aberration limited and brightness limited spot sizes of the central 50% of the beam, respectively, I is the beam current and $B_{r,25}$ is the reduced brightness of the central 25% of the beam.

Whether chromatic or spherical aberrations predominate, is largely dependent on the current. The higher the current, the more important spherical aberrations become, as can be seen by the relative current dependencies of the spot sizes. This should be reflected in the measured spot size versus current curve [13].
The spot size of the beam is also in part determined by the initial focussing of the condenser lens (see Section 2.2.1). Stronger focussing should result in a smaller spot size and thus (see Equations 4.2.9 and 4.2.10) a higher brightness. Stronger focussing would also increase the effect of lens aberrations, however, which would in turn negatively affect spot size and brightness.

4.3 Implementation

The FIB used in the experiments is described in Chapter 2. The goal is not to determine the spot size and brightness of this FIB, but to investigate the applicability and limits of this method. To that purpose the method will be tested experimentally and compared to the results of a model.

4.3.1 The model

The working of the used FIB was modelled using General Particle Tracer [28], a simulator that keeps track of the movement of individual particles, as they react to electric and/or magnetic fields and space charge effects and the like. The particle source is modelled as a small flat circle, representing the liquid metal tip from which the ions originate. The ions are represented by a 100 particles, modelled as spheres with a positive charge and a radius of 10^{-15} m. They leave the tip at a rate corresponding to the set current, within the set opening angle (see Figure 4.3.1).

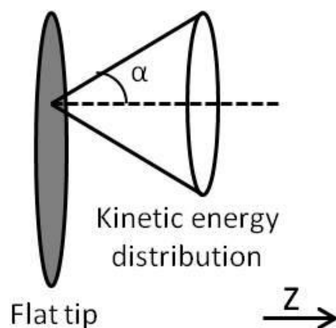

Figure 4.3.1: The initial particle distribution within the model. The particles originate on a flat circle, initially distributed in an approximately 2D Gaussian profile with a standard deviation corresponding to the rms virtual source size of the FIB: 20 nm. The kinetic energy distribution is confined within opening angle α. The kinetic energy spread in the z-direction is also an approximately Gaussian profile, this time with a standard deviation corresponding to the rms energy spread of 3 eV. Particles are originated within the distribution at a rate corresponding to the chosen current. α is determined according to the known angular current density of $20 \cdot 10^{-6}$ A/sr.

The initial spatial spread of the particles is approximated by a 2D Gaussian profile. The initial kinetic energy spread along the axis is also approximated by a Gaussian profile.

While the exact industrial build of the used FIB is proprietary information and could not be known, a closest approximation of internal fields was provided by the manufacturer of the FIB and used for this model.

The model uses a simple configuration of an extractor surrounding the source and two lenses (see Figures 4.3.2, 4.3.3, 4.3.4, 4.3.5 and 4.3.6). The extractor field was modelled by positive and negative uniform electric fields as formed when separated by isolated plates with a small hole (r = 0.5 mm) in them. The other fields were approximated by a multitude of superadded fields surrounding the positions of the condenser lens and the objective lens. These fields were provided to closely approximate the entire effect of the electric fields on the particles passing through the FIB.

The structure of the FIB this model approximates can be seen in Figure 2.2.2 in Chapter 2.

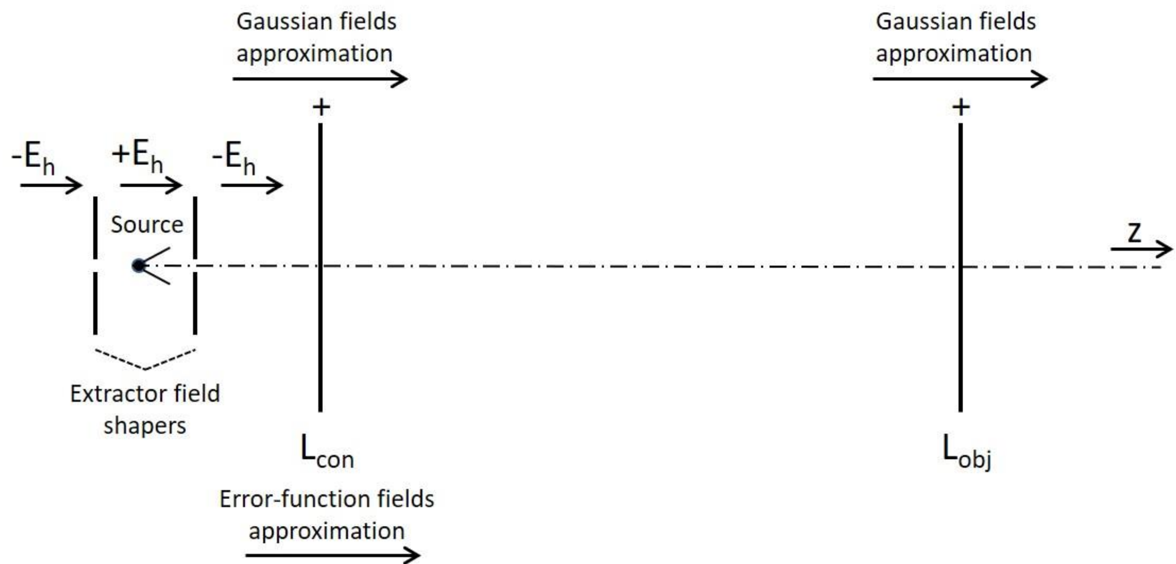

Figure 4.3.2: The layout of the electric fields within the model. The extractor field is modelled by positive and negative uniform electric fields (±E_h) separated by isolated plates with a small hole in the middle with a radius of 0.5 mm (here named the Extractor field shapers). The Extractor field shapers lie at a distance of +/- 5.55 mm from the source. Over this distance the extraction voltage of 9.6 kV is reached. The fields within the layout are approximated by multiple superadded fields surrounding the position of the condenser lens (L_{con}) at 15.27 mm from the source and the objective lens (L_{obj}) at 329.71 mm from the source. A trace of the particle movement through the model can be found in Figure 4.3.3. An example of the electric fields within the model can be found in Figures 4.3.4, 4.3.5 and 4.3.6.

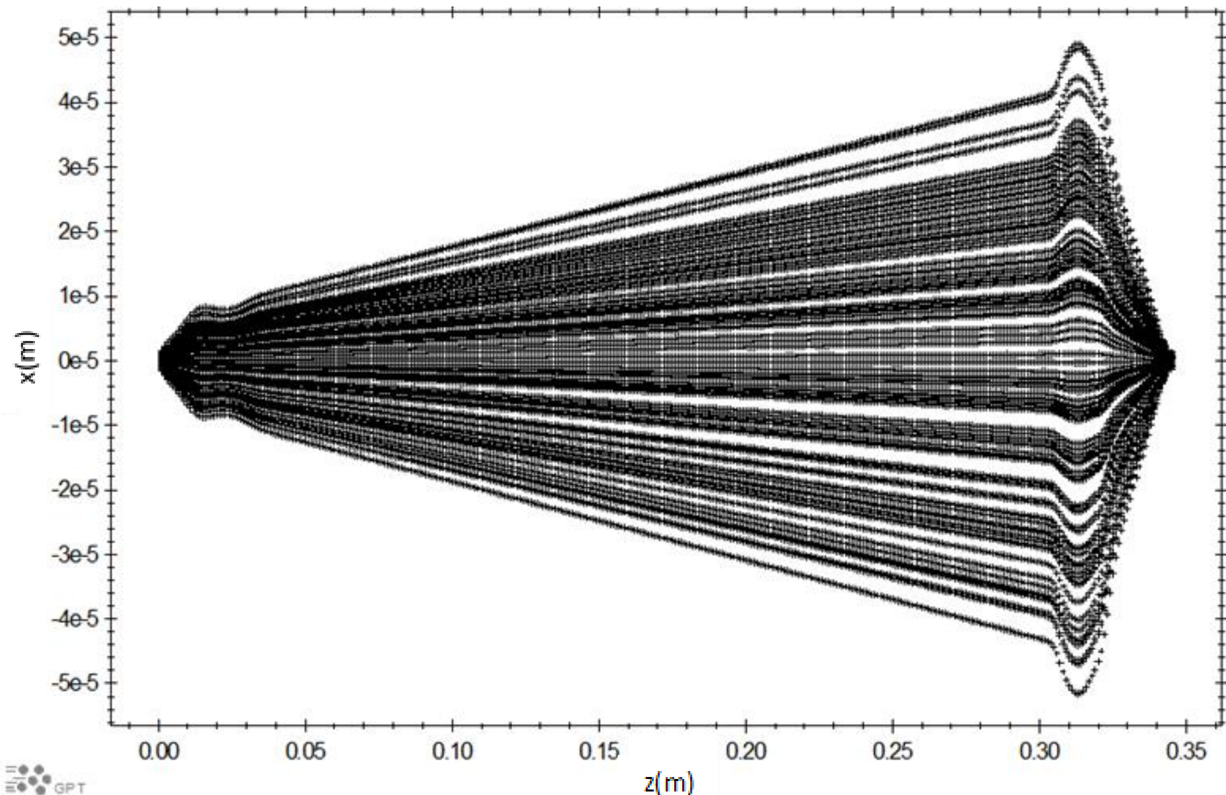

Figure 4.3.3: An example of the trajectory of the particles along the 'ion beam column' as calculated by the model. The source is at z = 0 m, the condenser lens can be found around z = 0.015 m and the objective lens can be found around z = 0.33 m.

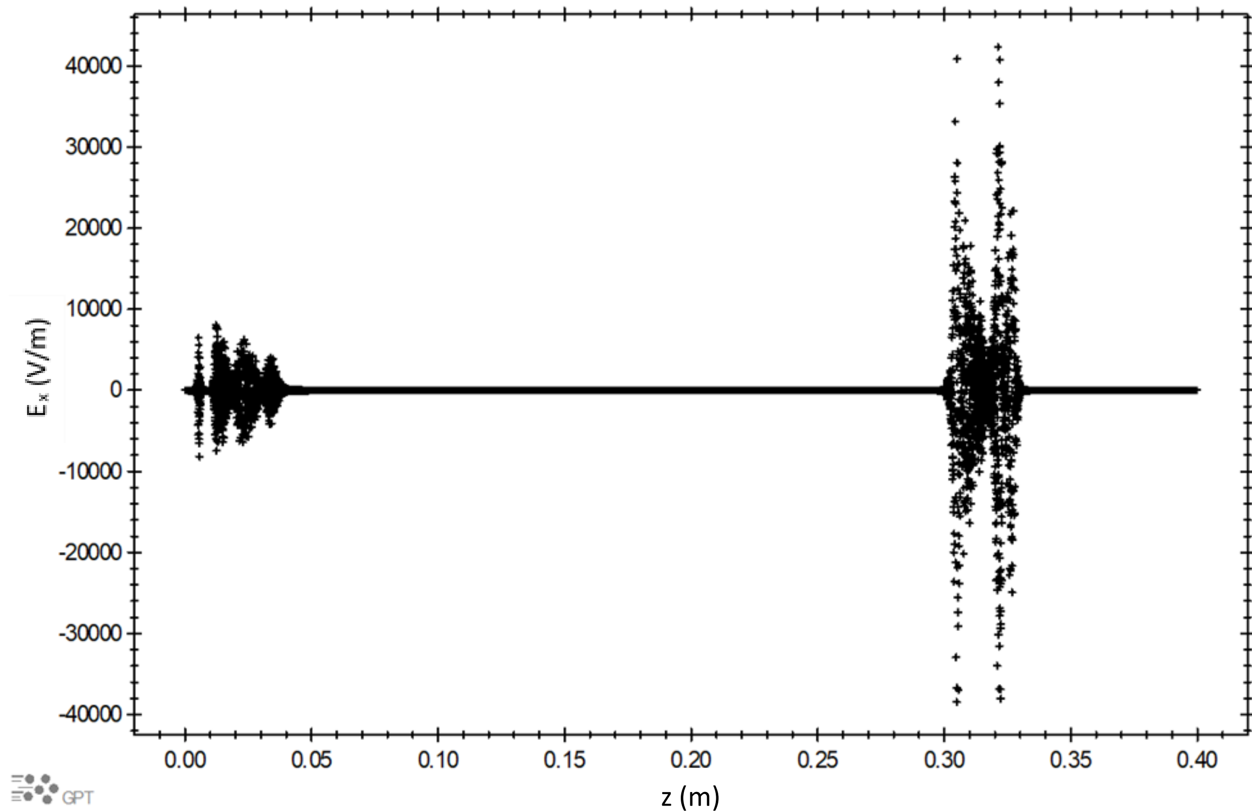

Figure 4.3.4: The electric fields in the x-direction E_x as undergone by each particle when moving along the ion beam column in the model, at a condenser lens voltage of 17.5 kV and a beam current of 40 pA. The fields are spherically symmetrical perpendicular to the z-axis, thus the fields in the y-direction are equivalent to this. The source is at $z = 0$ m, the condenser lens can be found around $z = 0.015$ m and the objective lens can be found around $z = 0.33$ m. Particles farther out in the x-direction from the x-axis experience stronger fields, as can also be seen in Figure 4.3.5.

With the model it was possible to determine the particle positions each point and compare this directly to the experimental results. To do so the circumstances of each experimental measurement (see Section 4.4.1) were duplicated in the model, using the matching lens voltages and current. The standard deviation σ of the particles in the beam at each position was automatically calculated when running the model. The radius of the spot size and the beam at various other positions were thus taken as the standard deviations at those positions, since calculating the radius containing 50% of the beam r_{50} at any point proved difficult. Brightness calculation was then done from this information the same way as in the experimental measurements, using the information granted by the model on the beam size at several distances from the waist (see Section 4.3.2).

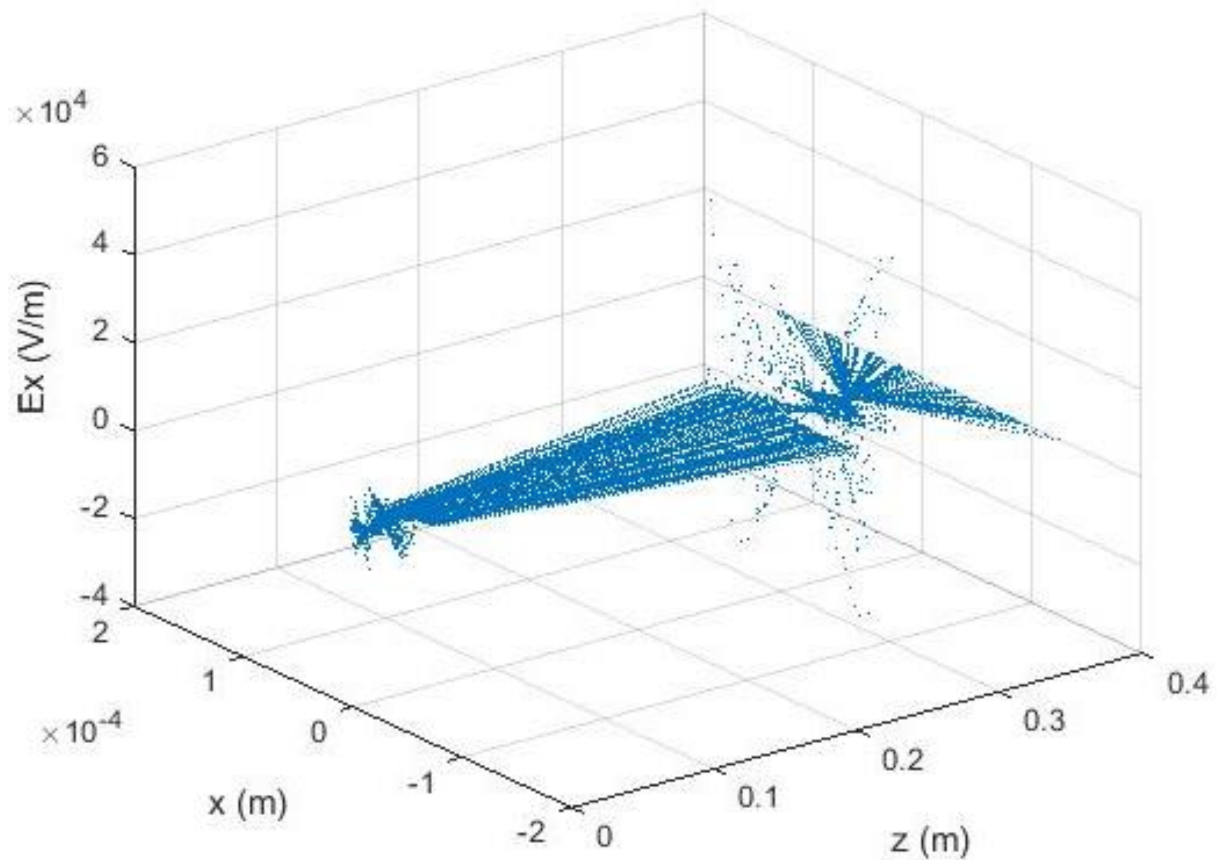

Figure 4.3.5: The electric fields in the x-direction E_x each particle undergoes in the model at a condenser lens voltage of 17.5 kV and a beam current of 40 pA, as dependent on their positions in the x- and z-direction. The fields are spherically symmetrical perpendicular to the z-axis, thus the fields in the y-direction are equivalent to this. The source is at $z = 0$ m, the condenser lens can be found around $z = 0.015$ m and the objective lens can be found around $z = 0.33$ m. A flattened out version of this image, showing only the dependence of E_x on z, can be found in Figure 4.3.4.

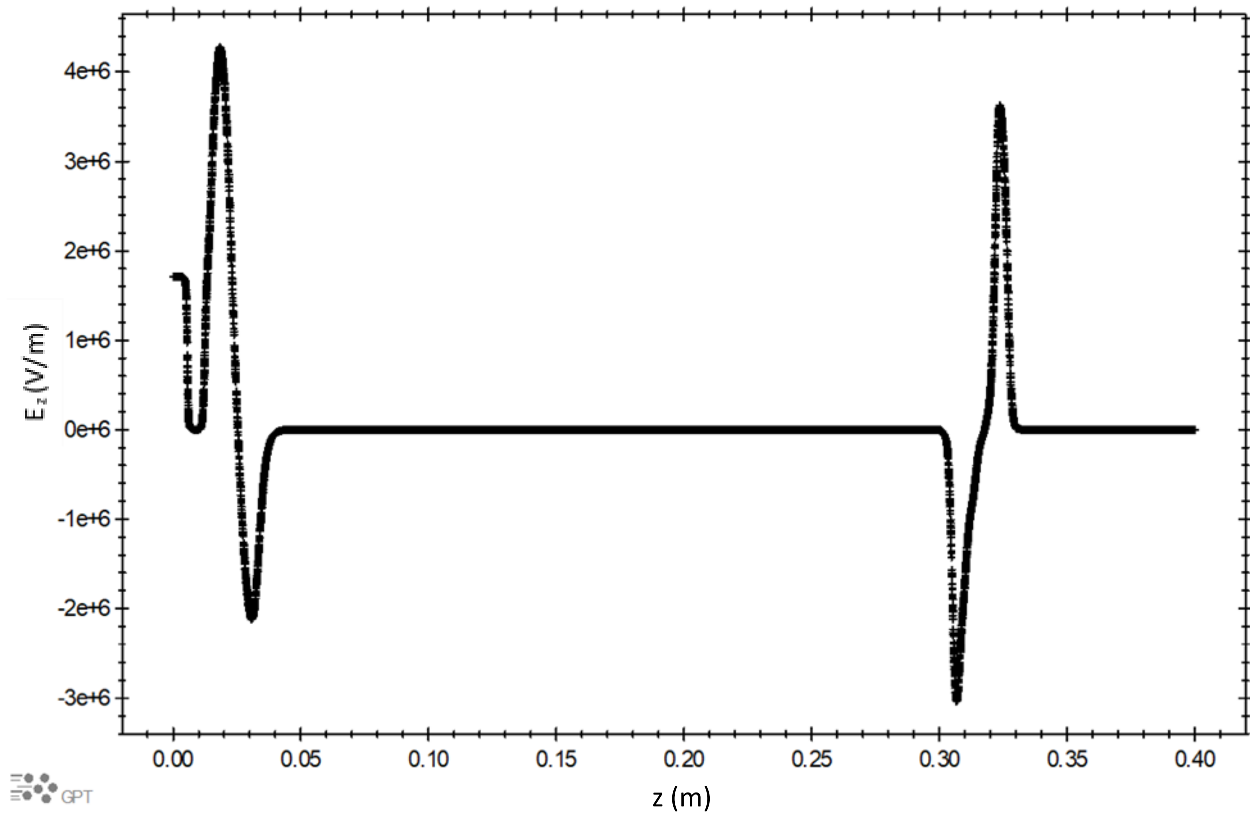

Figure 4.3.6: The electric fields in the z-direction E_z as undergone by each particle in the model as they move along the ion beam column, at a condenser lens voltage of 17.5 kV and a beam current of 40 pA. The source is at $z = 0$ m, the condenser lens can be found around $z = 0.015$ m and the objective lens can be found around $z = 0.33$ m.

4.3.2 Experimental Implementation

The Knife Edge Measurement

A knife edge measurement is done by focusing the ion beam onto a substrate material consisting of a flat surface with a very sharp edge (also see Section 1.3.2). As the ion beam scans the edge it crosses from the side onto the surface. The secondary electrons emerging from the material of the substrate when the ion beam hits the material can be measured (see Figure 4.3.7).

Assuming the edge itself is sharp enough, the slope as the beam crosses onto the edge as seen in a picture made with these secondary electrons is only determined by the size of the beam. The edge-scan then gives an accurate representation of how much of the beam covers the edge at any scanned place on the picture. The difference in distance between where none of the beam is hitting the edge and the beam is fully on the substrate itself (on the other side of the edge) then corresponds directly to the spot size (see Figures 4.3.8 and 4.3.9).

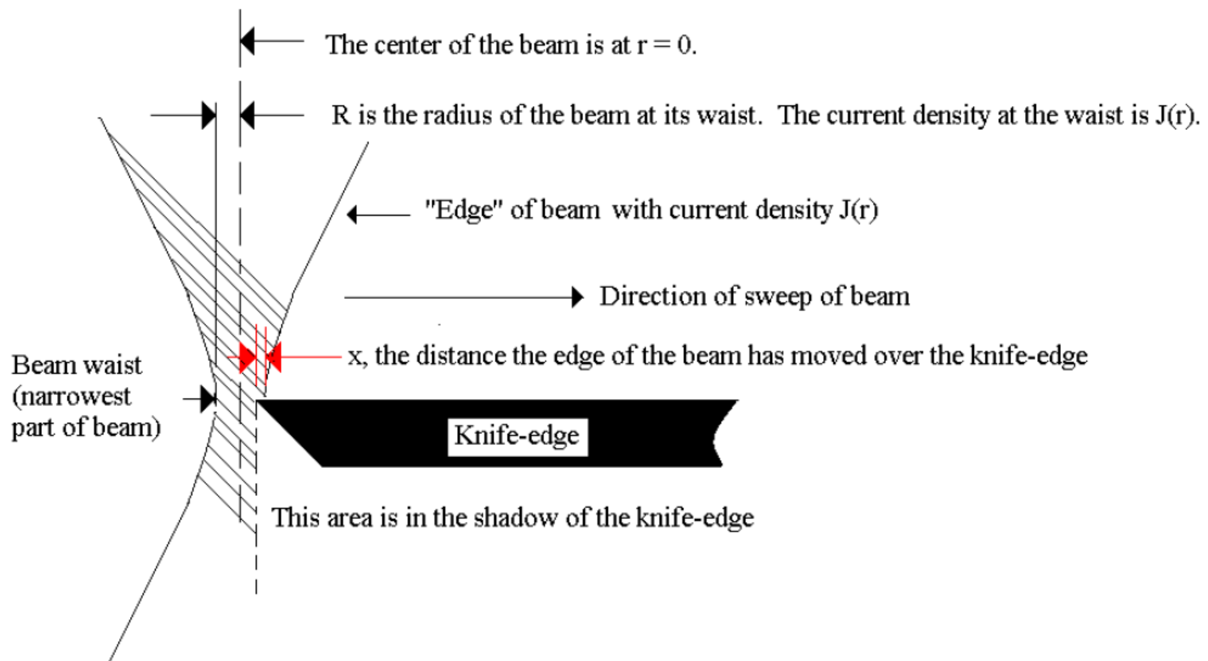

Figure 4.3.7: Schematic illustration of a knife edge measurement [17]. As the beam is swept across the knife-edge, the amount of electrons emitted by the surface, corresponding to the distance x, are measured by a secondary electron detector. This results in a secondary electron picture of the edge, which can be processed into a graph of the electron yield corresponding to the place where the beam is focused across the edge (see Figures 4.3.8 and 4.3.9).

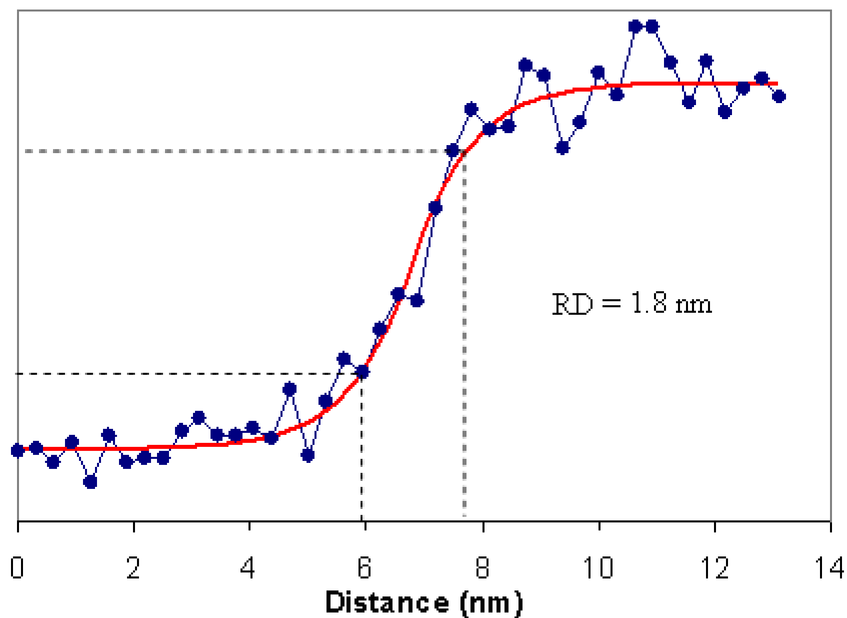

Figure 4.3.8: An example of a low current Ga FIB rise distance measurement, showing the significant statistical fluctuations in the results for a single line scan (dots) [17]. The best fit to the data is given by the smooth line. The distance over which the secondary electron yield increases, here taken from 20%-80%, is called the rise distance D_R (or RD in this image).

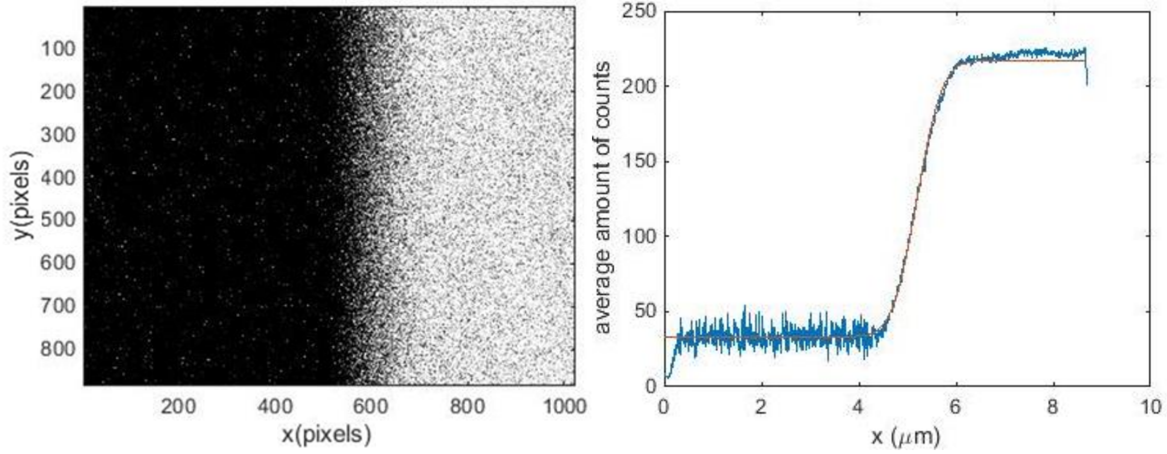

Figure 4.3.9: The result of a knife edge measurement. The figure to the left shows the picture resulting from the secondary electron measurement during the edge scan. The figure to the right shows the average secondary electron yield across the y-axis in the left picture at each position x, with Equation 4.3.2 fitted through it. From this figure the rise distance can be calculated. This scan was taken from the waist-scan at a condenser lens voltage of 18.5 kV, a magnification of 17500, a beam current of 41 pA and a beam voltage of 30.0 kV. The size of the left picture corresponding to its pixels is directly determined within the FIB, corresponding to the known magnification of the image (see Section 2.2.2).

To minimize the influence of noise, the intensity values as a function of x (the direction perpendicular to the edge) for the rise-distance graphs in this thesis were calculated by averaging the intensities along the y-direction (parallel to the edge) in each knife edge measurement (see Figure 4.3.9).

The corresponding distance in the graph at which the secondary electron yield increases is called the rise distance (D_R). The chosen standards for calculating the rise distance vary. A rise distance at 12-88% of the maximum has been used in the past, as well as rise distances of 35-65%. What rise distance is chosen is generally dependent on the applications the FIB is meant for (milling or imaging for instance) [17].

In the following experiments the 25-75% rise distance has been used, both for determining the beam sizes in the measurements and in the model. The 25%-75% rise distance corresponds to the beam diameter containing 50% of the beam. Assuming an approximately gaussian current density distribution, the corresponding beam radius containing 50% of the beam r_{50} is close to the standard deviation σ of the beam. In a beam with an exactly gaussian current density distribution they relate as [27]:

$$r_{50} = \sqrt{-2\ln 0.5} \cdot \sigma \approx 1.18\sigma \,. \tag{4.3.1}$$

To further account for the statistical fluctuation, while calculating the rise distance, a fit is made through the data (see Equation 4.3.2). Since the rise distance measurement shows results in an approximate integral of the current density distribution and the current density distribution of the beam approximates a Gaussian shape (more on the expected shape of the current density distribution in Section 4.2.2), the fitted function should be an error-function:

$$N = N_{av} + A \cdot \mathrm{erf}\left(\frac{x - x_o}{\sqrt{2}a}\right), \tag{4.3.2}$$

where N is the average amount of counts (intensity) at a point x along a line in the scan across the knife-edge, x_0 is the offset of the image, corresponding to the location of the edge, N_{av} is the secondary electron intensity at the centre of the edge, A is de amplitude of the function (the difference in intensity between N_{av} and the minimum and maximum intensities) and A is related to the steepness of the error-function. Both N_{av} and A were predetermined before fitting, by calculating the minimum and maximum intensities as the average over a 100 points well off the

edge and a 100 datapoints well on the edge respectively. After making a general estimate of their values, x_0 and a were then determined by fitting Equation 4.3.2 through the data. The code used to calculate the rise distance for each image can be found in Appendix A.2.

The Waist-scan

This experiment was performed using automated waist-scans. In a waist-scan the beam size is measured along the beam axis surrounding the waist of the beam, by moving the knife edge sample to several positions along this axis and performing a knife edge measurement at each position (see Figure 4.3.10).

To do so, the voltage of the objective lens, which determines the exact position of the waist of the beam and is thus used to focus the beam on the sample (see Section 2.2.1), is kept constant during each waist-scan. Unlike in Chapter 3, where the beam is focused on the sample for each image taken, the knife-edge scans made on different positions along the beam above and below the waist are thus deliberately out of focus, showing the width of the beam outside of the waist. In general, the spot size was measured at 17 positions along the waist, each 30 µm apart, from -240 µm to +240 µm surrounding the focal point, which should coincide with the beam waist (see Figure 4.3.11). Ten images were taken at each position. From each image the 25%-75% rise distance was determined and the average of these was taken as the beam size at that position.

The instruction code used to make the FIB perform a waist-scan can be found in Appendix A.3.

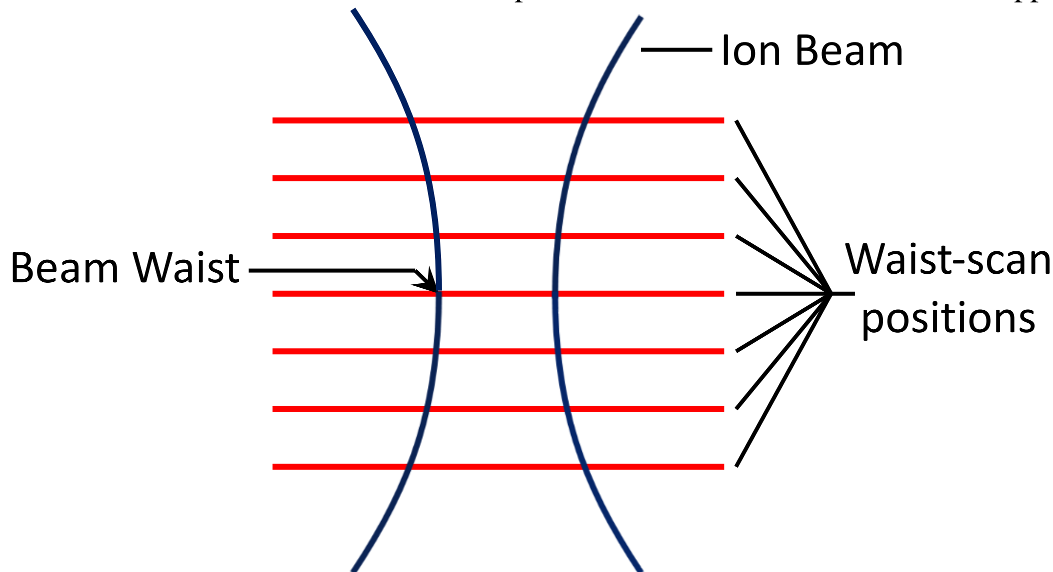

Figure 4.3.10: The knife edge sample is moved along the ion beam axis. At several positions (the waist-scan positions) along the axis a scan of the knife edge is then made. These centre around the beam waist and can be used to determine how the size of the beam changes along the waist. In general, 17 positions along the ion beam axis were used for the scan, each 30 µm apart, from -240 µm to +240 µm distance to the focal point (which should coincide with the waist). 10 images were taken per position. From each of these scans (or knife edge measurements) the 25-75% waist size can later be determined (see Figure 4.3.9).

From the waist-scan the spot size and emittance of the beam can be determined. Equation 4.2.9 was transformed for the fitting function used to do this:

$$x_{max,L}^2 = x_{max,0}^2 + \frac{\varepsilon^2}{x_{max,0}^2} L^2 \rightarrow x_{max,L}^2 = a + bL^2 \,, \qquad (4.3.3)$$

in which a and b are the fitting parameters. In Figure 4.3.11 Equation 4.3.3 was fitted as a function of L. For the purposes of calculating the spot size and emittance more accurately, Equation 4.3.3 was fitted in Figure 4.3.12 as a function of L^2. In the example of Figure 4.3.12, $a = (1.4 \pm 0.2) \cdot 10^{-16}$ m^2 and $b = (1.59 \pm 0.04) \cdot 10^{-7}$ sr. This means that here the radius of the spot $x_{max,0} = (12 \pm 1)$ nm and that the emittance $\varepsilon = (4.7 \pm 0.4) \cdot 10^{-12}$ m·rad. The uncertainties were calculated from the fit, incorporating the uncertainties in the data points as well as the closeness of the fit to the datapoints. In these examples the proposed fit matches the datapoints closely, allowing for a relatively low uncertainty.

Assuming the beam is spherically symmetrical perpendicular to the beam axis, Equation 4.2.10 can then be used to determine the reduced brightness of the beam, since the beam current is determined within the FIB setup (see Section 2.2.1). In the example of Figures 4.3.11 and 4.3.12, where $I = 9$ pA and $U = 30.0$ keV, then $B_R = (3.5 \pm 0.6) \cdot 10^5$ Am^{-2}sr^{-1}eV^{-1}.

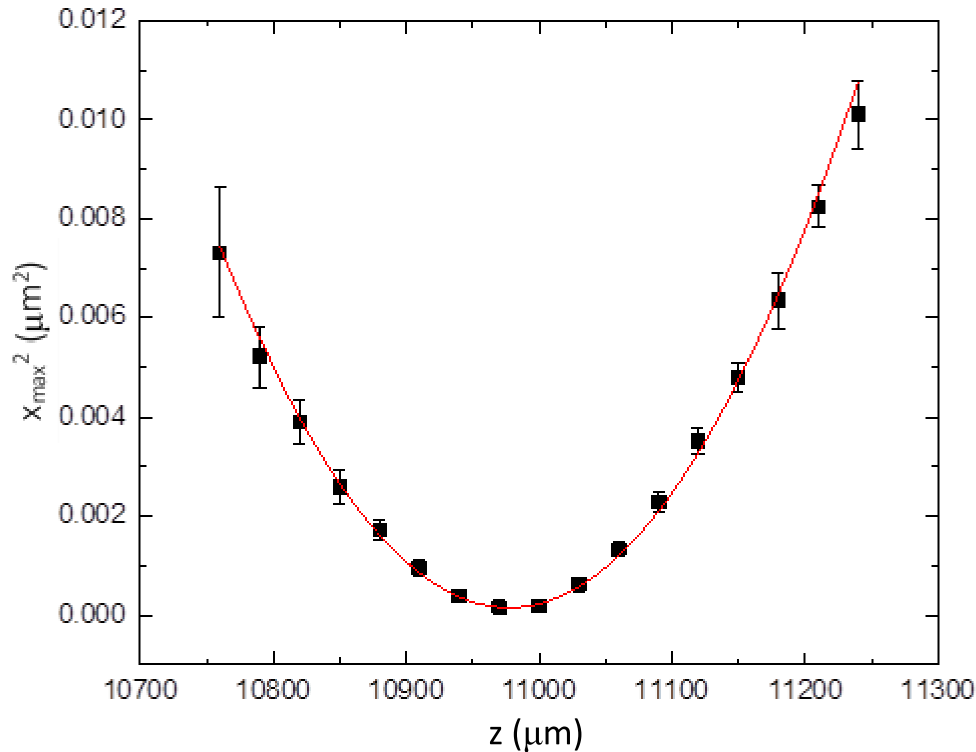

Figure 4.3.11: The results of a waist-scan, showing the squared beam size as a function of the height of the measurement in the FIB (its position along the z-axis). This data comes from the waist scan made at a magnification of 17500, a beam current of 9 pA and a beam voltage of 30.0 kV. Each point is the average calculated rise distance from 10 scans, each determined as seen in Figure 4.3.9. Equation 4.3.3 was fitted through the results. As expected, the proposed fit closely matches the data, making it possible to accurately determine the spot size and emittance from these results.

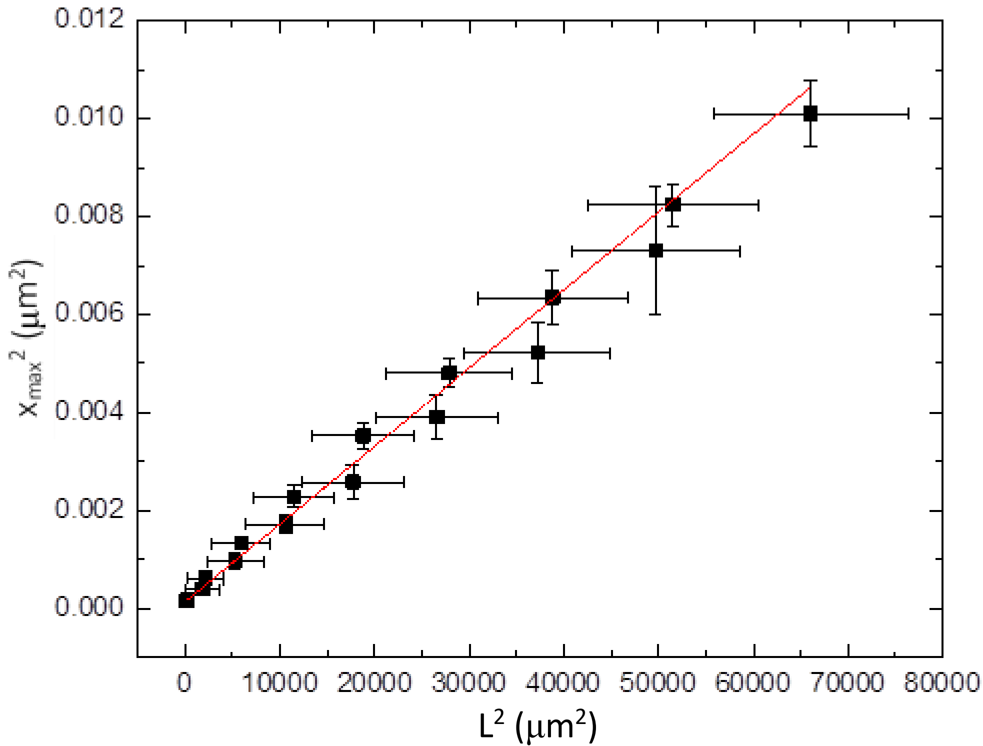

Figure 4.3.12: The squared beam size as a function of the squared distance along the beam axis to the focal point of the focused ion beam. This data comes from the waist scan made at a magnification of 17500, a beam current of 9 pA and a beam voltage of 30.0 kV. Each point is the average calculated rise distance from 10 scans, each determined as seen in Figure 4.3.9. Equation 4.3.3 was fitted through the results. As expected, the proposed fit closely matches the data, making it possible to accurately determine the spot size and emittance from these results.

4.3.3 Expected Experimental Difficulties

While the Knife Edge method itself is fairly straightforward, making sure the results are accurate and dependable is not. Two clear problems are encountered when employing this method: statistical variations and differing quality of the knife edge [17].

Statistical Effects

Statistical variations can have a heavy impact on the results of the knife edge measurement. At small currents the beam itself is noisy. Quite aside from that, the generation of secondary electrons by the ion beam is itself a statistical effect and can thus alter the measurement. Orloff [17] investigated this effect. The results from Orloff's paper (see Figure 4.3.13 and 4.3.14) are provided below to further explain the implications on measurements using the Knife Edge method.

The effect of noise is shown in Figure 4.3.8, which shows an example of a knife edge measurement. The noise in this figure is not negligible. In fact, using the image in Figure 4.3.13, many knife edge measurements were performed, which resulted in highly varying rise distances.

Part of this effect may also be due to the quality of the edge. As can be seen in Figure 4.3.13, the edge is not equally well-defined across the picture. Not only this, secondary electron yield may vary by position due to specimen crystallinity and chemical effects and the like. All in all, the 20%-80% rise distances from Figure 4.3.13 varied from < 2 nm to about 6 nm.

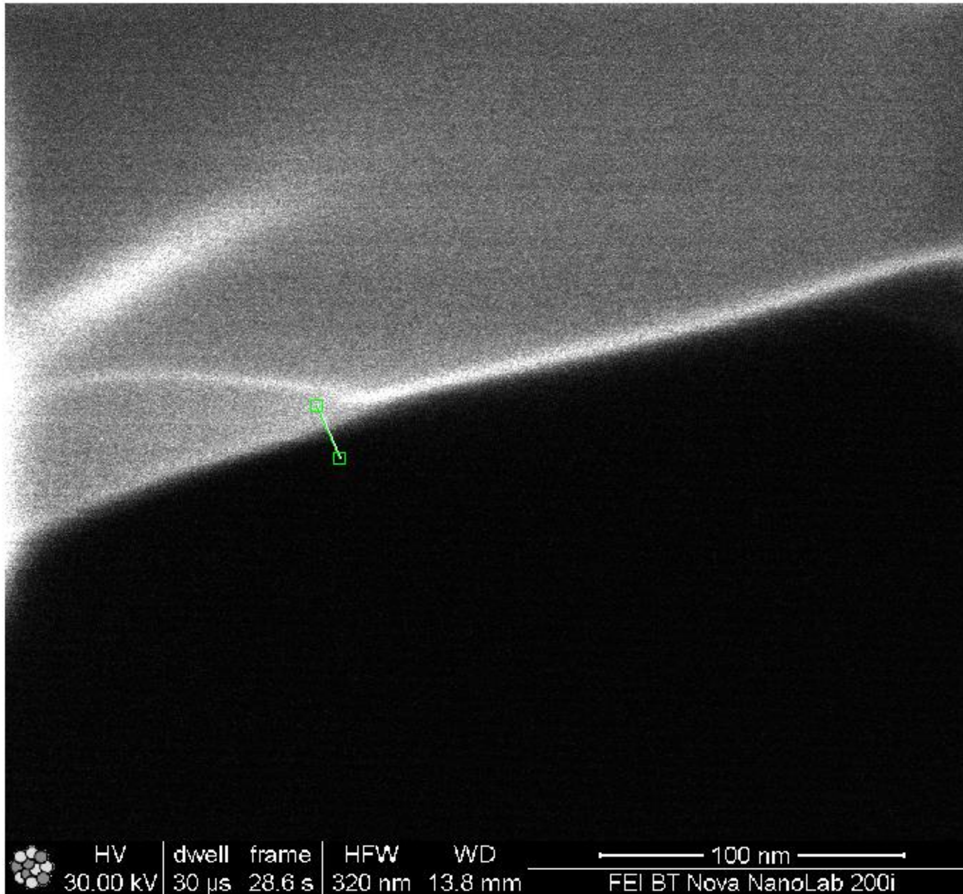

Figure 4.3.13: Image of a knife-edge taken with a 1 pA Ga FIB at 30 keV. The dwell time per pixel was 30 µs. The line terminated by boxes indicates where the rise distance of Figure 4.3.8 was measured. The specimen is graphite [17].

In a numerical experiment Orloff further investigates the statistical effects on the rise distance method. For this a current density distribution of a FIB was calculated for a beam current of 10 pA and an acceptance angle of 0.4 mrad where the current density distribution would be limited primarily by the source size and chromatic aberrations. The 35%-65% rise distance of this distribution was 3.7 nm. By adding random noise to this distribution 10.000 "noisy" distributions were generated. The rise distances were calculated from these "noisy" distributions to show the effect of noise on the rise distance result (see Figure 4.3.14).
These results show that it is highly important to take the statistical variations into account and that, to find the rise distance, it is important to use the average of a statistically significant amount of measurements.

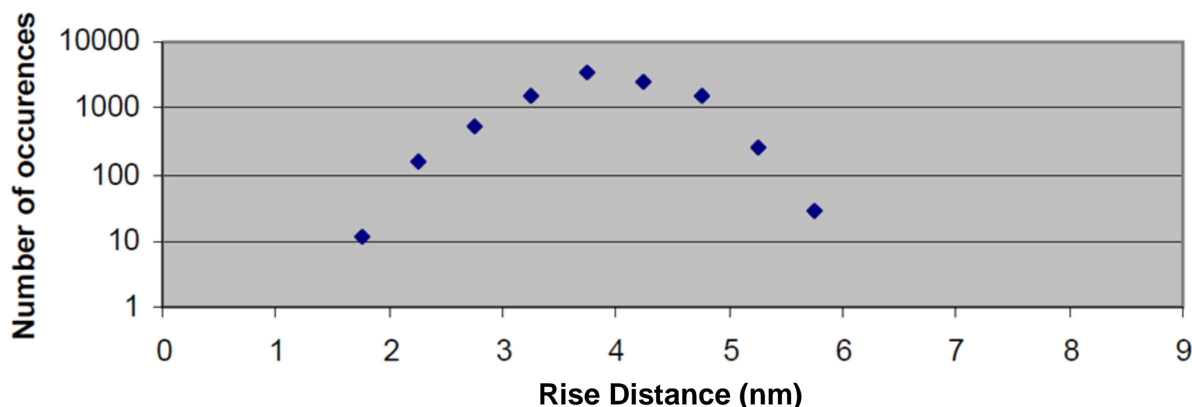

Figure 4.3.14: The distribution of 35% - 65% rise distances of 10,000 "noisy" current distributions. A point lying at 1.75 nm represents the data where the rise distances were between 1.5 and 2.0 nm, etc. The mean rise distance is 3.9 nm and the variance is 1.4 nm. The 4 nm range for the rise distances is purely the result of statistical fluctuations in the beam current [17].

Edge Quality

Making a statistically significant amount of measurements is made difficult by the variations in edge quality mentioned before. As can be seen in Figures 4.3.15 and 4.3.16 the sharpness of the edge greatly influences the found result.

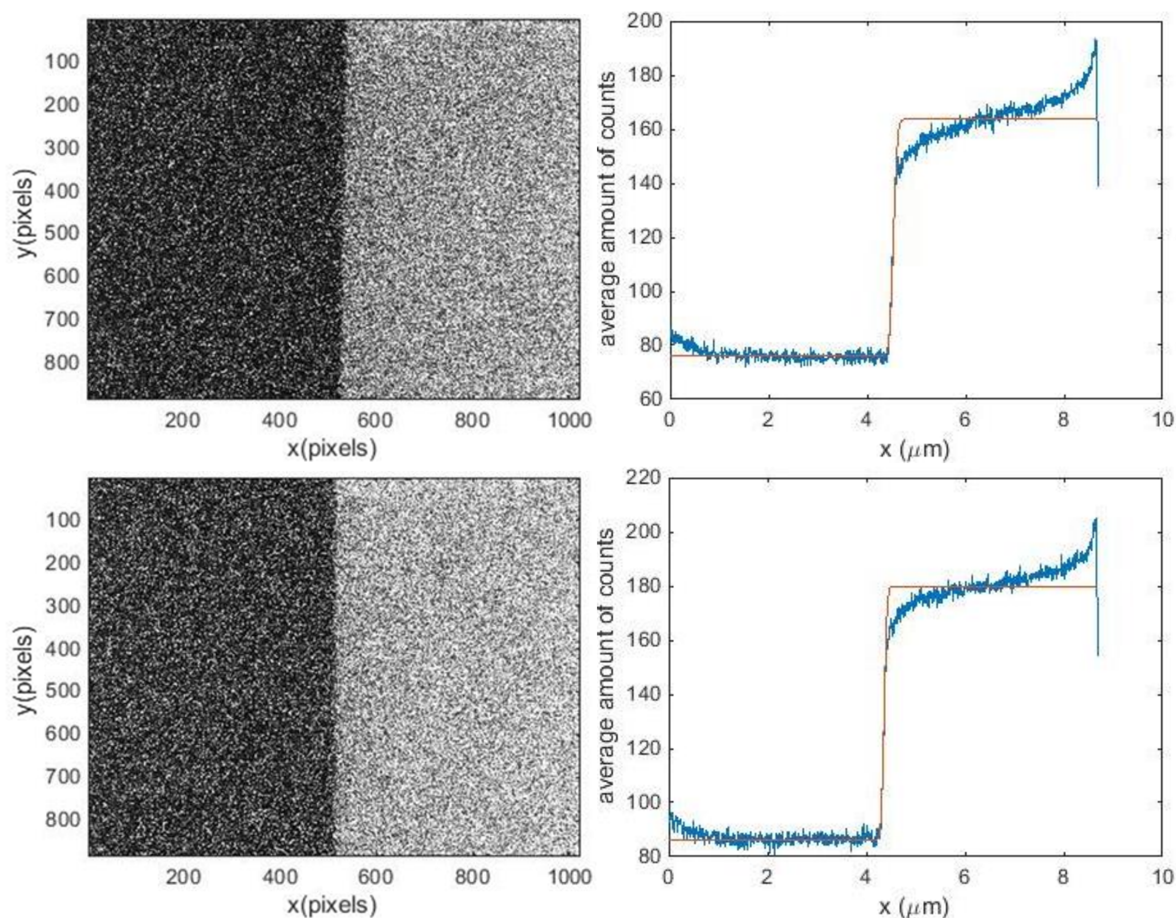

Figure 4.3.15: Two knife edge scans showing seemingly sharp edges, taken at different places along the same knife edge. The figures to the left show the pictures resulting from the secondary electron

measurements during the edge scan. The figures to the right show the average secondary electron yields across the y-axis in the left corresponding pictures as a function of position x, with Equation 4.3.2 fitted through it. The size of the left pictures corresponding to their pixels is directly determined within the FIB, corresponding to the known magnification of the image (see Section 2.2.2). These scans were taken from the waist-scan at a condenser lens voltage of 15.5 kV, a magnification of 17500, a beam current of 41 pA and a beam voltage of 30.0 kV. These scans can be compared to Figures 4.3.9 and 4.3.16, which show blunter edges.

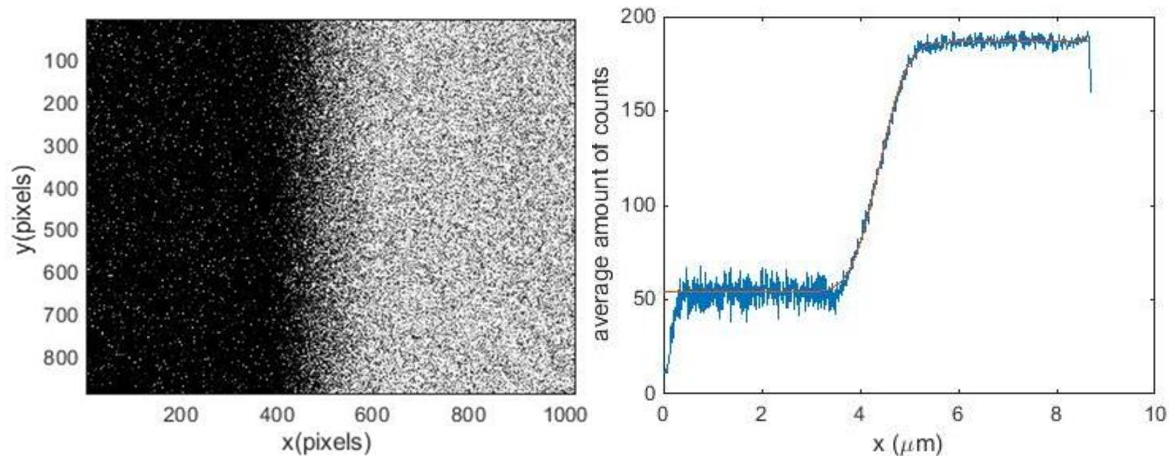

Figure 4.3.16: A knife edge scan showing an edge that is relatively blunt. The figure to the left shows the picture resulting from the secondary electron measurement during the edge scan. The figure to the right shows the average secondary electron yields across the y-axis in the left picture as a function of position x, with Equation 4.3.2 fitted through it. The size of the left picture corresponding to its pixels is directly determined within the FIB, corresponding to the known magnification of the image (see Section 2.2.2). This scan was taken from the waist-scan at a condenser lens voltage of 18.5 kV, a magnification of 17500, a beam current of 41 pA and a beam voltage of 30.0 kV. Figure 4.3.9 shows an edge close by from the same waist-scan. These can be compared to Figure 4.3.15, which shows two sharper edges.

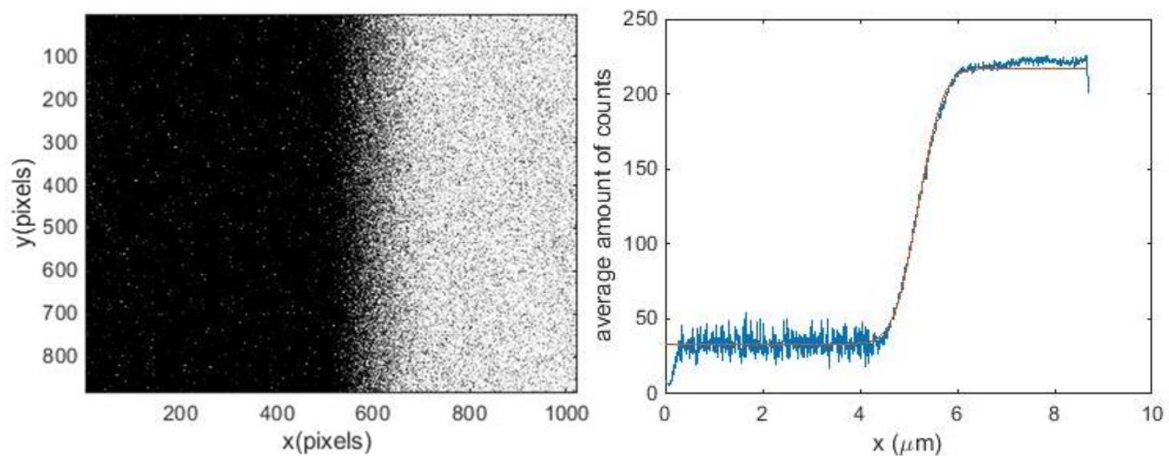

Figure 4.3.9: An edge-scan showing an edge that is relatively blunt. The figure to the left shows the picture resulting from the secondary electron measurement during the edge scan. The figure to the right shows the average secondary electron yields across the y-axis in the left picture as a function of position x, with Equation 4.3.2 fitted through it. The size of the left picture corresponding to its pixels is directly determined within the FIB, corresponding to the known magnification of the image (see Section 2.2.2). This scan was taken from the waist-scan at a condenser lens voltage of 18.5 kV, a magnification of 17500, a beam current of 41 pA and a beam voltage of 30.0 kV. Figure 4.3.16 shows an edge close by from the same waist-scan. These can be compared to Figure 4.3.15, which shows two sharper edges. See also Section 4.3.2 where this Figure is first shown.

To find the correct rise distance it is important to use the parts of the edge that are most well-defined and thus most sharp [17]. These will result in the lowest and most accurate rise distance measured. However, the use of heavy ions such as gallium ions makes it difficult to perform many accurate measurements in the same spot, since the ions themselves will deform the edge due to sputtering, implantation and other damages. Therefore, each picture was made at a different location along the used edges.
The edges were created by splicing silicon wafers. While it is difficult to create a sharp edge without defects, there is generally a clear visible consistency in quality along the same edge (see Figures 4.3.9 and 4.3.16, which were taken along the same edge, as well as 4.3.15, that also shows two pictures along the same edge).
To limit the effect of deteriorated edges, the results were processed manually to find pictures that showed a deteriorated (and thus not sharp enough) edge, so that these pictures resulting in clearly erroneous data could be taken out (see Figure 4.3.17).

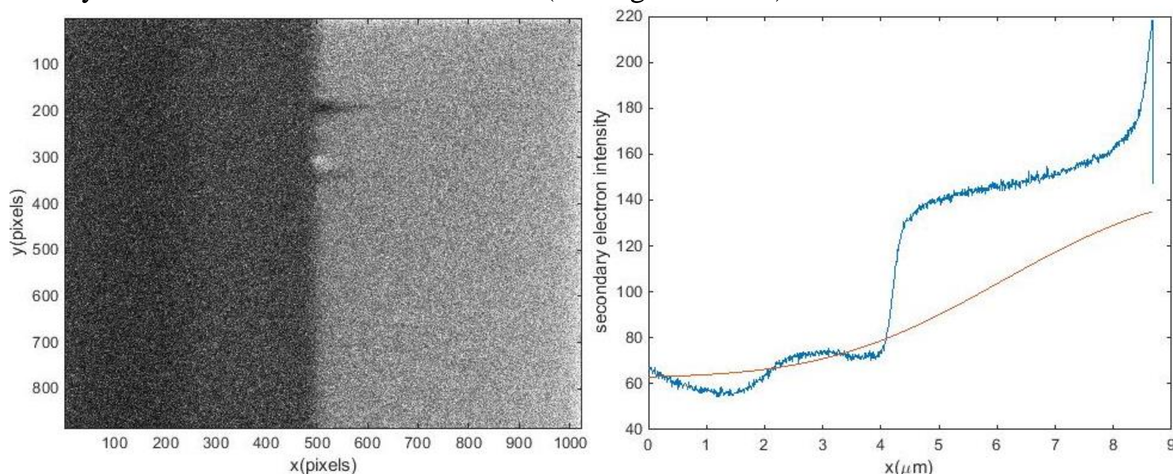

Figure 4.3.17: An example of a clearly deteriorated edge (seen to the left) resulting in an unusable rise distance graph (seen to the right). This picture was taken at a condenser lens voltage of 17.5 kV, a magnification of 17500, a beam current of 260 pA and a beam voltage of 30.0 kV. It was not used for calculation of the brightness or the spot size.

This did not account for the differences as seen in Figure 4.3.15 and Figures 4.3.16 and 4.3.9, however and some of the results have been influenced by moving to a different edge (see Figures 4.4.1 and 4.4.3).

In conclusion

The effect of edge sharpness added to the statistical effects make the spot size difficult to determine accurately. The best way to gain an accurate rise distance is thus to make many measurements in different spots along a knife edge and use from these the measurements made in the areas at which the edge is most well-defined. The average of these should give an accurate approximation of the spot size of the beam.
As spot size and emittance (and from them the reduced brightness) are determined with this method, however, they do not depend on measuring the beam size accurately at a single point, since their values are determined by a fit through the calculated beam size at several points along the beam axis surrounding the focal point (see Figure 4.3.12). This allows for correction for bad data points and, because of this, the spot size and brightness may be determined with higher accuracy than when the waist-scan is not used.

4.4 Results

To evaluate the usability of the Knife Edge method, the experimental results gained by using this method will first be explained and compared to expectations. After that, the results about the effectiveness of the method itself will be shown.

4.4.1 Experimental measurements

By comparing the measurements with the Knife Edge method to the expectations and the results of the model, the Knife Edge method can be further evaluated. These results are shown here. During each waist-scan the voltage of the objective lens was kept constant, as described in Section 4.3.2.

Voltage of the condenser lens

The voltage of the condenser lens should partly determine the eventual spot size of the beam (see Section 2.2.1), which makes it possible to compare its effects on spot size and beam brightness to the results of the model and expectations. The spot size and brightness of the beam were thus measured as dependent on the voltage of the condenser lens to consider, compare and evaluate these trends. This was done with a magnification of 17500, a beam voltage of 30.0 kV and a beam current of 41 pA. The results can be seen in Figures 4.4.1, 4.4.2 and 4.4.3. Each data point was calculated from a waist-scan, as described in Section 4.3.2.
The radius of the spot size is given as the radius containing 50% of the beam for the knife edge measurements and the standard deviation of the spot for the model data respectively (see Figures 4.4.1 and 4.4.2). As can be seen in these figures the measured results seem to show two different disjointed curves. These two sets of measurements, the first consisting of the measurement data at the voltages of 14.5 kV, 15.5 kV and 17.5 kV and the second of the measurement data at the voltages of 16.5 kV, 18.5 kV, 19.5 kV and 20.5 kV, were performed on two separate edges. This explains the disjunction of the results and immediately shows the result of using an insufficiently sharp edge, as turned out to be the case for the measurements in the second set (16.5 kV, 18.5 kV, 19.5 kV and 20.5 kV). Edge morphology can be a real problem when trying to determine the spot size using the Knife Edge method, as can be seen when comparing Figure 4.3.15 to Figures 4.3.16 and 4.3.9.
Figure 4.4.2 shows a zoomed in portion of Figure 4.4.1, showing only the 14.5 kV, 15.5 kV and 17.5 kV measurements. It shows that, at higher condenser lens voltages, the spot size decreases. This is not unexpected as the spot size of the beam is in part determined by the initial focussing of the condenser lens (see Section 4.2.2). Stronger focussing should result in a smaller spot size. The data from the model shows a linear decrease, with the spot size radius between 10 and 20 nm across the measurements. The data from the experimental measurement also shows a decrease as the condenser lens voltage increases, but the data points are too few to see whether this is a linear dependence. The spot size radii found in the experimental measurements are higher, however, between 25 and 40 nm. This is a far greater difference than can be explained by the difference caused by using the radius containing 50% of the beam for the measurement data and the standard deviation for the model data, which would account for a factor of about 1.18 difference in an approximately gaussian beam (see Equation 4.3.1). This may be caused partly by inaccuracies in the experimental setup. Even this edge may not have been sufficiently sharp to get an entirely accurate result. It may also be caused by the inaccuracy of the model. In the model the assumption of a Gaussian shaped current density distribution was made, an assumption that is not entirely in tune with reality (see Section 4.2.2). The so-called beam tails

can really increase the apparent spot size, especially when the spot size is small [8], though this effect should increase with increasing current.

Also, these spot sizes are all larger than 5-10 nm (2.5-5 nm for the radius of the spot), but that is to be expected, since spot size increases with higher current. The 5-10 nm mark is set at low current (in the order of several pA) and the current for these measurements was significantly higher (41 pA). To go into more detail about the match of these measurements with expectations, the current dependency of the measurements should be looked at (see Figure 4.4.5).

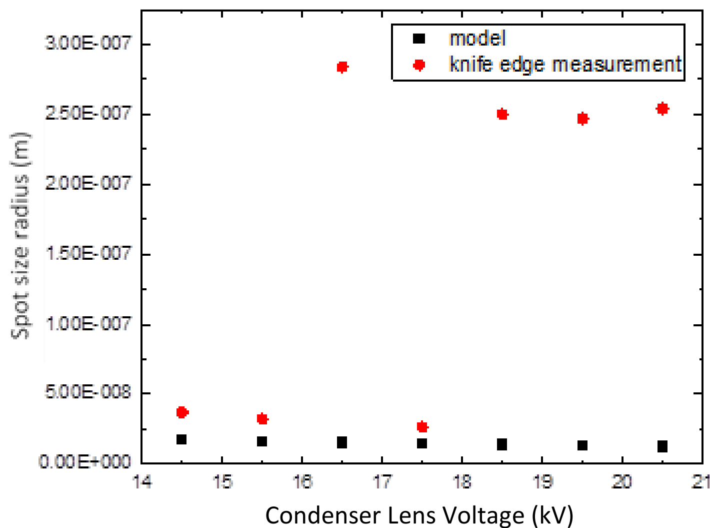

Figure 4.4.1: The radius of the spot of the FIB as a function of the voltage of the condenser lens at M = 17500, a beam current of 41 pA and a beam voltage of 30.0 kV, as determined by the waist-scan, using the Knife Edge method, and determined by the model. The measurements at 14.5, 15.5 and 17.5 kV were performed with a different knife edge than the ones at 16.5, 18.5, 19.5 and 20.5 kV. A zoomed in portion of the lower part of this graph can be seen in Figure 4.4.2.

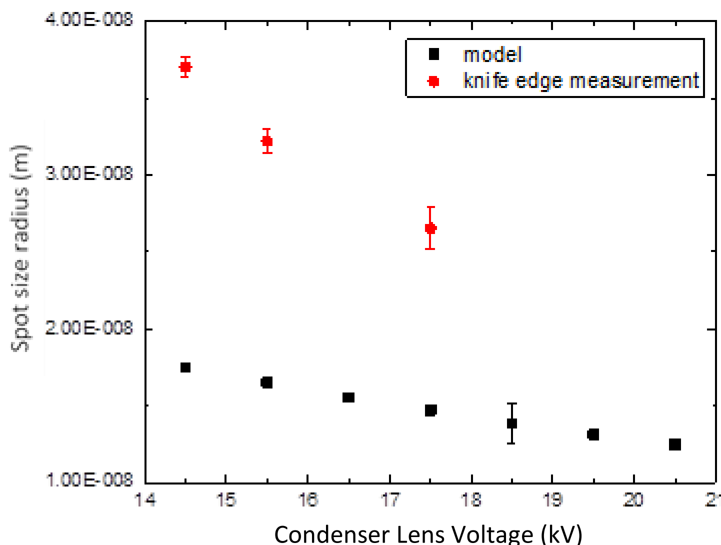

Figure 4.4.2: Part of Figure 4.4.1, zoomed into the measurements at 14.5, 15.5 and 17.5 kV, which were performed using the same knife edge.

Even at the blunter edge the spot size seems to decrease with increasing condenser lens voltage, though this pattern is less clear and even appears to contain a minimum. This rising spot size at the end may indicate that at some point lens aberrations form a larger contribution to increasing the spot size than the stronger focussing decreases spot size, but there is insufficient data here

to conclude this. All in all, this data is not very useful. Very close attention should thus be paid to the quality and sharpness of the edge to make proper knife edge measurements.

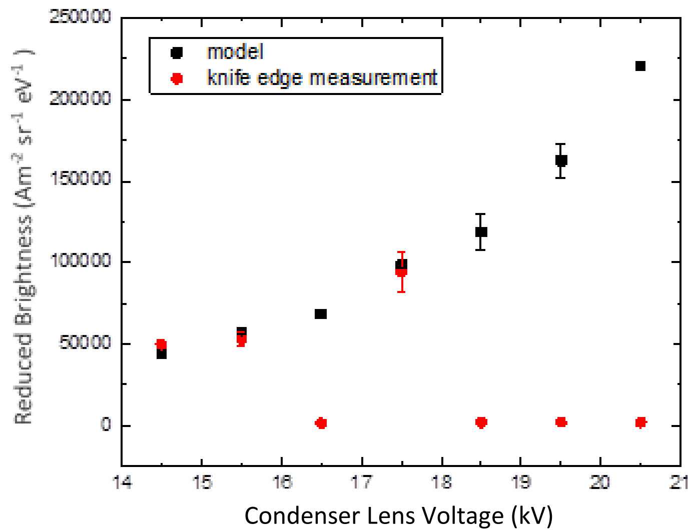

Figure 4.4.3: The reduced brightness of the FIB as a function of the voltage of the condenser lens at M = 17500, a beam current of 41 pA and a beam voltage of 30.0 kV, as determined by the waist-scan, using the Knife Edge method, and determined by the model. The measurements at 14.5, 15.5 and 17.5 kV were performed with a different knife edge than the ones at 16.5, 18.5, 19.5 and 20.5 kV.

In Figure 4.4.3 the reduced brightness can be seen as a function of the condenser lens voltage. The model data shows that B_R increases as the voltage of the condenser lens increases. Given that the spot size decreases at higher condenser lens voltage, this is not unexpected, since B_R is dependent on the spot size (see Equations 4.2.9 and 4.2.10).

In the experimental measurements, once again the measurements made using the blunt edge (at 16.5 kV, 18.5 kV, 19.5 kV and 20.5 kV) are very different from the model data and do not even appear to follow the same shape. These are thus quite useless for determining the actual reduced brightness of the beam.

The measurements performed using a sharper edge (14.5 kV, 15.5 kV and 17.5 kV) coincide far better with the model data. In the model the matching currents and lens voltages were used, together with the expected angular current density, virtual spot size, beam energy and energy spread of the FIB beam. Overall the data from the model and these experimental measurements coincide very well, apparently better even than the results for the spot size. From Figure 4.4.2 it might be expected that, as there the experimental values for the spot size radius are higher than the model values, in Figure 4.4.3 the experimental values for the reduced brightness should be lower than the model values.

This difference can already be seen in the emittance calculation (see Figure 4.4.4), indicating that the difference occurs here. It may be that this measurement is less prone to error than measuring only the spot size, since more data points are directly taken into account from the waist scan in determining the emittance than the spot size (see Section 4.3.2). In Equation 4.3.3 the emittance is determined from both fit parameters, whereas the spot size is only determined from fit parameter a. Thus, when calculating the emittance, the determination of b may somewhat compensate for the more error-prone determination of a. Otherwise it is unclear what causes this.

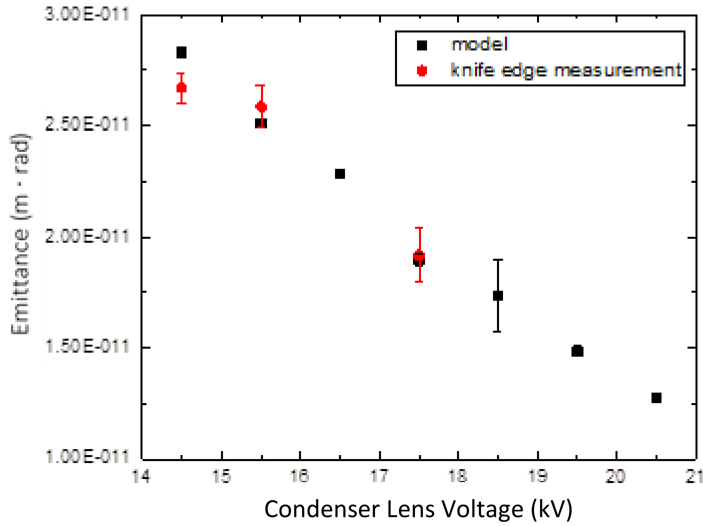

Figure 4.4.4: The emittance of the FIB as a function of the voltage of the condenser lens at M = 17500, a beam current of 41 pA and a beam voltage of 30.0 kV, as determined by the waist-scan, using the Knife Edge method, and determined by the model. Only the measurements at 14.5, 15.5 and 17.5 kV are shown.

At the very least Figure 4.4.3 shows that this method can result in an accurate prediction of the reduced brightness' dependency on the condenser lens voltage, since the trend does match. This is still conditional, though, on sufficient attention being paid to the sharpness of the edge.
Depending on the voltage of the condenser lens, the reduced brightness seems to be between $4 \cdot 10^4$ and $2.25 \cdot 10^5$ $Am^{-2}sr^{-1}eV^{-1}$. While the reduced brightness doesn't coincide with the expected 10^6 $Am^{-2}sr^{-1}eV^{-1}$ this may once again be caused by the higher current, since this brightness is expected at a lower current in the order of several pA. To go into more detail about the match of these measurements with expectations, once again the current dependency of the measurements should be looked at (see Figure 4.4.6).

Beam Current

The effect of the used beam current can also be used to compare the experimental method to the model results and expectations, since it should influence both the spot size and the beam brightness. The spot size versus current curve is furthermore particularly interesting for determining beam quality (see Section 1.2). The spot size and brightness of the beam were thus also measured as dependent on the beam current to consider, compare and evaluate these trends. This was done at a magnification of 17500, a beam voltage of 30.0 kV and a condenser lens voltage of 17.5 kV. The results can be seen in Figures 4.4.5 and 4.4.6. Each data point was calculated from a waist-scan, as described in Section 4.3.2.
Once again, the experimental values for the radius of the spot size represent the radius containing 50% of the beam, whereas the model values represent the standard deviation of the beam (see Figure 4.4.5). As can be seen in Figure 4.4.5 the spot size in general increases with higher current, as is expected. The values from the experimental measurement are both higher and more spread out, however. In fact, the fit of the measurement data (see Equation 4.4.1) resulted in a fit parameter a of about a factor 4 greater than the fit of the model data. This difference cannot be explained by the difference of using the radius containing 50% of the beam for the measurement values, while using the standard deviation for the model values, since in an approximately gaussian beam this should only cause a difference of a factor 1.18 (see Equation 4.3.1). Furthermore, unlike the model values, the experimental values do not lie on a

clear line. Both of these differences may be caused by the earlier mentioned errors that can occur when determining spot size experimentally. Differences in the used edges may contribute, though unlike in Figure 4.4.1, this difference could not be so clearly attributed to that, and more than this seems to have caused this effect. The simplifications of the model versus reality, for instance the use of a Gaussian current density distribution, may also partially be responsible for the difference.

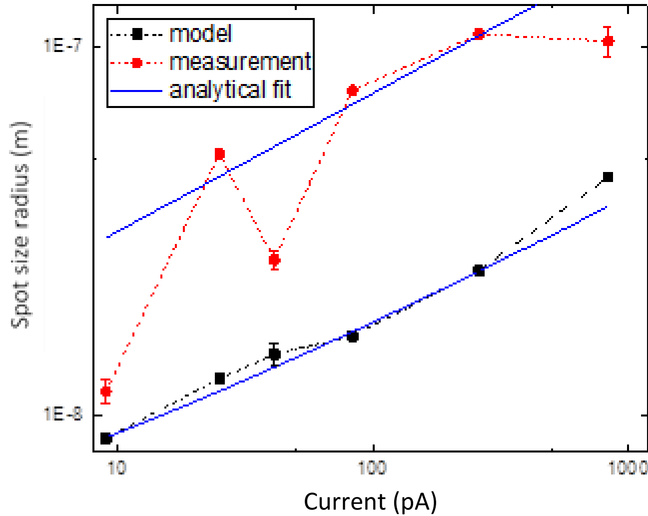

Figure 4.4.5: The Spot Size of the FIB as a function of the beam current at M = 17500, a beam voltage of 30.0 kV and a condenser lens voltage of 17.5 kV, as determined by the waist-scan, using the Knife Edge method, and determined by the model. The blue lines are analytical fits through the data corresponding to the spot size dependency on the beam current of a spherical aberration limited beam (see Equation 4.4.1).

The experimental values of the spot size radius seem to lie between 10 and about 110 nm, as the current increases. The expected value at low current (in the order of several pA) is about 5-10 nm (see Section 4.2.2), meaning the radius should be between 2.5-5 nm. From this graph it can be extrapolated that the spot size at that current should be within an order of magnitude difference of the expected result, but more than an order of magnitude approximation cannot be taken from this measurement. The model values, however, do seem to coincide with the expected spot size at low current, since the value of the spot size radius at 9 pA is already close to 5 nm and the spot size values from the model do form a clear trend.
To analyse the shape of the spot size versus current curve, Equation 4.2.11, 4.2.12 and 4.2.13 were used. Depending on whether the spot size is limited by chromatic aberrations, spherical aberrations or the brightness, one of these should coincide most closely with the found trend (see Section 4.2.2). The fit that coincided best with the data and was eventually fitted through both the experimental and model values, was derived from Equation 4.2.11, the trend for a spot size limited by spherical aberrations:

$$x_{max,0} = aI^{\frac{3}{8}}, \quad (4.4.1)$$

in which a is the fitting parameter. That Equation 4.4.1 generally follows the trend of the data, shows that the current dependency of the spot size coincides with the situation where the spot sizes are mainly limited by spherical aberrations. This agrees with expectations, since at higher currents spherical aberrations should predominate.
At lower currents, however, chromatic aberrations may predominate. This may be reflected by the experimental measurements, since in the lower current region (around 10 pA) these data

points' coincidence with Equation 4.4.1 is less clear. This could not be clearly tested, though, since there are not enough dependable data points in this region.
In the model spherical aberrations seem to dominate throughout, since here the fit with Equation 4.4.1 coincides with the data very well. That a matching trend could be found in the experimental data means that, at the least, the overall trend of the spot size versus current curve can be detected using these measurements, even if the exact spot size is uncertain.
Figure 4.4.6, which shows the reduced brightness as a function of the current, shows a clear difference between the reduced brightness as determined from the model and the experimental values. While the model values seem relatively constant as the current increases, the experimental values for reduced brightness clearly decrease with higher current. The increase in chromatic and spherical aberrations at higher currents, should affect both the experimental values and the model values (as seen in Figure 4.4.5), so cannot be used to explain so large a difference.

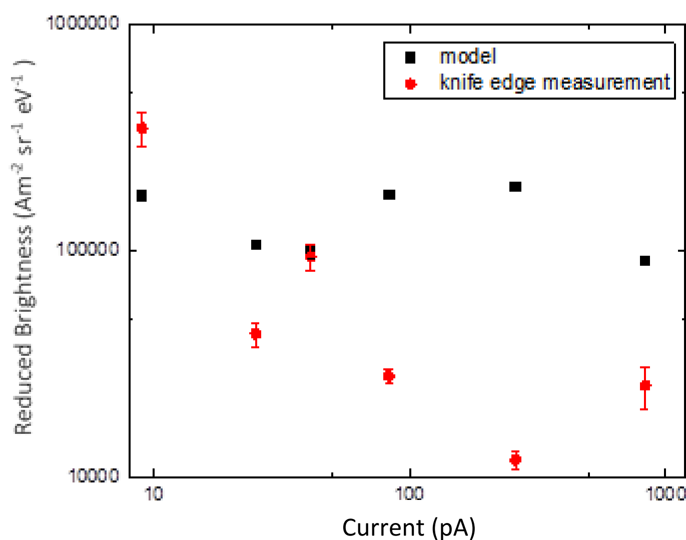

Figure 4.4.6: The reduced brightness of the FIB as a function of the beam current at M = 17500, a beam voltage of 30.0 kV and a condenser lens voltage of 17.5 kV, as determined by the waist-scan, using the Knife Edge method, and determined by the model.

In real setups the reduced brightness can decrease at higher currents, however, in part due to the enlargement of the beam tails (see Section 4.2.2), a difference that would not occur in the model, where the beam current density distribution is a simple Gaussian.
Thus, the difference between the model and experimental values does not necessarily mean that the experimental values cannot be depended on.
There is a high spread in the experimental data, however, which would make any exact determination of the reduced brightness uncertain. The model shows the reduced brightness to be about 10^5 $Am^{-2}sr^{-1}eV^{-1}$, which is one order of magnitude lower than the expectation of 10^6 $Am^{-2}sr^{-1}eV^{-1}$. Since reduced brightness may decrease at higher currents, the brightness for a system is usually given at low current. In this area the experimental value is close to the expectation, $(3.5 \pm 0.6) \cdot 10^5$ $Am^{-2}sr^{-1}eV^{-1}$, instead of 10^6 $Am^{-2}sr^{-1}eV^{-1}$, yet given the spread of the other data points its exactness is uncertain and it is still about a factor 3 lower than expected.
Overall at the very least a rough estimate of order of magnitude of the reduced brightness may be made with this method, but no more, unless more attention is paid to edge sharpness and other troublesome factors.

4.4.2 Difficulties of the Knife Edge Method

The sharpest limitation to accuracy encountered during the implementation of this method was the sharpness of the edge, as has been discussed in Section 4.3.3. As can be seen in Figures 4.4.1 and 4.4.3 the difference in results between different edges is far greater, than the effect of statistical errors (this is supported by Figures 4.3.15, 4.3.16 and 4.3.9 in Section 4.3.3).
It may be partially due to this that the results found in Section 4.4.1 were so uncertain. It seems that particular care needs to be taken when using this method and many suggestions have been made to counter its problems [16,17,21,22]. According to most papers, however, the knife edge measurement, while accurate enough for most purposes, is not the most accurate way to determine the spot size of a beam and for high accuracy it is better to use different methods instead [4,15,21,24].
On the other hand, implementing the Knife Edge method itself was relatively easy. Both performing the waist-scan and the analysis of the pictures to determine spot size and brightness could be easily automated. The only thing that had to be done manually throughout this method is finding scans among the bulk data of parts of the edge that were too deteriorated, but with image recognition software even this should be possible, since all that needed to be done was to check if the scan formed a straight line (see Figure 4.3.17).

4.5 Conclusion

The method described in this chapter makes it possible to find a rough estimate for both the spot size of a FIB and the reduced brightness. While the method is easy to implement and all steps of it can easily be performed automatically, there were clear problems with the results.
In the implementation, the main problem were the edges (as shown in Figures 4.3.15, 4.3.16 and 4.3.9). When the beam is scanned over an edge of insufficient sharpness, the results suffer. Furthermore, it is impossible to use the same part of an edge over and over again, since the ion beam deteriorates the substrate material, causing the edge to grow blunt.
Because of this it was necessary to move the beam to different parts of the edge while measuring. The results gained along the same edge of a sample did show that it is possible to make edges with very consistent sharpness, at least when using a spliced silicon wafer (see Figure 4.3.15). Having to move to a different edge can have a great impact on the results, however, and the use of an overly blunt edge can result in useless data (see Figures 4.4.1 and 4.4.3). Therefore, particular care should be applied to the selection of an edge.
Statistical errors and noise in the result were expected and could (for the most part) be accounted for by taking many measurements and averaging and/or fitting the results as needed (see Section 4.3.2). Nonetheless, as previous research about the Knife Edge method has also shown [17], the accumulation of problems such as improper edge morphology and statistical errors generally prevent getting an accurate result, resulting in a rough estimation of the spot size rather than an exact value. This can also be seen in Figures 4.4.2, 4.4.5 and 4.4.6. Figures 4.4.5 and 4.4.6 in particular show the difficulty in determining an exact value for the spot size or reduced brightness with this method. The experimental results were spread out and showed up to an order of magnitude difference with expectations or the model. The results from Figure 4.4.2 shows only a factor 2 difference with the model values. And when only the results of the sharper edge are taken into account in Figure 4.4.3 the experimental data coincides with the model values very well. This shows that it is possible to get more accurate results. Other additions or alterations to knife edge measurements to improve accuracy have also been suggested, such as using an additional Faraday cup to measure the current passing the knife edge or using the boundary between two elements, instead of an actual edge [16,17,21,22].
The results do agree with the trends in the model (see Figures 4.4.2 and 4.4.3) and with the expected spot size versus current curve as limited by spherical aberrations (see Figure 4.4.5), however. This indicates that these estimations are close enough to allow the measuring of important trends to determine beam quality, such as the aforementioned spot size versus current curve.
All in all, this method can be used to roughly determine beam quality, though it should perhaps be used in conjunction with further, more exacting measurements (see Section 1.3 for other methods of determining beam quality), if the exact value of the brightness or spot size needs to be determined. To get more exact results from this method a lot of care should particularly be taken in the selection of an edge. A lot may also be gained in the way the experiment is performed, by eliminating most of the sources of extra error, by taking the average result of many measurements to account for statistical effects and by optionally trying some of the improvements upon this method suggested by others. This extra care somewhat defeats the purpose of having a quick and easy method to determine beam quality, however, and the Knife Edge method may best be considered as a way to easily gain some understanding of the important trends in the ion beam properties, at least when enough measurements are taken.

5 Conclusion and discussion

In this thesis methods of determining the beam quality of a focused ion beam (FIB) were researched. FIBs are important instruments in the field of nanomachining, particularly because of their ability to directly modify structures at the nanometer length scale.
Particular emphasis was put on two of these methods: a method for determining the resolution of a FIB (see Chapter 3) and the Knife Edge method for determining the spot size and reduced brightness of a FIB (see Chapter 4). These methods were chosen, because they should be able to give clear indications of the properties of a FIB (namely resolution, spot size and brightness) and should be relatively easy to implement. The goal was to test and evaluate these methods, find their limitations, see if they could be further automated and determine whether they could be used to possibly measure the beam quality of future FIBs with higher reduced brightness and smaller spot size than the Ga LMIS (see Section 1.1.2), such as created by the ABLIS [2,5,6,13] or LoTIS projects [14].

5.1 Conclusions

5.1.1 The resolution measurement

The explored resolution measurement shows good results, when taking the time to manually determine where the edges in the pictures lie (see Chapter 3). The contrast response on distance between two sharp features in an image can be determined well enough to show a clear trend, allowing for the determination of the resolution. The resolution could not be determined more accurately than to find a range wherein it should lie, though: 2-7 nm and 4-10 nm were for instance found at magnifications of M = 120000 and M = 65000 respectively, and at lower image magnifications the spread in data increased, leading to a range of 15-35 nm at a magnification of M = 25000 (see Section 2.2.2 for more information on the magnification). None of these ranges were outside of expectations, though, since the resolutions at the two higher magnifications were expected to be in the order of 7 nm, so at the least this method results in a decent estimate of resolution, as long as the magnification is high enough.
It is also an easy method to determine the resolution of a FIB, especially since nothing is needed beyond the scanning capabilities of the FIB itself and a sample with sharp edges. It makes it possible to determine the optical transfer function of the FIB (the image contrast frequency response) without knowing the exact current density distribution, which is useful since the current density distribution of a FIB is not easily determined (see Section 1.3.3).
It is not a fast method, however, and requires manual post-processing outside of the use of the FIB. A method to use software to automatically find the edges, making manual post-processing obsolete, has not been found. Noise interfered too much with finding the accurate positions of edges in an image, leading either to edges being found where there were none or edges being overlooked, when trying to correct for the effect of noise, or both (see Section 3.4.2). This results in extra erroneous data points being found and a large spread of data in the optical transfer function (also see Figure 3.4.8). With proper edge-finding software this method may not be impossible, however. Particularly software that focuses on finding shapes (the lines of the edges) instead of local maxima may offer a solution to this problem, but this remains a concern for future research. Since it would allow for easy direct estimation of the resolution of any FIB, however, this would be a worthwhile thing to further investigate.
When it comes to using this method on future FIBs, higher resolution and the corresponding smaller spot size may become a problem. This has not been a problem with this method so far, since the edges overall in an easily created sample such as broken graphite were sharp enough

to allow this method to be used and, furthermore, this method does not depend on the exactness and sharpness of a single edge, unlike the knife edge measurement (see Section 5.1.2). The moment that the resolution of FIBs gets too close to the size of the edges themselves, this method can no longer be used, however. The sharpness of the edges in a sample will thus most likely be the limiting factor for using this method on FIBs of higher beam quality.

5.1.2 The knife-edge measurement

The Knife Edge method explored is used not only to determine the spot size of the FIB, but also its reduced brightness. A benefit of this method is that, like for the resolution measurement described in Section 5.1.1, nothing is needed to implement this method but the scanning capabilities of the FIB itself and a proper sample. It can also be almost fully automated, since all that is currently done manually, aside from mounting the sample, is checking the scans for clear edge deteriorations (see Figure 4.3.17), and even this may be done by software that compares an image to a reference image. Being able to use a simple, automated method to determine not only the spot size but also the brightness of a FIB is very useful.

The requirements of the sample, the so-called knife edge, are strict, however. An insufficiently sharp knife edge could easily account for an order of magnitude difference between the values as determined by the model and the experimental values. The appearance of larger spot size when using a blunter edge was also clearly shown when comparing Figures 4.3.15, 4.3.16 and 4.3.9 (see Section 4.3.3).

There was overall a large spread in the data from the experimental measurements resulting from differences in edge sharpness and other probable factors, such as statistical effects. The experimental values sometimes differed almost an order of magnitude from the expectations calculated by the model, though never more. The method as tried out here thus did not allow for more than a rough estimate of orders of magnitude of the brightness and spot size of the FIB.

With a particular sharper edge (see Figure 4.4.2) the experimental results only differed a factor 2 from the expectations from the model, the experimental values for the radius of the spot size here lying between 25 – 40 nm, against model values of 10 – 20 nm. Within this same experiment, the reduced brightness was even found to coincide closely with the expectations from the model, with each experimental value for the reduced brightness lying within 10% of the corresponding value from the model (see Figure 4.4.3). This shows that, with some care, especially in the selection of the edge, a better estimate of the spot size and reduced brightness may be found. This is supported by other proposed methods of improving the quality of a knife edge measurement [16,17,21,22].

Some ways to improve the knife edge measurements were already implemented. Each knife edge measurement was averaged with 9 others in the same circumstances and, for the sake of determining exact waist size and brightness, multiple scans were made surrounding the waist at different positions along the beam axis, to be able to fit the minimum beam size (which is the spot size radius) and determine the emittance and reduced brightness from this. The averaging and fitting helped to account for statistical errors, though this process may be taken further. To account for edge deterioration by exposure to the heavy ions, each measurement was done at a different position along the edge. This also allowed for inconsistency in edge quality, however, and should partly account for the high spread in the results.

This method proved better at showing the general trends of the spot size and reduced brightness' dependency on other beam parameters than any exact values. The dependency of spot size and reduced brightness on the voltage of the condenser lens, at least for the measurements using a

sufficiently sharp edge, coincided well with the expected trend as determined by the model (see Figures 4.4.2 and 4.4.3). Also, the measured spot size versus current curve coincided with the trend expected for a spot size limited by spherical aberrations (see Figure 4.4.5). This indicates that this method can be used to measure important trends to determine beam quality, such as the aforementioned spot size versus current curve.

All in all, this method can be used to gain a rough estimate of beam quality, though it should perhaps be used in conjunction with further, more exacting measurements (see Section 1.3 for other methods of determining beam quality), if the exact value of the brightness or spot size needs to be determined. To get more exact results from this method a lot of care should particularly be taken in the selection of an edge. A lot may also be gained in the way the experiment is performed, by eliminating most of the sources of extra error, by taking the average result of even more measurements to account for statistical effects and by trying some of the improvements upon this method suggested by others. This extra care somewhat defeats the purpose of having a quick and easy method to determine beam quality, however, and the Knife Edge method may best be considered as a way to easily gain some understanding of the important trends in the ion beam properties, by using a mostly automatic measuring process, instead of a method to determine the exact values of the spot size and reduced brightness.

When it comes to using this method on future FIBs, the smaller spot size will probably be the biggest problem for this method. Already insufficiently sharp edges result in clearly erroneous data. As the spot size increases, the knife edges will have to even sharper to be able to continue implementing this method and even more care should be taken in creating and selecting these edges. This will also affect the calculation of the reduced brightness, since it is determined using knife edge measurements of the spot size and the beam surrounding the waist (see Section 4.3.2). Whether making measurements on a higher brightness FIB would be more difficult regardless of smaller spot size is uncertain.

5.2 Discussion

When it comes to the explored resolution measurement (see Chapter 3), the results show that the resolution could be estimated at least up to its order of magnitude. This is put into question somewhat, however, since the comparison of the measurements of resolution were not done in the exact same circumstances as for which the expectations could be determined. The specifications of the FIB stated that the resolution should be below 7 nm at a beam current of 1 pA and a magnification $M \leq 30000$ (see Section 2.2.3), whereas the measurements were performed at a beam current of 40 pA and magnifications of $M = 120000$, $M = 65000$ and $M = 25000$. While it is not unreasonable to expect the resulting resolution to be within the same order of magnitude as 7 nm, this comparison is not exact.

The conclusion about the difficulty of automating edge detection in Chapter 3 is supported by Orloff's paper in which this resolution measurement is proposed [1], where it is mentioned that analysing the sample through the use of software was difficult and thus not attempted. The advances in software since 1996, the year in which this paper was published, may make it easier to find a solution now, however, and this may, in fact, have already been done. The reason this was not further pursued in this thesis was that it included a software heavy focus that would have taken a lot of time, while for the purposes of this thesis it was deemed more important to focus on some of the other aspects of beam quality as well, since beam quality is indicated by more than just resolution.

As for the knife edge measurements (see Chapter 4), while it has long been known that it is difficult to get a dependable result for the spot size [17], it should have been possible to achieve

more accurate results than these. When exploring some of the difficulties, Orloff shows results with no more than a factor 2 or 3 between the spot size and the expected spot size [17]. This was achieved for part of the measured trends dependent on the condenser lens voltage as compared to the model values, but for these apparently more accurate measurements no exact specifications for the FIB were known and thus the data could not be compared to such.
Better results could possibly also have been achieved within the scope of this thesis, by making more measurements or trying to use a different method to create a sharper knife edge. The focus was placed on determining whether this method could be performed in a quick and easy and mostly automated manner, however, since that seemed to be most useful for future application. The automated method of determining the reduced brightness using only knife edge measurements was in fact developed for this thesis and not, unlike the other methods, taken from existing literature.
There is also a difference between the measurement data and the model data, which comes into play when comparing them. In the measurement data both the radius of the spot size and the reduced brightness were calculated using the radius containing 50% of the beam r_{50} as the half beam size. In the model data these were calculated using the standard deviation σ as the half beam size. This difference was caused because the radius containing 50% of the beam proved too difficult to calculate in the model. With an approximately gaussian beam profile, this should account for no more than about a factor 1.18 difference between r_{50} and σ (see Equation 4.3.1) and when analysing these results this was taken into account. This relates a factor 0.5 for the reduced brightness (see Equations 4.2.9 and 4.2.10), however, which is larger but still less than an order of magnitude, though this difference may partly account for the measured reduced brightness not coinciding with expectations (see Figure 4.4.6), since using the standard deviation (instead of r_{50}) to determine the emittance is a typical choice [27]. These factors may also be slightly different in reality, since the beam itself is not exactly gaussian in shape (see Section 1.2). This difference, however large, is constant across all values, though, and should thus not affect the shape of the found trends.
Aside from this some doubt can be placed on the exactness of the trend found in the spot size versus current curve, however. While the expectation of a spherical aberration limited spot size showed the best fit for the experimental values overall, the spread in the data was quite large. Furthermore, at lower currents chromatic aberrations might be expected to dominate. Whether this could be seen in the corresponding data could not be determined, however, since too few measurement points were taken in the lower current range (see Figure 4.4.5).
One of the biggest benefits of both of the methods explored in this thesis, is that they do not require knowing the current density distribution of the beam, which makes them directly applicable on a FIB, without further knowledge. However, knowing the current density distribution is handy in its own right, since it affects the interaction of the FIB with a sample, and should thus not be neglected.
Lastly, the experiments in this thesis were limited to an exploratory research of the two methods and were thus only tested on an old FIB model. Thus, all conclusions about how useful the methods would be for future FIBs can only be speculation.

5.3 Recommendations for future research

First of all, the exactness of some of the methods in this thesis could be investigated further. The use of more data points would lead to more clearly defined conclusions. While knife edge measurements in particular have already often been researched further, the method proposed in this thesis for determining not only the spot size using knife edge measurements, but also the

reduced brightness, may not have been, since it was developed for this thesis. A further exploration of how this method can be made to be more exact, without sacrificing its main factor of ease of use too much, would be interesting, particularly since this Knife Edge method can be performed almost fully automatically, and could thus be of great use.

When it comes to the other method explored in this thesis, the method for determining the resolution explored in Chapter 3, it would mostly be interesting to research whether or not this method could be fully automated. For this, proper edge-finding software would be needed, particularly software that is capable of finding shapes, instead of determining local maxima, since simply finding local maxima makes this method too vulnerable to noise. Since the original paper describing this method stems from 1996 [1], this may by now have already been done, however, so a literature study of possibilities in this area would have to be done first.

Aside from this, it would be particularly useful to try out current methods of determining FIB quality on higher quality FIBs, particularly those with smaller spot sizes and resolutions and higher brightness, to find out how the changed parameters affect how well these old methods work.

Lastly, determining the current density distribution of the beams should not be ignored, since the exact form of the distribution can strongly affect the operation of a FIB (see Section 1.2). Some methods to do so have already been developed (see Section 1.3.3). Faster and easier methods to directly determine the current density distribution would be useful and could also help to better determine the exact spot size and brightness of a beam.

Bibliography

[1] J. Orloff, L.W. Swanson and M. Utlaut. *Fundamental limits to imaging resolution for focused ion beams*. J. Vac. Sci. & Technol. B **14**, 3759 (1996)

[2] S.H.W. Wouters, G. ten Haaf, R.P.M.J.W. Notermans, N. Debernardi, P.H.A. Mutsaers, O.J. Luiten and E.J.D. Vredenbregt. *Performance predictions for a laser-intensified thermal beam for use in high-resolution focused-ion-beam instruments*. Phys. Rev. A **90**, 063817 (2014)

[3] B. Knuffman, A.V. Steele, J. Orloff and J.J. McClelland. *Nanoscale focused ion beam from laser-cooled lithium atoms*. New J. of Phys. **13**, 103035 (2011)

[4] A. Lugstein, B. Basnar, G. Hobler and E. Bertagnolli. *Current density profile extraction of focused ion beams based on atomic force microscopy contour profiling of nanodots*. J. App. Phys. **92**, 4037 (2002)

[5] G. ten Haaf, S.H.W. Wouters, S.B. van der Geer, E.J.D. Vredenbregt and P.H.A. Mutsaers. *Performance predictions of a focused ion beam from a laser cooled and compressed atomic beam*. J. App. Phys. **116**, 244301 (2014)

[6] S. Wouters. *A compact, ultracold atomic beam source for use in a focused ion beam system*. Ph.D. thesis, Eindhoven University of Technology (2016)

[7] V. Castaldo, C.W. Hagen, B. Rieger and P. Kruit. *Sputtering limits versus signal-to-noise limits in the observation of Sn balls in a Ga+ microscope*. J. Vac. Sci. & Technol. B **26**, 2107 (2008)

[8] R.L. Kubena and J.W. Ward. *Current-density profiles for a Ga+ ion microprobe and their lithographic implications*. App. Phys. Letters **51**, 1960 (1987)

[9] G.E. Moore. *Cramming more components onto integrated circuits*. Electronics, pages 114-117 (1965)

[10] *Samsung Starts Mass Producing Industry's First 10-Nanometer Class DRAM*. https://news.samsung.com/global/samsung-starts-mass-producing-industrys-first-10-nanometer-class-dram, dated April 05, 2016, retrieved March 8, 2019

[11] *Exynos 9 Series (8895): A Mobile processor that goes beyond mobile innovation*. http://www.samsung.com/semiconductor/minisite/Exynos/w/solution/mod_ap/8895/, undated, retrieved March 8, 2019

[12] B. Knuffman, A.V. Steele and J.J. McClelland. *Cold atomic beam ion source for focused ion beam applications*. J. App. Phys. **114**, 044303 (2013)

[13] G. ten Haaf. *Ultracold Rb Focused Ion Beam*. Ph.D. thesis, Eindhoven University of Technology (2017)

[14] A.V. Steele, A. Schwarzkopf, J.J. McClelland, B. Knuffman. *High-brightness Cs focused ion beam from a cold-atomic-beam ion source*. Nano Futures **1**, 015005 (2017)

[15] S. Tan, R.H. Livengood, Y. Greenzweig, Y. Drezner and D. Shima. *Probe current distribution characterization technique for focused ion beam*. J. Vac. Sci. & Technol. B **30**, 06F606 (2012)

[16] C. Otis, M. Maazouz, D. Logan, J. Orloff. *Pitfalls in the Measurement of FIB Beam Size. On the way to an accurate estimation of the Focused Ion Beam Size*. Imaging & Microscopy (2012)

[17] J. Orloff. *Measuring the beam size of a focused ion beam (FIB) system*. Scanning Microscopy (2010)

[18] Y. Greenzweig, Y. Drezner, S. Tan, R.H. Livengood, A. Raveh. *Current density profile characterization and analysis method for focused ion beam*. Microelectric Engineering **155** (2016)
[19] N. Vladov, J. Segal and S. Ratchev. *Apparent beam size definition of focused ion beams based on scanning electron microscopy images of nanodots.* J. Vac. Sci. & Technol. B **33**, 041803 (2015)
[20] J. Orloff. *Highresolution focused ion beams*. Rev. Sci. Instruments **64**, 1105 (1993)
[21] T. Ishitani, H. Tamura and H. Todokoro. *Scanning microbeam using a liquid metal ion source*. J. Vac. Sci. & Technol. **20**, 80 (1982)
[22] H. Arimoto, A. Takamori, E. Miyauchi and H. Hashimoto. *Novel Method for Measuring Intensity Distribution of Focused Ion Beams*. Japanese Journal of Applied Physics **22** (1983)
[23] L.R. Harriot. *Beam-size measurements in focused ion beam systems*. J. Vac. Sci. & Technol. A **8**, 899 (1990)
[24] G. Ben Assayag, C. Vieu, J. Gierak, P. Sudraud and A. Corbin. *New characterization method of ion current-density profile based on damage distribution of Ga+ focused-ion beam implantation in GaAs*. J. Vac. Sci. & Technol. B **11**, 2420 (1993)
[25] C.W. Hagen, E. Fokkema and P. Kruit. *Brightness measurements of a gallium liquid metal ion source*. J. Vac. Sci. & Technol. B **26** (2008)
[26] J. Buon. *Beam Phase Space and Emittance*. CERN Accelerator School (1992)
[27] Barletta, Spentzouris and Harms. *USPAS notes*. U.S. Particle Accelerator School, http://uspas.fnal.gov/materials/12MSU/emitlect.pdf, undated, retrieved at 26-06-2019
[28] www.pulsar.nl/gpt

Appendix: Code

This appendix contains the code used to process the data in the experiments described in Chapter 3 (see Section A.1) and Chapter 4 (see Section A.2). These codes were written in Matlab. It also contains the code used to control the FIB for the experiment in Section 4.3.2 (see Section A.3). This was written in the internal programming language of the FIB.

A.1 Matlab codes for the experiments in Chapter 3

A.1.1 Code for manual edge determination

This code was used to determine the contrast between two manually found edges (see Section 3.3.2):

```
%This matlab program calculates the contrast between two edges
clear all;

f = imread('2,34muM_short_50pA4.TIF');
line = 690;          %pick a line from the image
e1 = 741;            %pick the x-coördinate of the first edge
e2 = 798;            %pick the x-coördinate of the second edge
xmaxSet = 2.34;      %set image width

%Don't change the rest of the code
k = f(line,:);       %take the chosen line
[irr,sk] = size(k); %determine the length of the line

%determine x axis
dx = xmaxSet/(sk-1);

%determine distance between the edges
r = e2-e1;
r = r*dx

%determine maximum and minimum intensity
mx = max(k(e1:e2));
mn = min(k(e1:e2));

%change the types of the maximum and minimum intensity
for j=1:1000
    if(mn==j)
        mn=j;
    end
end
for j=1:1000
    if(mx==j)
        mx=j;
    end
end

%Calculate the contrast
C = (mx-mn)/(mx+mn)

%determine the total contrast for normalization purposes
mxF = max(k);
mnF = min(k);

%change the types of the maximum and minimum intensity
```

```
for j=1:1000
    if(mnF==j)
        mnF=j;
    end
end
for j=1:1000
    if(mxF==j)
        mxF=j;
    end
end

%determine the contrast of the entire picture
CF = (mxF-mnF)/(mxF+mnF)
```

A.1.2 Code for automatic edge determination

The following code was used to find all edges in a picture automatically and determine the contrasts between them (see Section 3.3.3):

```
%This matlab program calculates the contrasts found in several lines of a
%picture, as a function of the distances between "edges" in the picture. It
%calculates this from each pair of edges lying next to eachother.

clear all;
f = imread('1,27muM_short_50pA4.TIF');
line = 1:885;  %pick lines from the image
tr = 0.75;          %pick the minimum relative intensity needed to determine
an edge
n = 5;                %pick the amount of neighbours on both sides, an edge
has to be greater than
xmaxSet = 1.27;     %set image width
numAve = 100;       %set amount of points over which the endpoint averaging
is done

%Don't change the rest of the code
k = f(line,:);      %take the chosen lines
[one,sL] = size(line);

%initialize variables
mx = zeros(1,sL);
Pmx = zeros(1,sL);
mn = zeros(1,sL);

%determine the maximum and minimum intensity per line
for l=1:sL
    [mx(l),Pmx(l)] = max(k(l,:)); %determine the maximum intensity and it's
place
    mn(l) = min(k(l,:));          %determine minimum intensity
end

%change the types of the maximum and minimum intensity
for l=1:sL
    for j=1:1000
        if(mn(l)==j)
            mn(l)=j;
        end
    end
end
for l=1:sL
    for j=1:1000
        if(mx(l)==j)
            mx(l)=j;
        end
    end
end

%initialize variables
kTr = zeros(1,sL);

%determine the threshold intensity for edges per line
for l=1:sL
    kTr(l)=tr*mx(l);
end
```

```
%initialize variables
[one,sk] = size(k);
kNear1 = zeros(sL,sk);
kNear2 = zeros(sL,sk);

%determine the neighbours of each pixel
for l=1:sL
    for j=1:sk
        if((j-n)<1)
            kNear1(l,j) = 1;
        else
            kNear1(l,j)=j-n;
        end
    end
    for j=1:sk
        if((j+n)>sk)
            kNear2(l,j) = sk;
        else
            kNear2(l,j)=j+n;
        end
    end
end

%initialize variables
i = ones(1,sL);
kEdge = zeros(sL,sk);
edges = zeros(sL,sk);

%find the edges, using the given variables
for l=1:sL
    for j=1:sk
        if(k(l,j)>kTr(l))
            temp = k(l,kNear1(l,j):kNear2(l,j));
            m = max(temp);
            if(k(l,j)==m)
                kEdge(l,i(l))=j;
                i(l) = i(l) + 1;
                edges(l,j) = 1;
            end
        end
    end
end

%To determine lengths of vectors later
iMax = max(i);

%plot the lines and their edges
%for l=1:sL
%    figure;
%    colormap('gray');
%    subplot(2,1,1); imagesc(k(l,:));
%    subplot(2,1,2); imagesc(edges(l,:));
%end

%determine the distances between the edges
res = zeros(sL,(iMax-2));
for l=1:sL
    for j=1:(i(l)-2)
        res(l,j) = abs(kEdge(l,j+1)-kEdge(l,j));
```

```
    end
end

%determine the maxima and minima between each pair of edges
kMax = zeros(sL,(iMax-2));
kMin = zeros(sL,(iMax-2));
for l=1:sL
    for j=1:(i(l)-2)
        kMax(l,j)=max(k(l,kEdge(l,j):kEdge(l,j+1)));
        kMin(l,j)=min(k(l,kEdge(l,j):kEdge(l,j+1)));
    end
end

%determine the contrast between each pair of edges
kC = zeros(l,(iMax-2));
for l=1:sL
    for j=1:(i(l)-2)
        kC(l,j) = (kMax(l,j)-kMin(l,j))/(kMax(l,j)+kMin(l,j));
    end
end

%intialize variables
resLong = res(1,:);
cLong = kC(1,:);

%make one long vector
for l=2:sL
    resLong = [resLong,res(l,:)];
    cLong = [cLong,kC(l,:)];
end

%sort the distances
[resSortZero,ind]=sort(resLong);

%sort the contrasts
[one,srZero] = size(resSortZero);
CSortZero = zeros(1,srZero);
for j=1:(srZero)
    CSortZero(j) = cLong(ind(j));
end

%count the amount of zeros
counter = 0;
for j=1:srZero
    if (resSortZero(j)==0)
        counter = counter+1;
    end
end

%take out the zeros
resSort = resSortZero((counter+1):srZero);
CSort = CSortZero((counter+1):srZero);

%determine x axis
dx = xmaxSet/(sk-1);

%transform the resolution to micrometers
resSortT = resSort*dx;
```

```
%plot the contrasts as a function of the distances between the edges
figure;
plot(resSortT,CSort); title('Contrast');

%determine the new sizes of the long vectors
[one,srSort] = size(resSort);
[one,scSort] = size(CSort);

%normalize the contrast
ave = mean(CSort((scSort-numAve):scSort));
CSortNorm = CSort/ave;

%plot the normalized contrast
figure;
plot(resSortT,CSortNorm);  title('Normalized contrast');
```

A.1.3 Code for adding artificial noise

The following code structure was added to the code in Section A.1.2 to add artificial noise to an image, so that the effects of adding noise could be studied (see Section 3.4.2):

```
%Initialize variables
kM = max(max(k));
kNoise = zeros(sL,sW);

%Calculate random noise
randNoise = (rand(sL,sW)-0.5)*maxNoise*2;

%Add additional noise to the image
for l=1:sL
    for j=1:sW
        kNoise(l,j)=k(l,j)+randNoise(l,j);
        if(kNoise(l,j)<0)
            kNoise(l,j) = 0;
        end
        if(kNoise(l,j)>kM)
            kNoise(l,j)=kM;
        end
    end
end
```

A.2 Matlab code for the experiment in Chapter 4

This code was used to determine the rise distances from the knife edge scans (see Section 4.3.2):

```
clear all;

%Define the heights (z) pictured
zStart = 10760;      %The lowest z
zFinal = 11240;      %The highest z
zDiff = 30;          %The difference between two subsequent heights
neg = 0;             %Whether or not the z-values are negative. 1 is true, 0
is false.

%The amount of measurements per height
sStart = 1;
sFinal = 20;
sTot = 20;
sP = 100000;         %The place of the measurement number in the imagestring

%The image width in micrometers
imWidth = 36.632;

%Set how the rise distance is defined. Perc gives the percentage from 0 to
%1 that defines the rise distance. Thus if perc is 0.12, the rise distance
%is taken from 12%-88%. If perc is 0.25, the rise distance is taken from
%25%-75%. And so on and so forth.
perc = 0.25;         %Give the percentage as a value between 0 and 0.5

%Some estimated values for the fitting of the error-function. If the fit is
%y(x), these values change it like this: y = off+scY*erf((x-shift)/scX))
scX = 0.01;            %Estimation of the scaling in x of the fitted error-
function

%The boundaries for determining the minimum and the maximum values to
%calculate A and C
minL = 150;          %The left boundary for the average minimum
minR = 250;          %The right boundary for the average minimum
maxL = 700;          %The left boundary for the average maximum
maxR = 800;          %The right boundary for the average maximum

%Fitlimiters
limit1 = 200;        %The lower fit limit
frac = 1.5;              %The fraction of the maximum at which the upper fit
limit will be

%Do not change the rest of the code
zN = 1+(zFinal-zStart)/zDiff;        %Total number of heights
fullResult = zeros(sTot,zN);         %Initialize result matrix

allStart = zeros(sTot,zN);           %Initialize result matrix with minima
allFinish = zeros(sTot,zN);          %Initialize result matrix with maxima
allF4  = zeros(sTot,zN);                 %Initialize result matrix with the
variance of the error term of the fits
allR  = zeros(sTot,zN);                  %Initialize result matrix with the
residuals of the fits

fitCheck = zeros(sTot,zN);            %Checkboxes of user's choice to accept
the fit y/n
```

```
fitComment = cell(sTot,zN);          %Placeholder for user's comments on a
particular fit

%Place the heights in an array
heights = zStart:zDiff:zFinal;

stop = 0;   %Option to stop the script while executing

%Execute the script for all images
for s=sStart:sFinal
for z=heights
%Determine at what place the current imagedata should be placed in result
zNumber = 1+(z-zStart)/zDiff;

try
%Read the image
imN = (s*sP)+z;          %The current image number
imstr = sprintf('%u',imN);  %Convert the image number to a string
TIFstr = [imstr '.TIF'];    %Concatenate .TIF to the image number
f   =   imread(fullfile('D:\Metingen   Kathelijne\Knife   edge\Autoscan\Lens1
Voltage\15,5kV',TIFstr));          %Read the image with number im

%Determine the size of the image
kU = f;
[sL,sW] = size(kU);

%Change the information in the image to type double
k = zeros(sL,sW);
for i=1:sL
    for j=1:sW
        k(i,j) = double(kU(i,j));
    end
end

%Calculate the average of all the lines over the knife edge
overlap = zeros(1,sW);
ave = zeros(1,sW);

for j=1:sW
    %Add the lines together
    for i=1:sL
        %Count the lines that overlap
        if(k(i,j)>0)
            overlap(j) = overlap(j)+1;
        end

        %Add the points together
        ave(j) = ave(j)+k(i,j);
    end

    %Calculate the average
    ave(j) = ave(j)/overlap(j);
end

%Calculate the place axis
pixWidth = imWidth/sW;  %Determine the width of one pixel
p = (0:(sW-1))*pixWidth;

%Make the fits
```

```
%Initizalizing variables
fitK = zeros(sL,sW);     %The fits of each line
checkPrecision = zeros(1,sL);   %If the fit is precise enough, shows a 1

%Find the average minimum and the average maximum to rise between
start = mean(ave(minL:minR));
finish = mean(ave(maxL:maxR));

%Calculate the estimated fitvalues from this
A = (finish-start)/2;
C = start+A;

%Calculate the shift estimate
leftBound = start + (finish-start)/3;    %The value at left boundary of the
range in which the centre lies
rightBound = finish-(finish-start)/3;    %The value at right boundary of the
range in which the centre lies
centreValue = start+(finish-start)/2;    %The value at the centre
pLeftBound = 0;     %The left boundary of the range in which the centre lies
pRightBound = 0;    %The right boundary of the range in which the centre lies
pCentreValue = 0;   %The estimated place of the centre

for i=1:sW
    if(ave(i)<leftBound)     %The left boundary is the rightmost place just
above the left boundary value
        pLeftBound = i+1;
    end
    if(ave(i)>rightBound && pRightBound==0)  %The right boundary is the
leftmost place just below the right boundary value
        pRightBound = i-1;
    end
end
for i=pLeftBound:pRightBound
    if(ave(i)>centreValue && pCentreValue==0);  %The estimated place of the
centre is the first place above to the centre value between the boudnaries
        pCentreValue = i;
    end
end

shiftEst = p(pCentreValue);        %The estimated place of the centre in
micrometers

%Calculate the second fit limit
%Find the place where the function is at 1/frac1 of the maximum
int1 = start+2*A/frac;
x1=0;
for i=2:sW
    if((ave(i)>int1)&&(ave(i-1)<int1)&&(x1==0))
        x1 = i;
    end
end
limit2 = x1-1;

%Set the limited plot that will be fitted
pFit = p(limit1:limit2);
aveFit = ave(limit1:limit2);

%Fit an error-function through the data
modelfun = @(b,x) C+A*erf((x-b(1))/(b(2)*sqrt(2)));
beta0 = [shiftEst,scX];
```

```
[fitCoef,f1,f2,f3,f4] = nlinfit(pFit,aveFit,modelfun,beta0);
fitK = modelfun(fitCoef,p);
fitKlim = modelfun(fitCoef,pFit);

%Show the fit in a plot and prompt y/n to accept it or not
%Show the corresponding picture
pic = figure('Position',[120 200 400 300]);
colormap('gray');
imagesc(kU);

%Create the fit title for the picture
sstr = sprintf('%u',s);
zstr = sprintf('%u',z);
figTitle = ['s=' sstr ', z=' zstr];

%Plot the fit
fig = figure('Position',[120 500 400 300]);
plot(p,ave,p,fitK);
title(figTitle);

%Prompt the choice
choice      =      'y';      %questdlg('Proper      fit?','Check      the
fit.','y','n','comment','y');
close(pic);
close(fig);

%Determine the rise distance boundaries for the first percentage
bound1 = C-A+(2*A*perc);  %The value at the left edge
bound2 = C+A-(2*A*perc);  %The value at the right edge

%Determine the rise edge distance
fineAxis  =  0:(p(sW)/200000):p(sW);        %A  finer  place  axis  to  determine
place more accurately
fineFit = modelfun(fitCoef,fineAxis);   %The fit as made with the finer axis
[irr, sfA] = size(fineAxis);
place1 = 0;     %The place of the left edge
place2 = 0;     %The place of the right edge
for i=1:sfA
    if((fineFit(i)>bound1)&&(place1==0))
        place1 = fineAxis(i-1);
    end
    if((fineFit(i)>bound2)&&(place2==0))
        place2 = fineAxis(i);
    end
end

REdist = place2-place1;    %The rise distance

%Check what the user decided
switch choice
    case 'y'
        fitCheck(s,zNumber)=1;
        fitComment(s,zNumber)={'y'};
    case 'n'
        fitCheck(s,zNumber)=0;
        fitComment(s,zNumber)={'n'};
    case ''
        fitCheck(s,zNumber)=0;
        fitComment(s,zNumber)={'User cancel'};
```

```
        stop = 1;
        break;
    case 'comment'
        fitCheck(s,zNumber)=0;
        comment = inputdlg('What do you have to add?','Comment');
        fitComment(s,zNumber) = {comment};
end

%Show the rise distances gleaned from the line-fit in result
fullResult(s,zNumber) = REdist;

%Show the start, finish and f4 found in the other result matrices
allStart(s,zNumber) = start;
allFinish(s,zNumber) = finish;
allF4(s,zNumber) = f4;

%Calculate the residual and show it in the last result matrix
f1sq = f1.^2;
R = mean(f1sq);
allR(s,zNumber) = R;

catch
%Set a 0 in result if the image does not exist or the fit gives an error
fullResult(s,zNumber) = 0;
allStart(s,zNumber) = 0;
allFinish(s,zNumber) = 0;
allF4(s,zNumber) = 0;

end
    if stop
        break
    end
end
    if stop
        break
    end
end

%Average the results per height
[hR,wR] = size(fullResult);
sumDist = zeros(1,wR);  %Summation of the found rise distances per height
countDist = zeros(1,wR);%The amount of distances found
avDist = zeros(1,wR);   %Average of the found rise distances per height

%Summate the rise distances per height
for j=1:wR
    for i=1:hR
        if((fullResult(i,j)>0)&&fullResult(i,j)<1)
            sumDist(1,j) = sumDist(1,j)+fullResult(i,j);
            countDist(j) = countDist(j) + 1;
        end
    end
    avDist(1,j) = sumDist(1,j)/countDist(j);
end

%Set the heights to their true negative value before calculating the result
if (neg==1)
    heights = -1*heights;
end
```

```
%Place the result in one matrix
result = [heights;avDist];

%Plot the result
figure;
plot(result(1,:),result(2,:),'o');
xlabel('height (\mum)');
ylabel('Rise distance (\mum)');
title('The average 25% rise distance at different heights');

%Calculate the differences between start and finish at each picture
allDiff = zeros(hR,wR); %The differences between start and finish
for j=1:wR
    for i=1:hR
        if((allFinish(i,j)>0)&&allStart(i,j)>0)
            allDiff(i,j) = allFinish(i,j)-allStart(i,j);
        end
    end
end
```

A.3 FIB instruction code used for Chapter 4

This code was used to instruct the FIB to perform a waist scan (see Section 4.3.2):

```
# This code scans along an edge at different
# z-values (heights) and is thus useful to
# help determine the brightness of the beam.

# Write the current date and time into the logfile
logtime
# Define how numbers are written in the logfile
sigfigs 1, 2
# Get the operating variables and print them
getbeamcurrent
printlog "Beam current = ", bcurrent, " pA"
getcolumnpressure
printlog "Column pressure = ", pressure, " mbar"
getemission
printlog "Emission current = ", ecurrent, " microA"
getextractor
printlog "Extractor voltage =", xvoltage, " V"
getfocus
printlog "Focus voltage of the control beam =", focus, " V"
gethv hvoltage
printlog "HV = ", hvoltage, " V"
getlens1 l1voltage
printlog "Lens 1 voltage = ", l1voltage, " V"
getlens2 l2voltage
printlog "Lens 2 voltage = ", l2voltage, " V"
getstagecurrent
printlog "Stage current = ", scurrent, " pA"
getsuppressor
printlog "Suppressor voltage = ", svoltage, " V"
getvislope
printlog "V/I slope = ", slope, " V/microA"

# The tilt (tilt is not set by the program)
tilt = -10
printlog "Tilt = ", tilt, " degrees"
printlog

# Initialize variables
# Stepsize in z
zstep = 1
# Number of images captured at each z
ns = 10
# Number of z-values scanned
nz = 9
# Get the initial position of the stage
getstagepos
# Save the initial value of z to z0
z0 = z
# Distance between scans along the edge
xshift = -2
# How much y shifts per scan to stay on edge
yshift = 0.06
# zcount counts up to nz
zcount = 0
# scount counts up to ns
scount = 0
```

```
# Determine the sine, cosine and tangens of the tilt
radian = tilt * (180/3.142)
tan ttan, radian
sin tsin, radian
cos tcos, radian

# Scan the images
loop:
# Move to the right place
stagemove xyz, x, y, z

# Capture an image of the edge
grabframe 0, 0, 1024, 884, 2, 500, 0

# Image saved as #0z.tif (# is (scount+1), the amount of scans at the current
z so far)
numb = ((scount+1) * 100000) + z
saveimagedatabar numb, 0

# Imagenumber saved to the log
printlog numb, " s=", scount, " z=", z

# Change location and z to next position
zcount = zcount + 1
x = x + xshift
y = y + yshift
y = y + (zstep * tsin)
z = z - (yshift * ttan)
z = z + (zstep * tcos)

# Cancel the program if user pressed "stop/cancel"
if (cancel=1) goto end

# Repeat the loop up to here until all z-values have been imaged (again)
if (zcount<nz) goto loop

# Return z to its starting value
z = z0
zcount = 0

# Adjust y to correct for z-movement under tilt
zshift = nz * zstep
y = y - (zshift * tsin)

# Repeat the entire loop until all z-values have been imaged ns times
scount = scount + 1
if (scount<ns) goto loop

# Move z back to its starting number
stagemove z, z0

# End the program succesfully
result = 1
```